Load-deformation Behavior Of Component Elements Of Ship Hull Structures (stiffended Plate, Grillage).

8418431

Surahman, Adang

LOAD-DEFORMATION BEHAVIOR OF COMPONENT ELEMENTS OF SHIP HULL STRUCTURES

Lehigh University PH.D. 1984

University
Microfilms
International 300 N. Zeeb Road, Ann Arbor, MI 48106

PLEASE NOTE:

In all cases this material has been filmed in the best possible way from the available copy. Problems encountered with this document have been identified here with a check mark __√__.

1. Glossy photographs or pages _____
2. Colored illustrations, paper or print _____
3. Photographs with dark background _____
4. Illustrations are poor copy _____
5. Pages with black marks, not original copy _____
6. Print shows through as there is text on both sides of page _____
7. Indistinct, broken or small print on several pages __✓__
8. Print exceeds margin requirements _____
9. Tightly bound copy with print lost in spine _____
10. Computer printout pages with indistinct print _____
11. Page(s) __________ lacking when material received, and not available from school or author.
12. Page(s) __________ seem to be missing in numbering only as text follows.
13. Two pages numbered __________. Text follows.
14. Curling and wrinkled pages _____
15. Other ____

LOAD-DEFORMATION BEHAVIOR OF COMPONENT ELEMENTS OF SHIP HULL STRUCTURES

by

Adang Surahman

A Dissertation

Presented to the Graduate Committee

of Lehigh University

in Candidacy for the Degree of

Doctor of Philosophy

in

Civil Engineering

Lehigh University

1984

Approved and recommended for acceptance as a dissertation in partial fulfillment of the requirements for the degree of Doctor of Philosophy.

May 16, 1984
(date)

Alexis Ostapenko
Alexis Ostapenko
Professor-in-Charge

Accepted May 17, 1984
(date)

Special committee directing the doctoral work of Adang Surahman

George C. Driscoll
Professor George C. Driscoll
Chairman

Alexis Ostapenko
Professor Alexis Ostapenko

Arturs Kalnins
Professor Arturs Kalnins

Le-Wu Lu
Professor Le-Wu Lu

David A. VanHorn
Professor David A. VanHorn

ACKNOWLEDGMENTS

This study was partially sponsored by the U.S. Coast Guard of the Department of Transportation under Contract No. DTCG23-81-C-20068. The author is grateful for this support and especially acknowledges the guidance provided by Messrs. Daniel Billingsley and Daniel Cox, the consecutive Technical Representatives for the program.

The author would like to thank Dr. Alexis Ostapenko, project director of the sponsored research program and Professor-in-Charge of the dissertation, for his guidance and support throughout the study. Also thanks are expressed to Dr. George C. Driscoll, Chairman, and Drs. Arturs Kalnins, Le-Wu Lu and David A. VanHorn for reviewing the manuscript and offering constructive criticism of this study.

All the work was conducted at Fritz Engineering Laboratory, Department of Civil Engineering, Lehigh University; Dr. L.S. Beedle is Director of the Laboratory and Dr. D.A. VanHorn is Chairman of the Department.

Table of Contents

List of Figures

List of Tables

ABSTRACT

Methods for reliably computing the maximum bending moment of a ship hull girder depend on the knowledge of the nonlinear axial behavior of its component elements. To be practically efficient, the definition of this behavior should be in the form of compact algorithms (analytical computational models) rather than large computer programs. Plate, longitudinally stiffened plate and grillage were the hull girder elements considered in this study.

Parametric study of the functional effect of individual geometrical and material parameters on the axial load-deformation behavior of individual plates and longitudinally stiffened plates was carried out to obtain suitable coordinate functions. The functions were then subjected to multi-variable regression analysis in developing the analytical computational models. These models are applicable to the pre- and post-ultimate ranges of deformation. The data base consisted of the load-deformation relationships available from tests and theoretical analyses, or computed specifically for this study. Typical practical values of initial imperfections and residual stresses were incorporated into the models.

The models consist of sets (matrices) of constants which, for a particular combination of material and geometric properties, are reduced to a continuous analytical relationship of the axial stress

and the axial deformation (strain). The standard deviation with respect to the data used in the development of the models is 7.0% for plates and 7.8% for stiffened plates.

A numerical method of analysis was developed for grillages. The method is based on the combination of iterative integration and the solution of nonlinear equations. Depending on the degree of nonlinearity, the secant method or the flexible polyhedron search method were used.

The grillage analysis provides load shortening curves, and together with the results from other sources can be used to develop analytical models similar to the models for plates and stiffened plates. A limited study on the effect of the size of the transverses and of the number of stiffeners on the load-shortening relationship was performed. For grillages with very rigid trans verses, the results obtained from this analysis agree very well with the model developed for stiffened plates.

Chapter 1

INTRODUCTION

1.1 General Remarks

A ship hull structure is basically a box-shaped girder with the outer shell comprised of watertight thin plates stiffened by a frame gridwork. This structure is subjected to the variable and nonuniformly distributed loads caused by cargo loads and water pressure.

Depending on the relative position of the ship to the wave motion, there are two different bending moments acting on the hull's cross section. The first is the sagging moment, i.e., bending action in which the mid-hull section bends downward and causes compressive stresses at the ship deck. The other is the hogging moment and it causes tension in the deck plating.

A proper ship hull design is one that provides the ship with sufficient rigidity and strength to resist these bending moments while the weight of the ship is kept as small as possible. Minimizing the weight of the ship hull is desired to provide benefits such as faster ship movements, shorter construction time and an increase in load-carrying capacity.

Current design practice is based on an elastic analysis where the load effect is set smaller than the yield or buckling strength of the structure by a certain safety margin. This method does not provide a true estimate of the bending capacity of the ship hull cross section as most of the hull's elements do not exhibit a linear stress-strain relationship, especially in the ultimate range. Thus, the method does not consider the resistance which still exists in those elements which have reached the post-ultimate range. To achieve these objectives simultaneously, a method of analysis that considers nonlinearities in the stress-strain relationships of the elements of the hull structure should be used in design.

The magnitude and direction of the bending moment acting on the ship hull is determined by the axial stresses of the elements along the hull's circumference. These stresses can be tensile, which causes yielding, or compressive, which causes buckling and yielding. The response of the elements under compression depends on their material and geometrical properties. The complete knowledge of the load-deformation behavior of these component elements is therefore necessary for estimating the hull bending moment capacity. The types of these component elements are indicated by the patterns of load-deformation relationships. This behavior basically depends on the stiffness ratios of the plates and their stiffening frames.

The three component elements considered are plates, longitudinally stiffened plates and grillages.

The word grillage in the context of this presentation signifies a plate stiffened both in the longitudinal and transverse directions with respect to the direction of axial loading as shown in Figs. 13 and 14. If both sets of stiffeners are relatively rigid so that during in-plane loading only the plate deflects out of plane, the component element can be treated as a simple plate. If the stiffeners are relatively more flexible, this structure becomes a grillage. Two basic modes of failure limit the ultimate capacity of a grillage: the overall grillage mode when the whole assembly of the transverse and longitudinal stiffeners deflects together with the plate (Fig. 13), and the panel mode which occurs when the longitudinals and the plate deflect between the transverses. Grillages which exhibit the panel mode of failure will be termed henceforth stiffened plates whereas the term grillages will be used only if the failure mode is the overall grillage mode.

1.2 Literature Review

There have been many attempts to develop methods for computing the load vs. deformation relationships for these three component elements. Most of them were for plates. Also, many tests were conducted on plates. Fewer numerical methods and test results are available, and no analytical methods have been developed to generate load-shortening relationships for stiffened plates. Soares made a survey on plate and stiffened plate analyses and provided an extensive list of available literature [61].

For grillages there are even fewer numerical methods developed to formulate load-shortening relationships. The available results are too few to be conclusive. Also, there are very few tests on grillages and most of them were conducted to find the ultimate load or the modes of failure rather than the complete axial behavior in the pre- and post-ultimate ranges.

1.2.1 Plates

There is some numerical work on the complete load-shortening behavior of plates, i.e, covering the pre- and post-ultimate ranges [10, 11, 12, 14, 21, 22, 38, 40, 43]. There is also some experimental work although most of it has been mainly to define the ultimate capacity [8, 9, 15, 68], with only a few tests providing deformation measurements in the post-ultimate range [44].

Probably the numerical work by Little was the most extensive, covering a wide range of plate variables [40]. By using the variational method and a Raleigh-Ritz type method of minimizing the energy, he generated load-shortening curves for plates considering all governing parameters involved. He used the large deflection theory to compute strains and the plastic flow theory to define yielding [38]. The plate was divided into several elements and layers. To compute the total energy of the whole plate, he used the Simpson integration method. The displacement functions were expressed in terms of a sine series. To find the numerical values of the coefficients of each term in which the energy was a minimum, he used the quasi-Newton iteration method. Some of the results of his work were systematically tabulated [40].

The Raleigh-Ritz method of solution was also used by Kmiecik and Moxham [30, 43]. The ranges of variables covered in their analysis were more restricted. Kmiecik analyzed load-deformation relationship for long plates (aspect ratio greater than unity). Realistic shapes of initial deformations were assumed; however, residual stresses were not considered. Moxham analyzed almost square plates (aspect ratio A = 0.875) and long plates with aspect ratio A = 4.00.

Another common method used to compute load-deformation relationships was the finite difference method [14, 21, 22]. Basically, only square plates were considered in these studies.

Crisfield [10] used a finite element method to generate load-deformation of plates with the aspect ratio of A = 0.875 for various slenderness values and initial imperfections. He then developed a computer program to interpolate the load-deformation relationships of plates with slenderness values and initial imperfections other than the ones he used [11]. This method seems to be sufficiently accurate and can supply the load-deformation relationship at a much faster rate. In his computations, residual stresses were assumed to be zero. However, he suggested a simple formula to take the effect of residual stresses into account.

Det Norske Veritas [12] used a computer analysis that was programmed to perform nonlinear shell analyses (STAGSC) to generate load-deformation curves for wide plates of various aspect ratio and slenderness values. Residual stresses were assumed to be zero.

The simplest algorithm suitable for design purposes was proposed by Billingsley [5]. He formulated equations for effective width of plate as functions of the aspect ratio, plate slenderness and the strain level. However, initial imperfections and residual stresses were not considered. Moreover, the effective width was assumed to be constant after the plate had reached ultimate strength.

1.2.2 Stiffened Plates

Relatively limited numerical work has been completed on stiffened plates [17, 32, 34, 37, 39, 51, 52, 53, 58, 63, 65]. Most of it was to find the ultimate load rather than the load-deformation for the full range of deformation. However, some of the methods developed in these studies could be used directly or with some modifications to define the load-deformation behavior for a certain range of deformations.

The experimental work, despite its small quantity, provided much more useful information for the load-deformation behavior of stiffened plates, than the information so far obtained from the numerical work [3, 24, 25, 26, 33, 29, 37, 45]. Most of the tests provided load-deformation relationships for the entire range of deformation. Although these theoretical and experimental results were not sufficient for the present study since not all ranges of the stiffened plate variables were covered, two of the available computer programs can be used to generate the complete load-deformation relationships for stiffened plates of various geometrical configurations and material properties [54, 59].

Except for Komatsu and Smith who used the finite element method [32, 58], all other researchers used equilibrium methods in their numerical work.

In the equilibrium method, the stiffened plate is divided into a number of segments. The boundary conditions are imposed and the moment-curvature-axial force relationships are defined for every cross section of the segments. To satisfy the boundary conditions, the equilibrium equations for every cross section are solved and then a stepwise integration along the segments is performed.

Kondo used this method to compute the ultimate strength of stiffened plates under axial and lateral loading with a low b/t ratio such that the plate was not expected to buckle [34]. In his study, the length of the segments was determined from the instability criterion.

Tsuiji used the same method to compute the ultimate strength of stiffened plates with large plate slenderness (high b/t ratio) [63]. His work was continued by Vojta and Ostapenko who then developed design charts after systematically identifying and non-dimensionalizing the governing design parameters [65].

Rutledge and Ostapenko [53] then developed a method for the more general case, stiffened plates with low and high b/t ratios. A similar method was developed by Little [37]. He presented a theoretical analysis of stiffened plates covering the entire range of deformations. His results were then used to formulate a simple design approach for predicting the ultimate strength of stiffened plates under axial compression [17].

1.2.3 Grillages

There are very few studies on load-deformation behavior of grillages. Kerfoot [28] developed a method of solution for grillages subjected to combined axial and normal loads. He used a displacement formulation and a type of collocation method to solve the differential equations of large-displacement inelastic plates and beam-columns. His work was basically a general type of analysis for grillages.

Mansour [41] idealized the grillages to be a homogeneous orthotropic plate of constant thickness. The plate thickness was obtained by computing the relative rigidities of plate and stiffeners in both directions. He then performed a large deflection elastic analysis of the orthotropic plate. Although in such an approach the postbuckling behavior of the plate can be approximately taken into consideration by means of the effective width, the limit on the capacity can be set only by the occurrence of first yielding, and thus, the postultimate range cannot be analyzed.

A more expedient method to find the ultimate load of grillages was used by Parsanejad and Ostapenko [50]. He used the equilibrium method that was used for stiffened plates. He made some adjustments to the method to make it applicable to grillage analysis such as inclusion of an elastic-plastic matrix analysis for the transverse stiffeners, imposition of compatibility at the junctions between the transverse and longitudinal stiffeners, and the use of the Newton-Raphson method to solve a large matrix of simultaneous nonlinear equations. It appears that this is the only method which allows both the overall grillage and the panel modes and considers the pre- and postultimate ranges. The computer program developed for this method gave reasonably good correlation with the results of grillage tests by Smith [57] who conducted tests on full-scale welded steel grillages with dimensions typical to those used in common navy ship structures. Smith also compared his test results with the available theoretical analyses and made some design recommendations. Unfortunately, in all these tests, the panel mode rather than the grillage mode of failure was controlling.

Very few tests are available in which the ultimate load was definitely reached by the overall grillage mode. Thus, the accuracy of the computer programs has not been properly checked for this mode. The only tests which exhibited the grillage mode of failure are shown in the work by Komatsu [31] who conducted tests on grillages with stocky plates (low b/t), and thus no plate buckling.

1.3 Purpose and Scope

1.3.1 Purpose

Determination of the ultimate strength of a ship hull cross section requires knowledge of the nonlinear behavior of its component elements. Previous research conducted on such structural elements has resulted mainly in solutions for some particular cases by using complicated computer programs or in experimentally obtained load-deformation plots [4, 19, 20, 36, 46, 57]. Incorporation of these results into the analysis of ship hull girders requires detailed preparation of the data and can be used only as a research tool rather than a design procedure [6, 47, 58]. However, the use of some computer programs for the ultimate strength analysis of ship hull girders (for example, the FLEXM-program [5], [48], and [59]) could be readily made more practical for design applications if the behavior of the individual components could be described by simple algorithms.

The purpose of this study is to develop such simple algorithms in the form of analytical models for individual plates and for longitudinally stiffened plates (stiffener-plate combination). These models provide accurate, as well as, simple formulations of the load-shortening relationship in the pre- and post-ultimate ranges for various geometrical configurations and material properties.

For grillages, the emphasis of this study is on the development of a numerical method which can provide a data base for an analytical model similar to those developed for plates and stiffened plates.

The analytical models will be useful for design practice and in evaluation of the present design rules, as well as in developing new design rules for unusual types of ship hull structures. Although the thrust of this work is on the components as they are encountered in ship structures, the results will also be directly, or with some modifications, applicable to many civil engineering structures such as bridge girders and other box-shaped girders.

1.3.2 Scope

The load-deformation behavior that determines the ultimate bending capacity of a ship hull is the axial (in-plane) stress-strain relationship of the individual component elements. Nonlinearities that arise in the stress-strain relationship are due to yielding, buckling and postbuckling large deformations. Since the tensile stress-strain curve can be easily obtained once the yielding is defined (no buckling is present), only the compressive axial load-deformation relationship, which will be termed load-shortening, is considered. The stresses and strains that exist in the component elements vary in the cross section and along the span. The term load is used here for the average stress (force per unit area of the element cross section) and shortening is for the overall strain (total shortening divided by the total length of the span considered).

As defined earlier, the component elements considered in this study are plates, stiffened plates, and grillages. Plates are component elements in which the plate element is very slender compared to its stiffening frame so that buckling or partial yielding of the plate occurs before the ultimate load is reached. Stiffened plates are component elements in which the longitudinal stiffeners are relatively slender such that they buckle together with the plate, whereas grillages are the component elements with a certain rigidity such that the plate and the stiffeners in both directions (longitudinal and transverse) undergo out-of-plane deformation.

This study makes use of all the available information and develops analytical models for plates and stiffened plates. At first, all the variables required to define these analytical models are identified. These variables are then simplified by nondimensionalizing them or combining them together to obtain nondimensionalized parameters. Then, a parametric study is performed to determine the effects of these individual parameters on the behavior of the component elements. The final form of the analytical models are the stress-strain relationships given as closed-form functions of the nondimensionalized parameters. In this way, the axial behavior of the component elements can be described in a simple manner with adequate accuracy. Finally, recommendations for simple algorithms/design procedures to be used by designers and further developments of the method are made.

The analytical models developed for plates and stiffened plates are feasible due to the availability of, or the ability to generate, the required information. For grillages, such information is not available. The task of this study with regard to grillages is then to develop a numerical method of analysis for defining load-shortening relationships for the grillages which exhibit an overall grillage mode of failure. The analysis covers the ultimate and post-ultimate ranges of deformation and considers the strain reversal.

The method used is based on the solution of equilibrium and compatibility equations. To overcome the high nonlinearity occurring in the ultimate and post-ultimate ranges of deformation, several methods of solving simultaneous nonlinear equations are employed.

Chapter 2

NUMERICAL METHODS

2.1 Multi-Variable Regression Analysis

In this study the multi-variable regression analysis is the method used to obtain the formula for stresses as functions of the variable parameters for plates and stiffened plates. Like any other regression analysis, this method requires a data base, that is, the values of variables and their corresponding values of functions. The data can be in the form of continuous functions and/or a set of some scattered discrete points, even though the final result will be a continuous function valid for any values of the variables within specified domains of parameters.

2.1.1 Least Squares Regression Analysis for One Variable

The multi-variable regression analysis used here is based on the standard method of least squares which is briefly reviewed here in order to establish a basis for discussing the techniques of this study.

Given a set of values as functions H_j of an independent variable x, it is desirable to establish a continuous analytical function $\bar{H}$ of the independent variable in such a way that the discrepancy between the given values and the analytical values be the smallest possible. The continuous function is assumed to be in the form of a series.

$$\bar{H}_j = \sum_{i=1}^{m} c_i f_i(x_j) \tag{2.1}$$

where c_i are numerical coefficients, $f_i(x)$ are the selected functions of the independent variable x and m is the number of terms in the series. By minimizing the error between the given and analytical values of the function, the values of coefficients c_i can be determined as follows.

The error at a particular j-th point (i.e., $x = x_j$) is

$$e_j = \bar{H}_j - H_j \tag{2.2}$$

The sum of all squared errors is given by

$$E_r = \sum_{j=1}^{n} e_j^2 = \sum_{j=1}^{n} (\bar{H}_j - H_j)^2 \tag{2.3}$$

where $\bar{H}_j$ is the approximation of the function per Eq. (2.1) at the j-th point (i.e., for $x = x_j$), H_j is the actual value of the function at this point, and n is the total number of the given discrete points.

The error is minimized by taking derivatives with respect to coefficients c_i and setting these derivatives equal to zero.

$$\partial E_r / \partial c_i = 0 \qquad i=1,m \tag{2.4}$$

or

$$\sum_{j=1}^{m} (\bar{H}_j - H_j) f_{ji} = 0 \tag{2.5}$$

where f_{ji} is the individual function for the i-th coefficient at the j-th point. The resulting m simultaneous linear equations [Eq. (2.5)] can then be solved for the m unknown coefficients c_i.

In matrix formulation, the analytical approximation for the given set of points becomes

$$U_{(n,m)}\, C_{(m,1)} = \bar{H}_{(n,1)} \tag{2.6}$$

where $U = [f_{ji}]$ is a rectangular matrix each row of which contains the values of the individual functions of the series for a particular point, that is, for a particular value of the independent variable; $C = \{c_i\}$ is the column matrix (vector) of the unknown coefficients; and $\bar{H} = \{\bar{H}_i\}$ is the column matrix of the approximations of the function values H_i according to Eq. (2.1). Thus, the column matrix of all the errors becomes

$$e = \{e_j\} = \bar{H} - H = UC - H \tag{2.7}$$

The sum of the squared errors [Eq. (2.3)] is then given by

$$E_r = e^T e = [UC - H]^T [UC - H] \tag{2.8}$$

or

$$E_r = C^T U^T UC - H^T UC - C^T U^T H + H^T H \tag{2.9}$$

Since $C^T U^T H = H^T UC$, Eq. (2.9) becomes

$$E_r = C^T U^T UC - 2CU^T H + H^T H \tag{2.10}$$

The derivative of E_r with respect to vector $\{c_i\}$, set equal to a zero column matrix, becomes

$$[U^TU]C + C^T[U^TU] - 2\{U^TH\} = \{0\} \tag{2.11}$$

Furthermore, since $[U^TU]C = C^T[U^TU]$, Eq. (2.11) is simplified to

$$U^TUC - U^TH = \{0\} \tag{2.12}$$

which is equivalent to Eq. (2.5). In a more compact form, Eq. (2.12) is given by

$$V\{C\} = Q \tag{2.13}$$

where

$$V = U^TU$$

$$\text{and} \tag{2.14}$$

$$Q = U^TH$$

The unknown coefficients $\{c_i\}$ can then be found by solving the simultaneous linear equations of Eq. (2.13), and the final analytical approximation is given by Eq. (2.1) which is repeated here in a slightly different form

$$\bar{H} = \sum_{j=1}^{m} c_j f_j = \{c_i\}^T[f_1 \; f_2 \ldots f_m]^T = C^T[f_1 \; f_2 \ldots f_m]^T \tag{2.15}$$

2.1.2 Coordinate Functions for Multi-Variable Regression

When there are more than one independent variables, it is often advantageous (as is the case in this study) to establish the effect of just one variable (say, the k-th variable) while all other variables are kept constant. The assembly of the h_{kj} terms of the series for this k-th variable is called the coordinate function F_k and the individual terms are selected to make a close approximation of this function to the given data points for various sets of the other variables. The aim of this step is to have as few terms as possible for an acceptable fit. The thus established coordinate function F_k for the k-th variable will contain m_k terms.

$$F_k = [h_{k1} \; h_{k2} \; \cdots \; h_{km_k}] \qquad (2.16)$$

With a coordinate function established for each variable, the terms of the final series shown in Eq. (2.15) will contain products of the terms of the individual coordinate functions. In other words, the final coordinate function will be obtained as a direct product*

$$\begin{aligned} F &= [f_1 \; f_2 \; \cdots \; f_m] = \mathrm{dir}(F_1 F_2 \ldots F_k) \\ &= [(h_{11} h_{21} \ldots h_{k1}) \; (h_{12} h_{22} \ldots h_{k2}) \ldots (h_{1m_k} h_{2m_k} \ldots h_{km_k})] \qquad (2.17) \end{aligned}$$

*The term direct product will be used here for the apparent lack of an established designation for this operation. It will be indicated by $\mathrm{dir}(F_1 F_2 \ldots F_k)$

This way, a change in the coordinate function of a particular variable will not affect the coordinate functions of the other variables. The solution of the simultaneous linear equations remains the same as given by Eq. (2.13).

An illustration of obtaining Eq. (2.17) for the case of two variables, x_1 and x_2 is shown next. Assuming the coordinate functions have, say, $m_1 = 2$ and $m_2 = 3$ terms, respectively, they are,

$$F_1 = [h_{11} \quad h_{12}], \qquad \text{say,} \quad F_1 = [x_1 \quad x_1^2] \tag{2.18}$$

$$F_2 = [h_{21} \quad h_{22} \; h_{23}], \qquad \text{say,} \; F_2 = [x_2 \quad 1 \quad x_2^3] \tag{2.19}$$

The expanded function F becomes a matrix containing the products of the terms of these individual coordinate functions with the total number of terms m = 2x3 = 6.

$$\begin{aligned} F &= \text{dir}(F_1 F_2) \\ &= [h_{11}h_{21} \quad h_{12}h_{21} \quad h_{11}h_{22}h_{12}h_{22} \quad h_{11}h_{23} \quad h_{12}h_{23}] \\ &= [x_1x_2 \quad x_1^2x_2 \quad x_1 \quad x_1^2 \quad x_1x_2^3 \quad x_1^2x_2^3] \end{aligned} \tag{2.20}$$

If there is also a third variable with, say, $m_3 = 2$, then the number of terms in the F function will be

$$m = (m_1{=}2)(m_2{=}3)(m_3{=}2) = 12 \tag{2.21}$$

For a discrete point, the expanded function of Eq. (2.20) gives one row of matrix U of Eq. (2.6). The number of rows of U, n (which is also the number of points) must be at least equal to the number of columns, m, in order to have a solution of Eq. (2.13) for the unknown coefficients $C = \{c_i\}$.

2.1.3 Reduction of Coefficient Matrix C

If, after the solution for coefficients $\{c_i\}$ is obtained for a multi-variable problem of Eq. (2.17), it becomes desirable to fix the value of the j-th variable, the number of terms of the expanded function will be reduced from m to

$$m' = m/m_j \tag{2.22}$$

where m_j is the number of terms of the coordinate function for the variable whose value is preset.

If, for example, the $\{c_i\}$ coefficients found for the expanded function of Eq. (2.20) are to be reduced by presetting the second variable x_2, its coordinate function being given by Eq. (2.19), the reduced coefficients for the remaining variable x_1 and for its coordinate function of Eq. (2.18) become:

$$C' = \begin{bmatrix} c_1' \\ \\ c_2' \end{bmatrix} = \begin{bmatrix} c_1h_{21}+c_3h_{22}+c_5h_{23} \\ \\ c_2h_{21}+c_4h_{22}+c_6h_{23} \end{bmatrix} \tag{2.23}$$

The final formulation, as a function of x_1, is then:

$$\bar{H} = [c_1' \quad c_2'] \, [h_{11} \quad h_{12}]^T = [c_1' \quad c_2'] \, [x_1 \quad x_1{}^2]^T \qquad (2.24)$$

When there are more variables, the reduction of the general coefficient matrix $\{c_i\}$ for some preset variables is accomplished one-by-one in a similar manner and in any order.

The procedure described above has been found to be very efficient in studying the effects of individual variables and of the composition of their coordinate functions, on the accuracy of the function approximation.

Another application of the reduction concept is for the actual use of the final coefficients when the approximated function is to be given in terms of a single variable (in this study, the stress as a function of the strain) while all other variables are kept constant. Let, for example, consider a function of three variables A, B and e. Then, if the expanded function F is a direct product* of coordinate functions F_A, F_B and F_e

$$F = \mathrm{dir}(F_A F_B F_e) \qquad (2.25)$$

and the approximation function is

$$\bar{H} = C^T F^T \qquad (2.26)$$

*See Footnote on page 21

then $\bar{H}$ can be given as a function of F_e only. For this, the direct product of F_A and F_B is precomputed

$$F_{AB} = dir(F_A F_B) \tag{2.27}$$

and the $\{C\}$ column matrix is rearranged into a rectangular matrix $[C']$ analogous to the C' matrix in Eq. (2.23). Then,

$$\bar{H} = [[C]\ [F_{AB}]^T]^T[F_e]^T = [C'][F_e]^T \tag{2.28}$$

2.2 Numerical Methods for Nonlinear Problems

The multi-variable regression analysis as explained above can be used only if there are data points available from tests and/or previous analysis. This is the case for plates and stiffened plates. When this necessary information does not exist, as is the case for grillages, an analysis to provide such information must be performed. All common methods of structural analysis are based on fulfilling the equilibrium and compatibility requirements. In the linear range the analysis can be performed by using any familiar standard type of solution. However, in the post-buckling and post-ultimate ranges, the relationship between forces and deformations is nonlinear, and some method of solution for nonlinear problems must be used.

2.2.1 Linearization by Using Intersection of Several Hyperplanes

The method given here is an extension of the successful method to obtain a solution for nonlinear functions of two variables by using an intersection of two planes [48]. For functions of more than two variables, the solution is extended to an intersection of several hyperplanes. For illustrative purposes, the solution for the two-dimensional case is reviewed first.

Two relationships are expressed by two different functions of two variables X1 and X2

$$Y1 = Y1(X1,X2) \tag{2.29}$$

$$Y2 = Y2(X1,X2) \tag{2.30}$$

The solution of this problem is to find X1 and X2 such that both Y1 and Y2 become zero.

Graphically, these functions can be depicted in a three dimensional Cartesian coordinate system as the two surfaces shown in the top sketch of Fig. 2. The solution then becomes the point where the intersection line of these two surfaces, Y1(X1,X2) and Y2(X1,X2), passes through the X1-X2 plane (plane of zero Y). In order to linearize the probable solution, these two surfaces are approximated by two planes shown in the bottom sketch of Fig. 2.

Three points lying on the corresponding surfaces are required to define each plane. The three points on each surface are defined by Eqs. (2.29) and (2.30) for three* different sets of X1 and X2.

$$
\begin{array}{ll}
\text{Plane for Y1} & \text{Plane for Y2} \\
(X1_1, X2_1, Y1_1) & (X1_1, X2_1, Y2_1) \\
(X1_2, X2_2, Y1_2) & (X1_2, X2_2, Y2_2) \\
(X1_3, X2_3, Y1_3) & (X1_3, X2_3, Y2_3)
\end{array}
\tag{2.31}
$$

The equation of a plane passing through 3 points is

$$
\begin{aligned}
Y_1 &= D_0 + D_1 X1_1 + D_2 X2_1 \\
Y_2 &= D_0 + D_1 X1_2 + D_2 X2_2 \\
Y_3 &= D_0 + D_1 X1_3 + D_2 X2_3
\end{aligned}
\tag{2.32}
$$

or

$$
Y = D_0 + D_1 X1 + D_2 X2 \tag{2.33}
$$

where D_0, D_1, and D_2 are obtained by solving Eq. (2.32). To find the values of X1 and X2 which give zero values of Y for both planes, two solutions of Eq. (2.32) are required to define two different equations of Eq. (2.33) for planes Y1 and Y2 as given by Eq. (2.31). By setting Y = 0 , the two equations become

---

*In the method developed for the solution of the two-dimensional case [48], each surface may be defined by different sets of points, thus a maximum of six sets of X1 and X2 are possible. For coherence with other methods which will be subsequently discussed, in this study all the planes use the same set of points, that is, three points for the two-dimensional problem or, generally, n+1 points for an n-dimensional problem.

$$D1_0 + D1_1 X1 + D1_2 X2 = 0 \tag{2.34}$$

$$D2_0 + D2_1 X1 + D2_2 X2 = 0 \tag{2.35}$$

where $D1_0$ is the D_0-value for $Y_1 = Y1_1$, $Y_2 = Y1_2$ and $Y_3 = Y1_3$, and $D2_0$ is the D_0 value for $Y_1 = Y2_1$, $Y_2 = Y2_2$ and $Y_3 = Y2_3$... etc.

Solution of these equations results in a new set of X1 and X2, say, $X1_4$ and $X2_4$ with their corresponding values of the surface functions of $Y1_4$ and $Y2_4$. The above procedure is repeated by replacing the set of X1 and X2 having the largest absolute value of Y1 or Y2 with the new set of X1 and X2 until the desired solution is obtained, that is, when the resulting Y1 and Y2 become zero or close to zero within a specified tolerance.

For the solution of n nonlinear simultaneous equations, the method cannot be illustrated graphically. However, the formulas used can be extended from 2 variables to n variables. Then, Equations (2.29) and (2.30) become

$$\begin{aligned} Y1 &= Y1(X1, X2, \ldots, Xn) \\ Y2 &= Y2(X1, X2, \ldots, Xn) \\ &\ldots \\ Yn &= Yn(X1, X2, \ldots, Xn) \end{aligned} \tag{2.36}$$

Equation (2.31) becomes

$$
\begin{array}{lcl}
\text{Hyperplane for } Y1 & \ldots & \text{Hyperplane for } Yn \\
(X1_1,\ X2_1,\ \ldots,\ Y1_1) & \ldots & (X1_1,\ \ldots,\ Xn_1,\ Yn_1) \\
(X1_2,\ X2_2,\ \ldots,\ Y1_2) & \ldots & (X1_2,\ \ldots,\ Xn_2,\ Yn_2) \\
\ldots & & \\
(X1_{n+1}, X2_{n+1}, \ldots,\ Y1_{n+1}) & \ldots & (X1_{n+1},\ \ldots, Xn_{n+1},\ Yn_{n+1})
\end{array}
\tag{2.37}
$$

Equation (2.32) becomes

$$
\begin{aligned}
Y_1 &= D_0 + D_1X1_1 + D_2X2_1 + \ldots + D_nXn_1 \\
Y_2 &= D_0 + D_1X1_2 + D_2X2_2 + \ldots + D_nXn_2 \\
&\ldots \\
Y_n &= D_0 + D_1X1_n + D_2X2_n + \ldots + D_nXn_n
\end{aligned}
\tag{2.38}
$$

Equation (2.33) becomes

$$
Y = D_0 + D_1X1 + D_2X2 \ldots + D_nXn \tag{2.39}
$$

Equations (2.34) and (2.35) become

$$
\begin{aligned}
&D1_0 + D1_1X1 + \ldots D1_nXn = 0 \\
&D2_0 + D2_1X1 + \ldots D2_nXn = 0 \\
&\ldots \\
&Dn_0 + Dn_1X1 + \ldots Dn_nXn = 0
\end{aligned}
\tag{2.40}
$$

Then, the same procedure, as described for the two planes, can be used to obtain $\{X1_{n+2}, X2_{n+2}, \ldots, Xn_{n+2}\}$ and to perform the iteration until the largest absolute value of the resulting $\{Y1, Y2, \ldots, Yn\}$ is considered sufficiently small.

2.2.2 The Secant Method

The linearization method using the intersection of several hyperplanes has been proven to be very effective. It does not only give a visual illustration of the solution but also predicts the feasibility of the solution. For example, the problem cannot be solved when one of the hyperplanes cannot be defined since it is parallel to the Y axis, or when two of the hyperplanes are parallel to each other. All of these cases can be detected as the coefficient matrix of Eq. (2.40) becomes zero or if Eq. (2.32) cannot be solved. The complete list of such ill-conditions for $n = 2$ is presented in [48].

The linearization method using the intersection of several hyperplanes, however, requires lengthy computations, and a simplified version of it is used here. This version is usually called the secant method. The algorithm for the one-dimensional secant method is presented in [26, 34] and extended to the multi-dimensional case in [68]. The secant method does not have the ability to detect some of the ill-conditions mentioned above, for example, it still gives a solution although it is incorrect, since one of the hyperplanes is parallel to the Y axis.

To overcome this problem, an additional step which detects this particular ill-conditioning is introduced. First, consider the subspace X1-X2-...-Xn which is obtained by eliminating the Y axis (see Fig. 3 for the two- and three-dimensional cases). For the two-dimensional case this type of ill-conditioning occurs when the three trial points are colinear in the subspace X1-X2, whereas for the three-dimensional case, the four trial points are coplanar in the subspace X1-X2-X3. For a general case, the n+1 trial points are in the same "sub-hyperplane" (this would be a line for n = 2 and a plane for n = 3). Mathematically this can be verified by first isolating a point from the n+1 trial points. Then, a vector in the subspace which is normal to the "sub-hyperplane" passing through the remaining points is determined. A second vector, which passes through the isolated point and one of the remaining points, is also determined. If all of the n+1 trial points are on the same "sub-hyperplane", then the two vectors are orthogonal. For n = 2 this case will not only cause one of the hyperplanes to be parallel to the Y-axis but also all of them to be identical.

Coefficients D computed from Eq. (2.40) are no longer required. A vector of coefficients $c = \{c_1, c_2 \ldots, c_{n+1}\}$ is used instead. These coefficients are obtained by solving the following simultaneous equations

$$
\begin{aligned}
c_1 + c_2 + \dots + c_{n+1} &= 1.0 \\
Y1_1 c_1 + Y1_2 c_2 + \dots + Y1_{n+1} c_{n+1} &= 0.0 \\
Y2_1 c_1 + Y2_2 c_2 + \dots + Y2_{n+1} c_{n+1} &= 0.0 \\
\dots & \\
YN_1 c_1 + YN_2 c_2 + \dots + YN_{n+1} c_{n+1} &= 0.0
\end{aligned} \tag{2.41}
$$

The new values of the trial points are

$$
\begin{aligned}
X1_{n+2} &= c_1 X1_1 + c_2 X1_2 + \dots + c_{n+1} X1_{n+1} \\
X2_{n+2} &= c_1 X2_1 + c_2 X2_2 + \dots + c_{n+1} X1_{n+1} \\
\dots & \\
XN_{n+2} &= c_1 XN_1 + c_2 XN_2 + \dots + c_{n+1} XN_{n+1}
\end{aligned} \tag{2.42}
$$

The next step of iteration is identical with the previous method.

2.2.3 Error Minimization by Using A Flexible Polyhedron

The method of linearization discussed above can be used successfully if the equations are moderately nonlinear. The criterion for the degree of the nonlinearity is generally unclear. In this study, however, the value of Y is used to judge the degree of the nonlinearity. If the largest of the new absolute Y values obtained from Eq. (2.36), as functions of variables X obtained from the solution of Eq. (2.40), is larger than the largest of the previous absolute Y values listed in Eq. (2.37), then the iteration may not result in the minimization of the error Y. This implies that the equations are highly nonlinear and the secant method cannot achieve convergence. Another method, which will forcibly reduce the largest error Y, is presented next.

This method is known as the Flexible Polyhedron search [22] since it is one of the search methods used in optimization for objective functions with no derivatives or the functions in which the derivatives are difficult to obtain [1, 22, 66]. This method can also be used for error minimization (minimization of Y). In the optimization, however, the problem is to find the values of X which result in the minimization of the objective function and to find the minimized objective function Y. This means that there is an additional algorithm which verifies the optimality of the objective function Y. The search is then terminated when the value of Y is found to be a minimum. The latter algorithm is not required in the error minimization since the optimum is already known, that is, a zero error. The search or iteration can be terminated when the objective function Y, the largest absolute value of Y's in Eq. (2.36), is zero or close to zero within a specified tolerance.

In the polyhedron search method, the same n+1 trial points are used and their coordinates are defined in the subspace n. The Y-axis needs not be drawn since the function (error) values are used for comparative purposes only. For the two-dimensional case, contour lines (if known) for these values can be drawn on the X1-X2 plane (see Fig. 5). These n+1 points constitute vertices of a polyhedron (triangle for n = 2 and tetrahedron for n = 3) where the objective function for each of these vertices is

$$Y_i = \max \{|Y1_i|, |Y2_i|, \ldots, |Yn_i|\} \tag{2.43}$$

where Y_i is the largest absolute value of the functions at point i expressed by Eq. (2.36). Y_i will henceforth be referred to as the objective function of point i. As is the case for the previous method, the next step is to find point k with the largest objective function.

$$Y_k = \max \{Y_1, Y_2, \ldots\ldots Y_{n+1}\} \tag{2.44}$$

Then, the centroid of the vertices of the polyhedron is determined to compute the magnitude and direction of the search vector. Figure 4 shows the polyhedron with its search vector. These two steps can be formulated by

$$DXj = \left[\left(\sum_{i=1}^{n+1} Xj_i\right) - Xj_k\right]/n \quad i \neq k, \quad j=1, \ldots, n \tag{2.45}$$

where $\{DX1, DX2, \ldots, DXn\}$ is the directional search vector. The new point is defined by

$$Xj_{n+2} = Xj_k + C_r DXj \quad j=1,2,\ldots,n \tag{2.46}$$

where C_r is the reflection coefficient $0 < C_r < 1$ [1, 22]. This point becomes the new vertex of the polyhedron replacing the k-th point. This polyhedron is updated several times by repeating the above procedure until the objective function is small enough, and the search is terminated. In this study, C_r is taken to be 0.6 and one iteration cycle starts with Eq. (2.43) and ends with Eq. (2.46). Equation (2.46) is applied several times, before proceeding to the next iteration cycle, until the new Y_{n+2} defined by Eq. (2.46) does not become smaller than the previous one. However, this repetition must be limited so as to allow for adjustment of the magnitude and direction of the search vector and for maintaining the shape of the polyhedron. An example for the error minimization in a two dimensional case is shown in Fig. 5, where the vertices of each triangle represent the trial points for a particular cycle of iteration.

Two separate computer subroutines which perform the operations of the secant and flexible polyhedron methods were written and incorporated into the computer program for grillage analysis. The flexible polyhedron method is used only when the equations are highly nonlinear. In many cases, the equations are only slightly nonlinear and the secant method is sufficient to provide a fast converging solution.

Chapter 3

PLATE

3.1 Method Used

Many methods of analysis have been employed to define the load-shortening relationship for rectangular plates with various geometrical configurations and material properties. Large computer programs were used for these methods, and the resultant load-shortening relationships depended on the assumptions and the method used. Some of these results, together with test results have been given in tabulated or graphical form and they provided sufficient data for the multi-variable regression analysis.

3.2 Background and Assumptions

Previous work has shown that the load-shortening behavior of rectangular plates is affected by the following factors:

- boundary conditions
- plate length a
- plate width b
- plate thickness t
- properties of material (principally, modulus of elasticity E and yield stress S_y)

- initial imperfections (maximum initial deflection W_o)

- residual stresses (mainly, the compressive residual stress S_{rc} due to welding)

Since some of these factors, such as the boundary conditions, are not known or cannot be readily measured in actual structures, it was necessary to make suitable assumptions to approximate the actual conditions.

3.2.1 Boundary Conditions at Unloaded Edges

A. Rotational restraint

The degree of rotational restraint for the unloaded edges of real plates is intermediate between fixed and simply supported. In most of the previous research, the unloaded edges had been assumed to be simply supported [11, 12, 13, 20, 38]. This is a conservative assumption for real plates. However, results from experiments show that full rotational restraint increases the ultimate strength by only about 10% [43, 60]. Therefore, a modification to compensate for the additional restraint of intermediate cases in comparison with simple supports is not warranted.

B. In-plane restraint

The in-plane deformation of the unloaded edges can be either restrained or unrestrained. The increase of the ultimate capacity of the plates due to the restraint depends on the slenderness and initial imperfections. For stocky plates (low b/t ratio), the effect is significant in plates with small initial imperfections. This has been observed in plates with no initial imperfections [11] or small initial imperfections [21] in which the increase was about 10%. As the initial imperfections increase, the effect becomes less significant [20]. For slender plates, on the other hand, the strengthening effect of the in-plane restraint increases as the initial imperfections increase. For small and large imperfections, the strengthening effect is between 5 and 15%.

This complex relationship can be explained as follows. In stocky plates with small initial imperfections, the edge restraint causes compressive stresses at the unloaded edges. This results in biaxial compressive stresses which reduce the equivalent stress and hence delay the onset of yielding. As the initial imperfections increase, the compressive stresses at the unloaded edges decrease and, thus, reduce the strengthening effect. As the slenderness increases, the strengthening effect is also reduced. This occurs because the compressive stresses at the unloaded edges due to the restraint reduce the buckling stress. For slender plates with large initial imperfections, the edge restraint induces tensile stresses at the unloaded edges which restrain the out-of-plane deformation and lead to an increase of the ultimate strength.

For the plates considered, the initial imperfections are of average magnitude. In this case, the strengthening effect is expected to be less than 7%. Since in steel plated structures, the adjacent plates and the stiffeners between them force the edges of the plates to remain straight, it is reasonable to assume the unloaded edges to be simply supported rotationally and free to move in plane but to remain straight [11, 39, 60]. Such, so-called constrained, edges behave somewhere between restrained and unrestrained edges. The difference in the behavior between the plates with restrained and constrained edges and having initial imperfections is smaller than the values quoted above, and therefore, may be neglected.

3.2.2 Boundary Conditions at Loaded Edges

For the loaded edges, rotational restraint increases the stiffness of the plate mainly by increasing the buckling stress. The effect decreases as the plate becomes longer [61]. Likewise, the effect becomes less significant as the plate becomes stockier. The rotational restraint does not significantly change the ultimate strength of the plate; moreover, in real situations the degree of restraint is intermediate between fixed and simply supported. Therefore, it is commonly and conservatively accepted that the loaded edges may be modelled to be simply supported without any important loss of accuracy [42, 60].

3.3 Parameters and the Coordinate Functions

After the boundary conditions are set, the remaining variables (sometimes referred to as practical parameters [39]) become the governing parameters. Once these variables are known, the load-shortening relationship can be defined.

In order to have more flexibility in formulating the load-shortening relationship, it is desirable to define it in a non-dimensional form. The load is expressed by the nondimensional stress $s = S/S_y$ and the shortening is expressed by the nondimensionalized strain $e = \epsilon/\epsilon_y$. According to Little, two plates of the same type (having the same boundary conditions) will have the same nondimensionalized load-shortening relationship if the values of the following nondimensionalized parameters are he same [39]:

- Aspect ratio

$$A=a/b \tag{3.1}$$

- Slenderness ratio

$$B=0.526(a/t)\sqrt{S_y/E} \qquad \text{for wide plates } (a/b\leq 1) \tag{3.2}$$

or

$$B=0.526(b/t)\sqrt{S_y/E} \qquad \text{for long plates } (a/b>1) \tag{3.3}$$

where $0.526=\sqrt{3(1-u^2)}/\pi$ in which $u=0.3$ is the Poisson's ratio

- Initial imperfection

$$w_o = W_o/t \tag{3.4}$$

- Residual stress

$$S_r = S_{rc}/S_y \tag{3.5}$$

The magnitudes of the initial imperfections and residual stresses, however, are beyond control of the designer as they depend on the fabrication and construction procedure (e.g., welding procedure for welded plates). It is then necessary to set the values of initial imperfections and residual stresses to practical levels which are typical for ship structures. With the imperfection and residual stress preset, the load-shortening relationship is defined only by the aspect ratio A, slenderness ratio B, and the relative strain e.

To establish the functional relationship among these variables, a multi-variable regression analysis is performed and coordinate functions for these independent variables are selected. The objective for a particular variable is to determine a coordinate function containing the smallest number of terms yet giving adequately accurate values of the stress while all other variables are kept constant. A series of trials were performed using all available theoretical and experimental results and the following coordinate functions were selected.

3.3.1 Effect of Initial Imperfections w_o

Initial imperfections generally decrease the stiffness and the ultimate strength of rectangular plates [9, 13, 20, 39] and the shape of initial imperfections is usually assumed to be the same as for the buckling mode [13, 15, 42, 54, 60]. This reducing effect can be seen in the example shown in Fig. 8, in which the relative stress is given as a function of w_o for constant values of e, A, B and S_r. The available data points are shown by the small circles, triangles and rectangles whereas the curves approximate the relationship for particular values of e.

The functional relationship of relative stress, s, and w_o can be suitably represented by the following expression:

$$s = c_{w1}/(1+\sqrt{w_o}) + c_{w2}/(1+\sqrt{w_o})^2 \tag{3.6}$$

where c_{w1} and c_{w2} are coefficients which are functions of A, B, S_r, and e. Since the initial imperfection is beyond control of the designer, the use of w_o as one of the variable parameters has no practical meaning. Therefore, it is desirable to set w_o to a constant value which has been observed to be a common average value [12]. Such average values observed in practical design have been proposed for use in analysis [11, 12, 13, 60]. Also, since initial imperfections have been found to be related to b/t [11] or, more commonly, to B^2 [12, 13, 20, 59], the following average value is selected for this study:

$$w_o = 0.542\ B^2 \tag{3.7}$$

Then, the coordinate function $[1/(1+\sqrt{w_o})\ \ 1/(1+\sqrt{w_o})^2]$ becomes a matrix of constants and the coefficients C of Eq. (2.26) are included as described by Eqs. (2.23) and (2.24).

3.3.2 Effect of Residual Stresses S_r

Residual stresses have a detrimental effect on the stiffness and strength of rectangular plates [9, 20, 39]. The effect is most significant in the pre-ultimate range. An idealized but typical distribution of residual stresses across the plate width due to welding is shown in Fig. 7. The magnitude of the tensile residual stress, S_{rt}, is approximately equal to the yield stress, S_y. The width of the tensile residual stress determines the magnitude of the compressive residual stress in the middle portion since the stresses must be in equilibrium. The compressive residual stress S_{rc} in its nondimensional form, S_r, is then

$$S_r = 2nt/(b-2nt) \tag{3.8}$$

where nt is the width of the tensile residual stress at the edge of the plate. As in the case for initial imperfections, residual stress S_r is also beyond the designer's control. It was desirable therefore to set S_r or n to a value which corresponds to an average value. First, the residual stress was included as a variable where its effect was expressed by a coordinate function in form of a parabola. The suitability of the parabola is illustrated in Fig. 9:

$$s = c_{r1} + c_{r2}S_r + c_{r3}S_r^2 \tag{3.9}$$

where c_{r1}, c_{r2} and c_{r3} are coefficients which are functions of A, B, and e (after w_o is fixed). Then, the value of S_r was fixed by using an average value of n. Commonly, the value of n is between 3 and 4.5 [60], and the following formula was adopted to give the average values of the compressive residual stress for the plate model of this study:

$$S_r = 6/(48B-6). \tag{3.10}$$

The values given by this equation correspond to n=3.5 in Eq. (3.8) and are close to the values used in Ref. [12]. The process of setting the value of the residual stress to a fixed constant was performed in the same manner as for the initial imperfection w_o.

3.3.3 Effect of Aspect Ratio A

The aspect ratio affects the stiffness as well as the ultimate strength of rectangular plates. For wide plates, $A \leq 1.0$, the effect of the aspect ratio is very significant so that in some cases the plate stiffness is affected more strongly by the aspect ratio than by initial imperfections [39]. As A decreases from unity, the plate behaves more-and-more like a column as its axial behavior is less-and-less affected by the unloaded edges.

A parametric study [20] has shown that a curve of the relative peak stress vs. aspect ratio exhibited a parabolic relationship. To include this into consideration, a quadratic polynomial was chosen for the coordinate function. Then, for a given set of B and e, the stress became a function of A.

$$s = c_{a1} + c_{a2}A + c_{a3}A^2 \tag{3.11}$$

where c_{a1}, c_{a2}, and c_{a3} are the coefficients which are functions of B and e only. Figure 10 shows the functional effect of A for constant values of w_o, S_r, B and e.

For long plates, $A > 1.0$, the post-ultimate behavior is similar to the behavior of square plates and it has been suggested that the load-shortening behavior of square plates be used [12, 20, 57, 60].

Thus, the model for wide and long plates is simplified to the consideration of wide plates only ($A \leq 1.0$).

3.3.4 Effect of Slenderness Ratio B

The effect of slenderness ratio was approximated by a two term reciprocal polynomial of B.

$$s = c_{b1}(1/B) + c_{b2}(1/B^2) \tag{3.12}$$

where c_{b1} and c_{b2} are coefficients which are functions of A and e (see Fig. 11). This expression is similar to the formula for ultimate strength for plates used and recommended by many researchers [8, 17, 18, 63, 67] who used the terms $(1/B)$ and $(1/B)^2$.

3.3.5 Effect of Relative Strain e

For the strain range considered ($0.0 \leq \epsilon \leq 3.0\epsilon_y$), three different load-shortening curves were needed. For small strains, the load-shortening curve was taken to be linear. When the stress approaches the buckling and/or plastic range, the curve starts deviating from the straight line, and the load-shortening curve was approximated by a four term series with two separate ranges.

The resultant nondimensional stress-strain relationship is given by Eqs. (3.14) to (3.18) shown below in two ranges: (a) $e \leq 1.0$ and (b) $e > 1.0$. Coefficients d_1 to d_4 in these equations are functions of the aspect ratio A and the slenderness ratio B, as defined by Eq. (3.19). The procedure of using these equations and their limits is illustrated in Fig. 12.

a) for $e<1.0$:

For $e \le e_o$, where e_o is obtained from

$$e_o = (0.223\ AB)/(1+0.285B) \tag{3.13}$$

the relationship is a straight line

$$s = d_o e \tag{3.14}$$

where constant d_o is given by

$$d_o = d_1 + d_2/(1+0.5e_o^{\,3}) + d_3/(1+0.3e_o^{\,2}) + d_4/(1+3e_o) \tag{3.15}$$

but it should not exceed 1.0,

$$d_o \le 1.0 \tag{3.16}$$

For $e>e_o$, use Eq. (3.14) or

$$s = d_1 e + d_2 e/(1+0.5e^3) + d_3 e/(1+0.3e^2) + d_4 e/(1+3e) \tag{3.17}$$

whichever results in a smaller value of s.

b) for $e>1.0$:

$$s = d_1 e^{e^{-10}} + d_2 e/(1+0.5e^3) + d_3 e/(1+0.3e^2) + d_4 e/(1+3e) \tag{3.18}$$

Coefficients d_1, d_2, d_3 and d_4 for Eqs. (3.15), (3.17) and (3.18) are functions of A and B as given by Eq. (3.19)

$$
\begin{bmatrix} d_1 \\ d_2 \\ d_3 \\ d_4 \end{bmatrix} = C_p \begin{bmatrix} 1/B \\ A/B \\ A^2/B \\ 1/B^2 \\ A/B^2 \\ (A/B)^2 \end{bmatrix} \tag{3.19}
$$

This procedure is an application of the operations described by Eqs. (2.23) to (2.28).

3.4 Limitations

As mentioned above, initial imperfections and residual stresses are beyond the control of the designer. In this study these variables are set to typical values which are encountered in ship structures as given by Eqs. (3.7) and (3.10). Provided that deviations of these variables from the average values are within ordinary ranges, the error in the proposed model should be less than 10%.

The ranges of the remaining variables, A and B, are specified as typical for ship structure plating.

- $0.3 \leq A \leq 1.0$; for long plates, $A=1.0$
- $0.526 \leq B \leq 1.85$; this means, for example, for $S_y=350$ MPa (50 ksi), $24 \leq (a/t \text{ or } b/t) \leq 110$

The range of the relative shortening, e, is limited to the values that have practical usefulness.

- $0.0 \leq e \leq 3.0$

Further discussion about these limitations and examples of the application of the formulas are presented in Chapter 6.

Chapter 4

STIFFENED PLATE

4.1 Method Used

Unlike the case for rectangular plates, there are only some theoretical and experimental results available for stiffened plates. Thus, in order to be able to use the multi-variable regression analysis for developing an analytical model, additional data had to be provided by a modified version of an available computer program [58].

There are more variables involved in the model for stiffened plates than for simple plates, since the material and geometrical properties of the stiffener must be also included as additional parameters. To make the multi-variable regression analysis easier, some simplifying assumptions were necessary.

4.2 Background and Assumptions

The load-shortening behavior of a plate reinforced with transverse and longitudinal stiffeners (a grillage) is much more complicated than the behavior of a single plate since it is affected by some additional modes of failure. The principal modes of failure of such stiffened plates under axial loads are the flexural and tripping failure between the transverses and the overall grillage failure. The occurrence of one or the other mode is controlled by the particular combination of the geometrical and material properties. When the transverses are adequately strong, the overall grillage mode of failure indicated in Fig. 13 will be inhibited. The tripping mode does not occur when the longitudinals have sufficient torsional rigidity. Then, the flexural mode between the transverses becomes the controlling one and it is shown in Fig 14. The load-shortening behavior which leads to the flexural mode of failure which will be referred to as load-shortening of the stiffened plate, is considered in this chapter. The load-shortening behavior which exhibits the overall grillage mode of failure will be discussed in the next chapter whereas the tripping mode of failure is beyond the scope of this study and will not be considered.

In the stiffened plate model, the longitudinals are continuous over the transverses and their axial behavior can be approximately represented by the response of a single beam column consisting of a longitudinal stiffener and a plate of the width equal to the spacing of the longitudinals (see Figs. 1, 14 and 15). The following parameters influence the load shortening behavior of longitudinally stiffened plates:

- Dimensions and material properties of plate (b, t, E and S_y)

  Dimensions and material properties of stiffeners (b_w, t_w, S_{yw}, E_w, b_f, t_f, S_{yf} and E_f)

- Panel length (a)

- Initial imperfections (w_0 for plate, w_{0s} for stiffener)

- Residual stresses (S_r)

- Boundary conditions

Previous studies have shown that individual parameters have different effects on the behavior of stiffened plates. For example, the slenderness ratio of the plate and the slenderness of the stiffened plate affect the behavior of stiffened plates significantly whereas the ratio of the area of the stiffener to the area of the plate and the ratio of the area of the flange to the area of the total stiffener were found to have only moderate effect [16, 41, 60]. Residual stresses in the plate tend to reduce the plate strength although this reduction becomes less important for large slenderness ratios of stiffened plates. Initial imperfections of the stiffener also have a reducing effect. Generally, the deflected shapes of two adjacent panels are opposite to each other, and one is larger than the other as shown in Fig. 14. The maximum amplitude of initial imperfection of the stiffener in ship structures has been found to be directly related to the panel length [57, 60, 65].

Not all of the above listed parameters are under the control of a designer and thus, some values have to be assumed on the basis of observations and parametrical studies. Specifically, this applies to the values of residual stresses and initial imperfections which subsequently have to be incorporated into the analytical model. The following conditions are assumed:

1. Residual stresses for the plate are the same as the average value used for the plate element model.

2. The shape of the initial deformation of the stiffener is as shown in Fig. 14 with the magnitude of the maximum initial deformation set to be [60]

$$W_{os} = 0.0015a = w_{os}a \tag{4.1}$$

Experimental and computed data taken from literature were adjusted by inter- or extrapolation to conform to these assumptions.

4.3 Parameters and the Coordinate Functions

4.3.1 Nondimensional Parameters

After setting the residual stresses and initial imperfections to be constant, the remaining parameters can be combined in order to simplify the parametric study of stiffened plates. The following nondimensional functional parameters are used in the study:

- Slenderness ratio of plate B [Plate slenderness, the same as Eq. (3.3)],

$$B = 0.526\ (b/t)\sqrt{S_y/E} \tag{4.2}$$

- Slenderness ratio of stiffened plate L (Panel slenderness),

$$L = (1/\pi)(a/r)\sqrt{\epsilon_y} \tag{4.3}$$

where r is the radius of gyration of the stiffened plate (cross section of the beam-column) with respect to its centroidal axis parallel to the plate and ϵ_y is the weighted average yield strain

- Effective stiffener-to-plate area ratio R,

$$R = (A_f S_{yf} + A_w S_{yw})/(btS_y) \tag{4.4}$$

where $A_f = b_f t_f$ and $A_w = b_w t_w$

- Effective flange-to-stiffener area ratio G,

$$G = A_f S_{yf}/(A_f S_{yf} + A_w S_{yw}) \tag{4.5}$$

The weighted average yield strain ϵ_y used for Eq. (4.3) is defined as follows

$$\epsilon_y = P_y/E(bt + A_w + A_f) \tag{4.6}$$

where

$$P_y = btS_y + A_w S_{yw} + A_f S_{yf} \tag{4.7}$$

The final load-shortening relationship is presented in the non-dimensionalized form as a function of the average stress s vs. the relative strain e.

$$s = f(B,L,R,G,e) \tag{4.8}$$

where

$$s = P/P_y \tag{4.9}$$

$$e = \Delta/(a\epsilon_y) \tag{4.10}$$

in which P is the compressive force acting on the stiffened plate, a is the original length and Δ is the total shortening of the panel.

4.3.2 Coordinate Functions for Stiffened Plate Parameters

The coordinate functions for the individual parameters (B, L, R, G, and e) are described next.

When, for example, parameters L, R, G , as well as the relative strain e are kept constant, s becomes a function of B only. This function is selected to be

$$s = a_1(1/B) + a_2(1/B^{1.5}) \tag{4.11}$$

where a_1 and a_2 are functions of the preset values of L, R, G and e, and the coordinate function for B is defined by

$$F_B = [1/B \quad 1/B^{1.5}] \tag{4.12}$$

Then, in a matrix form, Eq. (4.11) becomes

$$s = [1/B \quad 1/B^{1.5}] \begin{bmatrix} a_1 \\ \\ a_2 \end{bmatrix} \qquad \text{or} \quad s = [a_1 \quad a_2] \; F_B{}^T \qquad (4.13)$$

In a similar manner, a coordinate function (a matrix) can be defined for each of the other parameters. For example,

$$s = [1 \quad L^3] \begin{bmatrix} b_1 \\ \\ b_2 \end{bmatrix} \qquad \text{or} \qquad s = [b_1 \quad b_2] \; F_L{}^T \qquad (4.14)$$

in which b_1 and b_2 are constant for particular values of B, R, G, and e, and $[1 \; L^3]$ is the coordinate function for L, F_L.

In summary, the coordinate functions for B, L, R and G used in the proposed procedure are:

$$\begin{aligned} F_B &= [1/B \quad 1/B^{1.5}] \\ F_L &= [1 \quad L^3] \\ F_R &= [1 \quad R] \qquad\qquad (4.15) \\ F_G &= [1 \quad G] \end{aligned}$$

Illustrations for these coordinate functions are shown in Figs. 16 to 19. Whereas these coordinate functions are valid over the whole ranges, the coordinate function for e has three separate ranges depending on the value of e.

With the limitation that s should not be greater than e, the general form of the effect of e on s is given by

$$s = F_e \begin{bmatrix} d_1 \\ d_2 \\ d_3 \\ d_4 \end{bmatrix} = F_e D \qquad (4.16)$$

where d_1, d_2, d_3, and d_4 are constant for a specific set of values of B, L, R and G, and F_e is the coordinate function for e.

$$F_e = [f_1(e) \quad f_2(e) \quad f_3(e) \quad f_4(e)] \qquad (4.17)$$

where the elements $f_i(e)$ with their limits of applicability are

$$f_1(e) = e \qquad \text{for } 0 \leq e \leq 0.9$$
$$\text{or} \quad = 0.625(e+0.1)^{(4.3-3e)} + 0.275 \qquad \text{for } e > 0.9$$

$$f_2(e) = e \qquad \text{for } 0 \leq e \leq 0.7$$
$$\text{or} \quad = (e+0.3)^{(e+0.3)^{-3.5}} - 0.3 \qquad \text{for } e > 0.7 \qquad (4.18)$$

$$f_3(e) = e \qquad \text{for } 0 \leq e \leq 0.7$$
$$\text{or} \quad = 0.5\ (e+0.3)^{(16-20e)} + 0.7 \qquad \text{for } e > 0.7$$

$$f_4(e) = e/(1+0.4e^2)$$

These individual functions of the coordinate function for e, F_e, are plotted in Fig. 20 to illustrate their nature. Values of d_i are given as functions of B, L, R, and G by

$$D = \begin{bmatrix} d_1 \\ d_2 \\ d_3 \\ d_4 \end{bmatrix} = [C_s]F^T \qquad (4.19)$$

where $[C_s]$ is a (4x16) matrix of constants obtained from the multi-variable regression analysis, and F^T is the transpose of the direct product of the respective coordinate functions

$$F^T = [\ F_B\ F_L\ F_R\ F_G\ ] \tag{4.20}$$

and it contains a total of sixteen terms

$$F = [\ 1/B\ \ 1/B^{1.5}\ \ L^3/B\ \ L^3/B^{1.5}\ \ R/B\ \ R/B^{1.5}\ \ RL^3/B\ \ RL^3/B^{1.5}$$
$$G/B\ \ G/B^{1.5}\ \ GL^3/B\ \ GL^3/B^{1.5}\ \ RG/B\ \ RG/B^{1.5}\ \ RGL^3/B\ \ RGL^3/B^{1.5}] \tag{4.21}$$

4.4 Limitations

As in the case for plates, the variables considered here are those which are commonly encountered in ship structures. The initial deformation and residual stresses of the plate are set to the average values specified for plate models. The initial deformation of the combined plate-stiffener is given by Eq. (4.1). Since the plate aspect ratio values of stiffened plates are larger than unity, the response of the square plate is used. The remaining parameters of the stiffened plate model and their limits of application are

B	Plate slenderness	$0.52 \leq B \leq 2.10$
L	Panel slenderness	$0.20 \leq L \leq 1.30$
R	Stiffener-to-plate area ratio	$0.20 \leq R \leq 0.50$
G	Flange-to-stiffener area ratio	$0.00 \leq G \leq 0.60$
e	Relative strain	$0.00 \leq e \leq 2.00$

Further discussion about these limitations and examples of application of these formulas are presented in Chapter 6.

Chapter 5

GRILLAGES

5.1 Introduction

As previously stated, consideration of grillages is limited to those exhibiting the overall grillage mode of failure. The panel mode of failure, in which the longitudinals fail between the transverses with the transverses remaining essentially straight, was treated in Chapter 4 as the failure of longitudinally stiffened plates. The question still remains open as to what requirements must be satisfied by the transverses in order to induce the panel rather than the grillage mode of failure. However, present design rules, e.g., those of the USN [63], apparently result in adequate transverses when applied to traditional structures. This conclusion is supported by the tests on grillages which conformed in their relative scantlings to typical ship hull structures and did not fail in the grillage mode [56]. However, if the transverses are relatively weaker, the stiffened plate method cannot be used, and an analysis of grillages exhibiting the overall grillage mode of failure must be performed.

A parametric study of the overall grillage mode of failure requires an adequate data base in order to arrive at optimal coordinate functions for all the variables involved. For example, in addition to the parameters used for stiffened plates, at least the following should be included: total length, material and dimensional data for transverses, support conditions for transverses, and the number of longitudinals. The presently available information does not supply sufficient data required for such a study, and at present, no numerical method is available to generate the required data. A method which is suitable for providing such information was developed in this study and will be described here.

5.2 Background and Assumptions

The grillage mode of failure occurs when the longitudinals together with the transverses undergo out-of-plane deformation. This implies that the transverses no longer remain as rigid supports and the structure becomes three-dimensional. To reduce the complexity of this problem, appropriate assumptions must be made, and these are described next.

A grillage system consists of a plate stiffened in both longitudinal and transverse directions as shown in Fig. 13. The supports at the edges are provided by frames perpendicular to the plane of the grillage system. It is assumed that the stiffeners, both longitudinal and transverse, combined with a strip of plate attached to them interact as a grid system. That is, each plate-stiffener combination behaves independently from the adjacent plate-stiffener combination. The only interaction exists at the junctions between the longitudinals and the transverses where the compatibility conditions are enforced.

In imposing equilibrium on the combined plate-stiffener cross sections, the assumption of a plane section remaining plane is used. Strain reversal is considered. For longitudinals, the response of the plate is represented by the model developed in Chapter 3 with the aspect ratio of one (a square plate) as used for long plates. For transverses, the effective width of the plate is assumed to be constant for all strain levels and along the span. An average value, equal to the relative stress at a strain equal to the yield strain, is taken. This effective width is a function of the aspect and slenderness ratios of the plate which are known. This provides is an approximation close to the suggested conservative value of 30t [49] or 50% of the beam spacing [6]. Both references agree that, in general, these assumptions do not have any significant effect on the result of the analysis since there is no axial load on the transverses and the centroid of the resultant cross section is very close to the plate.

Since the axial loads and deformations are imposed only on the longitudinals, the large-deflection analysis is applied only to the equilibrium equations in the longitudinal direction. The edge supports of the longitudinals are free to move in the axial direction; however, they are restrained to remain straight. For the transverses, the small deflection elasto-plastic analysis is used.

5.3 Grillage System

5.3.1 Parameters of Grillages

After all the assumptions are made, the grillage becomes a gridwork of longitudinals and transverses. In the longitudinal direction, every longitudinal stiffener together with the plate strip of width b is treated as a beam column which is divided into a number of segments as shown in Fig. 21. The strain and curvature in the mid-length cross section, ϵ_0 and ϕ_0, are the only unknown variables since slope θ_0 and shear V at this section are zero due to symmetry, whereas the axial force P and the moment M_0 are functions of ϵ_0 and ϕ_0. At every junction with the transverses there is an additional unknown, the redundant R, applied to the longitudinals due to the reaction exerted by the transverses. In the transverse direction, the stiffener together with the plate strip of width a_e (see Fig. 23), where $a_e < a$ is the effective width, is treated as an elasto-plastic beam. Redundant forces R at the junctions with the transverses are treated as point loads.

For a grillage system with an even number of stiffeners, 2m transverses and 2n longitudinals, there are (m+2)n unknowns to be found since only one quarter of the grillage system need be analyzed.

5.3.2 Procedure of Iteration for Grillage System

The analysis of the grillage structure requires the solution of simultaneous equations with the following variables:

- n unknowns for ϵ_0
- n unknowns for ϕ_0
- mxn unknowns for R

The flow of the computational procedure is described next.

For the assumed values of ϵ_0 and ϕ_0 at the midsections of the longitudinal stiffeners, the values of P and M_0, the axial force and the moment, can be computed whereas the values of Θ_0 and V, the slope and shear, at the midsection are known to be zero. Through numerical integration and the application of equilibrium requirements, (described in the next sections), the values of all internal forces and deformations at any cross section of each segment can be computed. At the segments where there are junctions with the transverses, the assumed redundant forces R are included as point loads in the equilibrium equations. After the integrations along the n longitudinals are completed, the m transverse stiffeners are analyzed, using the redundant forces transmitted from the longitudinals as point loads.

The following conditions have to be satisfied:

- Total axial deformations of the n longitudinals as defined on page 71 by Eq. (5.20) should be equal to each other and to the value preset for a particular increment.

- For simply supported grillages, the support moments of the longitudinals defined on page 67 by Eq. (5.4) or on page 71 by Eq. (5.16) should be zero, or for fixed supports, the slope defined on page 70 by Eq. (5.10) should be zero.

- Vertical deformations at mxn junctions between longitudinals and transverses computed on page 71 by Eq. (5.20) and on page 73 by Eq. (5.22) or (5.23) should be equal.

The above procedure results in a set of (m+2)n simultaneous nonlinear equations to be solved for (m+2)n unknowns (see Section 2.2).

5.4 Longitudinals

In order to arrive at a solution of the simultaneous equations, it is necessary to perform integration along the longitudinals and to impose equilibrium at every cross section of the longitudinal segments. These two procedures are described below.

5.4.1 Cross-Sectional Equilibrium

The cross section of the longitudinal plate-stiffener combination is shown in Fig. 23. The following sign convention is adopted:

- Bending moment and curvature are positive in the direction causing compression in the top flange (plate).

- Stresses, strains and axial forces are positive when they cause compression.

Top flange width b is equal to the spacing between two adjacent longitudinal stiffeners. For a given strain ϵ (strain measured at the elastic centroid) and a curvature ϕ, the strain and stress variations over the cross section are as shown in Fig. 24. The strain at any location is

$$\epsilon(z) = \epsilon + z\,\phi \tag{5.1}$$

where z is the distance from the elastic centroid.

The stress at the top flange is obtained by multiplying the nondimensional stress for the plate (as a function of nondimensional strain described in Chapter 3) by the plate yield stress. For the web and the stiffener flange, the bi-linear elasto-plastic stress-strain relationship is used. The flanges are considered thin enough so that the variation of stress over the thickness can be neglected. Then, the flange stress is taken equal to the stress at the centroid of the flange. The stress-strain relationships for the web and flanges are shown in Fig. 25.

The stress diagram therefore can be divided into several stress blocks as shown in Fig. 24. The stress resultant, F, for each stress block is

$$F_j = (z_j - z_{j-1})tS \tag{5.2}$$

where z_j and z_{j-1} are coordinates of the fibers limiting the stress block, t is the width of the block (b, t_w or b_f) and S is the average stress in the domain considered.

The total axial force P is

$$P = \sum_{j=1}^{K-1} F_j \tag{5.3}$$

where K is the total number of the stress fibers.

The total moment M with respect to the elastic centroid is

$$M = \sum_{j=1}^{K-1} F_j C_j \tag{5.4}$$

where C_j is the distance of the stress block centroid to the elastic centroid of the cross section.

5.4.2 Segmental Integration

The integration method described next is to find the moment or the slope at the end supports of the longitudinals, vertical deflections at the junctions of the longitudinal and transverse beams, and the total shortening of the longitudinal beams. To perform segmental integration, the segments are isolated from each other, and the equilibrium equations are imposed on the first segment from the mid-length. The known variables at the beginning of the integration are the internal forces and deformations at the middle cross section. Since the strain and curvature (ϵ_0 and ϕ_0) are assumed in the iteration, the moment M_0 and P_0 are functions of ϵ_0 and ϕ_0. Coordinates x_0, y_0 and s_0 are taken as the origin and the slope Θ_0 and shear V_0 are zero due to symmetry. The forces and deformation at the other end of the segment are found through an iterative process by imposing equilibrium and continuity. The process is then repeated for all other segments in turn. For example, for the i-th segment shown in the lower part of Fig. 21, the known variables are ϕ_i, Θ_i, V_i, x_i, y_i, P_i, M_i, s_i and s_{i+1} from the preceeding computation. The next step is to determine ϵ_{i+1} and ϕ_{i+1} which then can be used to compute V_{i+1}, P_{i+1}, Θ_{i+1}, M_{i+1}, x_{i+1}, and y_{i+1}. To find ϵ_{i+1} and ϕ_{i+1}, the two variables are assumed first. With these assumed variables, the other variables in the cross section are computed and the equilibrium is evaluated. The correct values of ϵ_{i+1} and ϕ_{i+1} are those which result in equilibrium. The iteration procedure to obtain the final values of ϵ_{i+1} and ϕ_{i+1} is illustrated by a flowchart in Fig. 22. This integration procedure is performed to determine the internal forces and deformations along each of the longitudinal beams.

In addition to the sign convention adopted in the computation of the cross sectional equilibrium, the following sign convention is used:

- The positive direction of the shear force couple is shown in Fig. 21
- The counter clockwise slope is positive
- The upward deflection is positive

The effect of the initial deformation is considered by adding the initial curvature ϕ^o to the curvature ϕ produced by forces.

$$\phi^t = \phi + \phi^o \tag{5.5}$$

The change of slope is then

$$d\Theta = \phi^t ds \tag{5.6}$$

Assuming that the variation of the curvature within the segment is linear, expressed by

$$\phi^t = \phi_i^t + (\phi_{i+1}^t - \phi_i^t)\ (s - s_i)/(s_{i+1} - s_i) \tag{5.7}$$

and by integrating Eq. (5.6), the slope at any point within the segment becomes

$$\theta = \theta_i + \phi_i^t(s-s_i) + 0.5(\phi_{i+1}^t-\phi_i^t)(s-s_i)^2/(s_{i+1}-s_i) \tag{5.8}$$

or

$$\theta = \theta_i + \Delta\theta(s) \tag{5.9}$$

and θ_{i+1} is

$$\theta_{i+1} = \theta_i + (\phi_i^t+\phi_{i+1}^t)(s_{i+1}-s_i)/2 \tag{5.10}$$

The effect of curvature on the deformed shape of the longitudinal beam is

$$dx = ds \cos \theta \tag{5.11}$$

and

$$dy = ds \sin \theta \tag{5.12}$$

These equations are then integrated with θ as given by Eq. (5.8) or (5.9). Terms $\sin(\theta+\Delta\theta(s))$ and $\cos(\theta+\Delta\theta(s))$ are expanded and, due to the relatively small magnitude of $\Delta\theta(s)$ with respect to θ, simplified to $\cos(\Delta\theta(s)) = 1$ and $\sin(\Delta\theta(s)) = \Delta\theta(s)$. These integrations yield [49]

$$x_{i+1}=x_i+(s_{i+1}-s_i) \cos \theta_i-(1/3)(\phi_i^t+\phi_{i+1}^t/2)(s_{i+1}-s_i)^2\sin \theta_i \tag{5.13}$$

$$y_{i+1}=y_i+(s_{i+1}-s_i) \sin \theta_i+(1/3)(\phi_i^t+\phi_{i+1}^t/2)(s_{i+1}-s_i)^2\cos \theta_i \tag{5.14}$$

Then, the following equilibrium equations are obtained

$$P_{i+1}= P_i = P \tag{5.15}$$

$$M_{i+1} = M_i + V_i(x_{i+1}-x_i) - P(y_{i+1}-y_i) \tag{5.16}$$

$$V_{i+1} = V_i \quad \text{in general, or} \tag{5.17}$$

$$V_{i+1} = V_i - R_j \tag{5.18}$$

where R_j is the force transferred from the transverse beam if the cross section i coincides with the junction with the j-th transverse beam.

The moment or slope at the support is obtained from Eq. (5.10) or (5.16).

The net vertical deflection of the j-th junction is

$$D_j = y_k - y_{i,j} - y_j^o \tag{5.19}$$

where $y_{i,j}$ is the vertical ordinate of the i-th cross section which is coincident with the j-th junction, y_j^o is the initial deflection of the j-th junction and y_k is the deflection at the support.

Initial deflection y^o is taken as a continuous function so that it can be defined at any point on the longitudinal and transverse beams.

The net shortening of one-half of the longitudinal beam is

$$Dx = L/2 - (x_k - x_0) + \sum_{i=0}^{k-1} (x_{i+1}-x_i)\epsilon_i - 0.5\int_0^{L/2} (dy^o/ds)^2 ds \tag{5.20}$$

where k is the number of equal length segments, L is the total length of the grillage and the last two terms are the shortening due to compression and initial curvature, respectively.

5.5 Transverses

A transverse stiffener together with a strip of plate of constant width a_e is treated as a beam. The effective width is

$$a_e = s\ a \tag{5.21}$$

where a is the spacing between two adjacent transverse beams and s is the relative stress obtained from Eq. (3.15) with e = 1.0.

In Eq. (3.15), coefficients d_1 to d_4 are functions of the slenderness ratio B and aspect ratio A which are computed from Eqs. (3.1) to (3.3). In using these formulas some adjustments have to be made since the stresses are applied in the transverse direction. This means that A = b/a rather than A = a/b and B is obtained from Eq. (3.3) rather than (3.2).

The cross-sectional properties, such as moment of inertia I (taken with respect to the elastic centroid of the cross section) and plastic moment M_p are then computed.

5.5.1 Flexibility Matrix

For the known vertical forces at the junctions between the transverses and longitudinals, the deflections can be computed by

$$D_i = d_{ij} R_j \tag{5.22}$$

where D_i is the deflection at point i, d_{ij} is the flexibility coefficient, and R_j is the vertical force applied at point j.

Equation (5.22) is the force-deformation equation for fixed-ended transverse stiffeners. Due to symmetry, only one-half of the stiffener need to be analyzed as shown in Fig. 26.

When the applied loads R are sufficiently large so that a plastic hinge is formed at point h, the deflection is computed by

$$D_i = d'_{ij}R_j + d''_{ih}M_h \tag{5.23}$$

where d'_{ij} and d''_{ih} are the flexibility coefficients of the transverse beam after the formation of the first plastic hinge and M_h is the moment at point h.

For pin-ended transverse beams, Eq. (5.23) is always used and the point h is assigned at the support. The value of M_h is taken to be equal to zero.

5.5.2 Collapse Mechanism

After the formation of a plastic hinge, the degree of static determinacy is decreased by one. If the loads are increased, additional plastic hinges can develop until a mechanism is formed. For the structure shown in Fig. 26, only two hinges are required to form a mechanism. For pin-ended beams, the hinge at the support with a zero plastic moment is considered as the first plastic hinge. After the formation of the last plastic hinge, the structure becomes unstable, which means that deflections become infinitely large for loads larger than the ultimate load. To maintain the load below this ultimate load, the following approximation is used.

First, a limiting moment, M_l, is specified. This moment is basically a limiting value over which the deformation (curvature at the cross section with this limiting moment) becomes very large. Since the true plastic moment M_p can never be reached (curvature cannot become infinite) unless the strain hardening of the material is considered, this limiting moment is taken to be

$$M_l = C_m M_p \tag{5.24}$$

where C_m is a coefficient close to but smaller than unity. This equation provides an early indication as to when the collapse load is approached.

In the grillage iteration for the next deformation increment after the formation of the second hinge, that is when M_1 is exceeded, the redundant forces R for this particular transverse beam are assumed to be constant. This eliminates them as unknown variables and, thus, the size of the simultaneous equations to be solved is reduced (see Section 5.3.2). This assumption underestimates the axial rigidity of the outer longitudinals and overestimates that of the inner longitudinals, since in actuality, redistribution of the redundant forces would be taking place. It is expected, however, that redistribution of the redundant forces would have small effect on the overall load-shortening behavior of the grillage as the responses of the outer and inner longitudinals are averaged.

A computer program was developed to perform the analysis to generate the load-shortening relationships for grillages. A brief flowchart of the program is shown in Fig. 27.

5.6 Limitations

The above described analysis is based on the assumptions some of which (such as the effective width of the plate in the transverse direction and the moment-thrust-curvature relationship of axially loaded beam-columns exhibiting reduction of strength in the post-ultimate region) are yet to be confirmed by experimental results and/or analytical proofs. Also, the convergence of the iteration procedure becomes relatively slow when the deformations go into the post-ultimate range. The simplifications made and these may limit the generality of the solution as described next.

5.6.1 Geometry

The grillage system analyzed in this study is doubly symmetrical with an even number of longitudinals and transverses. For an odd number of longitudinals and/or transverses, minor modifications should be made in some subroutines of the computer program. However, for a large number of stiffeners, the result for an odd number of stiffeners can be obtained by interpolation between the results of grillage analyses with two consecutive even numbers of stiffeners.

5.6.2 Boundary Conditions

The transverse stiffeners may be simply supported or fixed at the ends. The longitudinals are assumed to be simply supported. To change the longitudinals to the fixed support condition requires only the change in the compatibility conditions which are to be satisfied.

5.6.3 Initial Deformations

The initial deformation was assumed to be according to

$$y^{O}=W_{O}\sin(\pi/2+\pi s/L)\sin(\pi/2+\pi u/L_{t}) \tag{5.25}$$

for simply supported transverses and

$$y^{O}=W_{O}\sin(\pi/2+\pi s/L)\{1+\cos(\pi/2+\pi u/L_{t})\} \tag{5.26}$$

for fixed transverses, where L is the total length of the longitudinal stiffeners, u is the ordinate in the transverse direction measured from the middle, L_t is the total length of the transverse stiffeners and W_O is the initial deflection at the mid-point.

For other patterns of initial deformations, some changes should be made in the subroutines of the program where the effects of initial deformations are included.

5.6.4 Relatively Rigid Transverses

For relatively rigid transverses, the bending moment diagram of the longitudinal stiffener is as shown in Fig. 28. The restraint provided by the transverses results in a higher axial load to be carried by the longitudinal stiffener. The moment capacity of a cross section with a high axial force is shown in Fig. 29. It is lower than the moment obtained from the equilibrium equation of Eq. (5.16). In consequence, the relationships used in the iteration procedure described in Fig. 22 are no longer applicable.

Two alternate solutions are possible. The first is to use the method developed in Chapter 4 (for stiffened plates). This alternative, however, can be used only as an upper bound to the solution as it tends to over-estimate the load capacity. It can be used only for grillages with very rigid transverses (causing large axial load capacity of the longitudinals) so that the curvature and bending moment in the longitudinals can be negative (see Figs 28 and 29). When the transverses are moderately rigid so that only the bending moment in the longitudinals is negative while the curvature remains positive, another assumption which would simplify the solution is used. It consists of applying a plastic hinge rotation at the cross section where the maximum moment occurs.

$$\Theta_p=(M-M_m)/[P(s_{i+1}-s_i)] \tag{5.27}$$

where M is computed by Eq. (5.16) before the application of the plastic rotation. By using a plastic rotation, the maximum moment in the longitudinal stiffener is limited to a value smaller or equal to the maximum moment M_m as shown in Fig. 28.

5.6.5 Relatively Rigid Longitudinals

The bending moment diagram for relatively rigid longitudinals is shown in Fig. 28. The moment-curvature relationships for these longitudinals are shown in Fig. 29 as the moment-curvature curves for cross sections with high axial loads. At the post-ultimate stage of deformation the midsection curvature, ϕ_0, is in the post-maximum moment (M_m) region. The curvature of the next cross section (ϕ_1) is expected to be smaller than ϕ_0 as the moment at this cross section must be smaller than the midsection moment as shown in Fig. 28. This is inconsistent with the moment-curvature relationship shown in Fig. 29 since, for curvatures in the post-maximum moment region, smaller curvatures are associated with larger moments. As suggested by Sherman [55], a conservative estimate can be used by assuming a constant curvature along a region which is termed as the length of the plastic hinge, l_p. This assumption agrees with some test observations made by Sherman on circular tubular beam-columns [55].

By assuming that the moment-curvature curve is symmetrical in the vicinity of the maximum moment, the length of the plastic hinge in this study is approximated by

$$l_p = |s_{i+1} - s_i| (M_m - M_0) / |M_{i+1} - M_i| \tag{5.28}$$

where M_0 is the midsection moment and i is any cross section in the vicinity of the plastic region.

Examples of the application of the proposed method and a discussion of the obtained results is presented in the next chapter.

Chapter 6

APPLICATION, RESULTS AND DISCUSSION

The procedures for defining the stress-strain relationships for plates, stiffened plates and grillages were presented in Chapters 3, 4 and 5. Numerical results and illustrations for the application of these procedures are presented below.

6.1 Plate

6.1.1 Regression Analysis

Regression analysis using 1127 data points was performed to obtain the 144 constants shown in Table 1. Then, the variables for the residual stresses and initial imperfections were set to the practical average values (see Chapter 3) and the number of constants was reduced to twenty-four (24) given by the following (4x6) matrix:

$$C_p = \begin{bmatrix} -0.46790 & 1.64838 & -1.04823 & 0.30719 & -0.85944 & 0.50048 \\ -0.70316 & 2.41028 & -1.48401 & 0.42539 & -0.83704 & 0.26624 \\ 1.71876 & -5.92934 & 5.10363 & -1.09855 & 3.92163 & -3.09635 \\ -1.51186 & 8.33535 & -7.18090 & 1.61576 & -7.42777 & 6.22365 \end{bmatrix} \tag{6.1}$$

For a particular plate, with all the material and geometric parameters known, these constants can be further reduced to four by using Eq. (2.23) or (3.19). Then the stress becomes a function of strain only. A statistical comparison with all the input data was made and the standard deviation was found to be 7.0%.

This function was used to obtain a set of six coefficients for estimating the ultimate strength of plates for various slenderness and aspect according to Eq. (6.2).

$$s_{ult} = \sum_{i=1}^{6} c_i f_i(A,B) \tag{6.2}$$

Coefficients c_i and functions $f_i(A,B)$ for Eq. (6.2) are listed in Table 2. For the case of square and long plates, and using $\underline{B}$ = B/0.526 replacing B as variable, Eq. (6.2) becomes

$$s_{ult} = 1.82/\underline{B} - 0.93/(\underline{B})^2 \tag{6.3}$$

This equation is similar to the formulas in terms of $\underline{B}$ recommended by several researchers, such as, Conley, Faulkner, Frankland and Winter [8, 17, 18, 63, 67], for long plates. A comparison of these formulas with Eq. (6.3) is given in Fig. 30. The curve according to Eq. (6.3) is below the others since it includes the effects of residual stresses and initial imperfections for all values of slenderness $\underline{B}$. However, in this study, Eq. (6.2) is also applicable to the ultimate strength of wide plates since A<1.0 is a variable.

The resultant curves according to Eq. (6.2) for such plates are shown in Fig. 31.

6.1.2 Parametric Study

In this study, the values of residual stresses and initial imperfections were set to the average values observed in actual structures since both of these variables are beyond designer's control and, thus, maintaining them as variables has no practical significance. The remaining nondimensionalized variables are the aspect ratio, A, and the slenderness ratio, B, in addition to the relative strain. Figures 32 and 33 show the load-shortening curves for different A and B respectively. The aspect ratio affects the ultimate strength of plates whereas the slenderness ratio affects both the ultimate strength and rigidity of the plates.

6.1.3 Example of Application

The procedure for defining the load-shortening of plates was formulated as a simple function of nondimensionalized variables. An example of the application of this procedure to a sample plate is presented here.

<u>Given</u>:

A long plate with:

Length $a = 823$ mm, width $b = 381$ mm, thickness $t = 6.35$ mm, $S_y = 222.2$ MPa, and $E = 200000$ MPa.

Since this is a long plate $(a = 823 \text{ mm}) > (b = 381 \text{ mm})$, use aspect ratio $A = 1.00$ (see page 45), and compute B from Eq.(3.3)

$$B = 0.526(b/t)\sqrt{S_y/E} = 0.526(381/6.35)\sqrt{(222.2/200000)} = 1.052$$

Coordinate function for A (with A = 1.0):

$F_A = [1 \ A \ A^2] = [1 \ 1 \ 1]$

Coordinate function for B:

$F_B = [1/B \ 1/B^2] = [0.951 \ 0.904]$

The direct product of F_A and F_B: $F_{AB} = F_A F_B$

$$F_{AB} = [1/B \quad A/B \quad A^2/B \quad 1/B^2 \quad A/B^2 \quad (A/B)^2] =$$
$$= [0.951 \quad 0.951 \quad 0.951 \quad 0.904 \quad 0.904 \quad 0.904]$$

Obtain the coefficients of D by using Eq.(3.19): $\{D\} = [C_p] \, F_{AB}{}^T$

$$D = \begin{bmatrix} d_1 \\ d_2 \\ d_3 \\ d_4 \end{bmatrix} = \begin{bmatrix} 0.0790 \\ 0.0806 \\ 0.6021 \\ 0.0323 \end{bmatrix}$$

Compute e_o from Eq.(3.13):

$e_o = (0.223)(1.00)(1.052)/\{1.0+0.285(1.052)\} = 0.18$

Coefficients D are multiplied by the coordinate function F_e as given by Eq.(3.17) or (3.18), unless the value of e is less than e_o.

For example, for $e = 0.15$, since $(e = 0.15) < (e_o = 0.18)$, use Eq.(3.15): d_o=0.777, then, Eq.(3.14) gives the nondimensionalized stress $s = 0.777(0.15) = 0.117$.

For $e = 0.72$, since $(e = 0.72) > (e_0 = 0.18)$, use Eq.(3.17): $s = 0.488$.

The complete stress-strain diagram of s vs. e for this example is shown in Fig. 34.

6.1.4 Comparison with Test Results

In order to illustrate the validity of the proposed analytical model, a comparison with some available test results is presented next. However, this comparison is subject to a careful interpretation since the test specimens had initial imperfections and residual stresses with the values which often were unknown or quite different from the specific values which were used in the development of the model.

Most of the tests conducted on wide plates were to find the ultimate strength rather than the complete load-deformation relationship. Figure 35 is a comparison with the test conducted by Collier [7] on Specimen HTS with E = 215814 MPa (31300 ksi), S_y = 456.5 MPa (66.2 ksi), aspect ratio A = 0.3636, and slenderness ratio B = 0.583 (a/t = 32), where one of the loaded edges was fixed. Figure 36 is a comparison with the tests on Specimen HY-80 (the same series) with E = 210987 MPa (30600 ksi), S_y = 614.3 MPa (89.1 ksi), A = 0.3636 and B = 1.233 (a/t = 51). Both of the loaded edges were close to simply supported. The results for both cases agree well with the proposed model.

Figures 37, 38, and 39 are comparisons with the tests conducted on plates of aspect ratio A = 0.875 and slenderness ratios B = 0.815 (a/t = 55), 1.005 (a/t = 64), and 1.189 (a/t = 80), respectively [43]. The tests were conducted on unwelded (low or zero residual stresses), almost perfectly flat plates (very small or zero initial imperfections). Therefore, the test results are higher than the predicted values which are based on preset typical values of initial imperfections and residual stresses. The dashed curves in the figures show the load shortening relationships computed by the proposed method for plates with zero initial imperfections (perfect plates). These figures also show that, as the slenderness of the plate increases, the difference between the test plate claimed to be flat and the analytical plate with non-zero initial imperfections decreases. This tendency agrees very well with a number of theoretical studies which showed the decreasing effect of initial imperfections on the load-shortening behavior of wide plates [20, 39].

6.2 Stiffened Plate

6.2.1 Regression Analysis

For stiffened plates, 2115 points were used in the regression analysis to obtain 64 constants. A statistical comparison with all the data points gave the standard deviation of 7.8%. The constants are arranged in a 4x16 matrix which is shown in its transposed form by Eq.(6.4)

$$[C_s]^T = \begin{bmatrix} -0.08820 & 3.33314 & -1.01289 & -1.30577 \\ 0.03410 & -2.53633 & 0.72126 & 1.53022 \\ 0.30254 & -1.84088 & 0.32089 & 1.40126 \\ -0.11821 & 1.36843 & -0.17116 & -1.23825 \\ -1.44955 & 1.03995 & 1.20906 & 0.57116 \\ 2.09674 & -1.09834 & -0.54365 & -1.57902 \\ 0.95911 & 2.33213 & -0.30313 & -3.32766 \\ -1.21010 & -2.27392 & 0.10999 & 3.72225 \\ 0.83689 & -3.92283 & 0.95461 & 2.33082 \\ -0.72201 & 3.11582 & -0.74160 & -1.81497 \\ 0.32650 & 1.87236 & 0.51724 & -2.96740 \\ -0.23886 & -1.29017 & -0.41040 & 2.11919 \\ 3.78225 & 0.27975 & -1.69448 & -2.52897 \\ -3.81819 & 0.60350 & 0.90282 & 2.45707 \\ -2.81972 & -2.61326 & -1.82934 & 8.11895 \\ 2.67443 & 2.88827 & 1.45326 & -7.73726 \end{bmatrix} \tag{6.4}$$

The pertinent coordinate functions and the procedure of computing the average stress s as a function of the relative strain e are presented by Eqs. (4.15) to (4.21). This formulation gave the ultimate strength of a stiffened plate to be

$$s_{ult} = \sum_{i=1}^{16} c_i f_i(B,L,R,G) \tag{6.5}$$

The constants and functions for this equation are listed in Table 3.

6.2.2 Parametric Study

It has been found for stiffened plates subjected to lateral and axial loads that as the lateral load decreases, the load-shortening behavior of stiffened plates becomes less affected by the flange-to-stiffener area ratio, G, and the stiffener-to-plate area ratio, R [64]. This has also been observed in this study (no lateral load) as indicated in Figs. 18 and 19 by the almost horizontal lines. The most significant influence on the load-shortening behavior, is made by the plate slenderness ratio, B and the panel slenderness ratio L. The effects of these slenderness ratios on the load-shortening behavior are shown in Figs. 40 and 41, where the effect of the plate slenderness is the most pronounced.

6.2.3 Example of Application

The dimensions and material properties of the following example are those of Specimen T-1 of the series of tests conducted at Lehigh University [32].

<u>Given:</u>

Length a = 1486 mm (58.5 in.),

plate width b = 381 mm (15.0 in.),

plate thickness t = 6.61 mm (0.2604 in.),

depth of stiffener d_w = 74.2 mm (2.92 in.), thickness of stiffener web t_w = 4.27 mm (0.168 in.),

width of stiffener flange b_f = 99.8 mm (3.93 in.),

thickness of stiffener flange t_f = 5.16 mm (0.203 in.),

E = 200000 MPa (29100 ksi),

yield stress of plate S_y = 273.7 MPa (39.7 ksi),

yield stress of stiffener web S_{yw} = 275.8 MPa (40.0 ksi), and

yield stress of stiffener flange S_{yf} = 258.6 MPa (37.5 ksi).

Compute nondimensionalized parameters:

From Eq.(4.2): B=1.119

From Eq.(4.3): L=0.607

From Eq.(4.4): R=0.289

From Eq.(4.5): G=0.589

Compute the direct product of $[F_B F_L F_R F_G] = F$ from Eq.(4.21),

$$F=[0.894\ 0.845\ 0.200\ 0.189\ 0.258\ 0.244\ 0.058\ 0.055\ 0.526\ 0.498\ 0.118\ 0.111\ 0.152\ 0.144\ 0.034\ 0.032]$$

Obtain coefficients $D = [C_s]\,F^T$, from Eq.(4.19):

$$D = \begin{bmatrix} d_1 \\ d_2 \\ d_3 \\ d_4 \end{bmatrix} = \begin{bmatrix} 0.2245 \\ 0.4331 \\ -0.0908 \\ 0.1515 \end{bmatrix}$$

Then, the stress is given as a function of the strain according to Eq. (3.19).

For example, for e= 0.5,

$$s = d_1 f_1(0.5) + d_2 f_2(0.5) + d_3 f_3(0.5) + d_4 f_4(0.5)$$
$$= 0.2245(0.5) + 0.4331(0.5) - 0.0908(0.5) + 0.1515(0.445)$$
$$= 0.351$$

The complete relationship between s and e for this example is shown in Fig. 42.

6.2.4 Comparison with Test Results

There is only a small number of tests conducted on stiffened plates. An example is the series of tests conducted at Lehigh University [32]. The test points for Specimen T-1 of this series are shown in Fig. 42 together with the s-e curve computed according to the proposed analytical model. The stresses, including the ultimate stress agree quite well, but the test specimen exhibits somewhat greater stiffness (smaller e for the same s). This is apparently due to smaller initial imperfections than the imperfections preset in the analytical model.

Comparisons between the stress-strain curves computed by the proposed method and the curves obtained from some other tests are shown in Figs. 43, 44, 45 [32] and 46 [28]. Figures 43, 44 and

45 show the comparison of the proposed procedure with the test results for three geometrically identical specimens: Specimen T-7 (as fabricated), T-8 (annealed after fabrication), and T-9 (components annealed then welded) [32]. The measured compressive residual stress for Specimens T-7 and T-9 was approximately 0.1 S_y, that is, smaller than the value of 0.2 S_y assumed in the proposed method. This is the partial reason for the test results exhibiting higher ultimate stresses than the proposed method. It can be seen that there is a closer agreement between the predicted values (proposed method) and the test results for Specimens T-7 and T-9 which had residual stresses (Figs. 43 and 45) than for Specimen T-8 which was annealed and thus had essentially no residual stresses (Fig. 44).

Figure 46 shows the comparison for Specimen M-1 tested by Kmiecik [28]. This specimen exhibits a more rigid stress-strain curve in the initial stages partly due to smaller initial imperfection of the test panel (W_{os} = 0.0011a) than the assumed value of 0.0015a used in the proposed method. However, the ultimate capacity differs very little from the prediction.

It has been found that, in general, the laboratory test specimens have smaller values of initial imperfections and residual stresses than the values assumed in the proposed method on the basis of measurements on actual ship structures [12, 60]. It is expected, therefore, that the proposed procedure would give satisfactory load-shortening curves for stiffened plates with typical initial imperfections and residual stresses.

6.3 Grillages

In defining the load-shortening relationships for grillages, the dimensions and material properties of the transverse stiffeners must be taken into consideration. When the dimensions of the transverse stiffeners are relatively small, the transverses can no longer be treated as rigid supports even though they still provide some support. The pattern of the load-shortening curves for grillages is affected by the restraint, or lack of it after the transverses fail. None of the available test results, however, exhibited this type of failure. Thus, no experimental verification of the numerical results for a general grillage mode of failure is available. Some of the results obtained in the analysis of sample grillages in this study are presented below.

To illustrate the effect of the restraint provided by the transverses, several grillage configurations were considered. The dimensions of the longitudinals, which are taken to be the same as those for specimen T-1 of the stiffened plate [32], and spacings between the transverses, a, and between the longitudinals, b, are kept constant. The number of the longitudinal and transverse stiffeners and the dimensions of the transverses were varied as given in Table 4 and Fig. 47. The effect of these parameters is discussed separately below.

6.3.1 Dimensions of the Transverses

Figure 48 shows the load-shortening curves for grillages with two longitudinals and two transverses. The dimensions of transverses are varied. The upper bound for the load-shortening curve is the curve for the stiffened plate of Specimen T-1, i.e, a grillage with infinitely rigid transverses. The lower bound curve is taken for a simply supported beam-column of the full length with no transverse stiffeners. The upper bound agrees well with the sample G11-A which has the strongest transverses and thus behaves as a stiffened panel of length a. In this sample, the dimensions of the transverses are equal to those of the longitudinals given in Section 6.2.3 (see Table 4 for dimensions of the transverses).

Sample G11-B has smaller transverses (0.31 times as deep as those of Sample G11-A) but still sufficiently strong so that the longitudinals fail between the transverses. As the transverses become smaller, starting with the Sample G11-C (0.28 times as deep), the failure mode becomes a grillage mode and the transverses fail at earlier loading stages. The change of the failure mode is caused not only by the smaller moment capacity of the transverses, but also by the increase in the moment capacity of the longitudinals due to smaller axial loads.

Sample G11-F is the response of the grillage with even smaller transverses such that very little support is provided by them. The resulting redundant forces R (see Fig. 26) are too small to cause the formation of plastic hinges, even though the transverses have a smaller moment capacity.

6.3.2 Number of Longitudinals

Figure 49 shows the load-shortening curves for grillages G11-B and G21-B. Both have the same number of transverses but different number of longitudinals with the same spacing, thus, different overall widths of the grillages. As the number of the longitudinals increases, the length of the transverse stiffeners increases and each transverse stiffener has to restrain more longitudinals (see Fig. 47). Thus, the possibility of a formation of plastic hinges in the transverses is also increased as each longitudinal is subjected to less support from the transverses. The reduction of support from the transverses lowers the ultimate load and decreases the axial stiffness. The distribution of axial forces in the grillage sample G21-B between the outer and inner longitudinals is shown in Fig. 50. The outer longitudinals exhibit a more rigid axial stiffness since they undergo smaller out-of-plane deformations (see also Fig. 26).

6.3.3 Number of Transverses

Figure 51 shows the load-shortening curves for grillages G11-F and G12-F. Both have the same number of longitudinals but different number of transverses (two and four, respectively) with equal spacing, thus, a larger total length of the grillage. In general, the load-shortening curves are similar. Grillage G12-F (with four transverses) is more rigid in the pre-ultimate stage. After the plastification of the middle transverses, the axial stiffness deteriorates and the load-deformation curve drops at a faster rate. These curves show, that provided the transverses are strong, the model developed for stiffened plates (Chapter 4) can be safely used for grillages regardless of the number of the transverses.

Chapter 7

SUMMARY, CONCLUSIONS AND RECOMMENDATIONS

7.1 Summary

The proposed analytical models (algorithms) provide a method for determining the axial load-deformation relationships of plates and longitudinally stiffened plates in the pre- and post-ultimate ranges. The ranges of the geometrical and material parameters for which these models are valid are typical for ship structure components. These models are sufficiently short to be used on programmable calculators (or even manually) and can be readily incorporated as subroutines into computer programs for ultimate moment analysis of ship hull girders.

Some of the parameters, such as, boundary conditions, initial imperfections and residual stresses, were set approximately equal to the average conditions commonly encountered in actual ship structures since these parameters cannot be controlled by a practicing designer. The other variables of the geometrical configurations and material properties can be varied within the ranges that are typical for ship structures.

In developing these models, a multi-variable regression analysis was employed. The data base consisted of the experimental and theoretical results available in literature and of the data specifically generated for this study using large computer programs, particularly for the stiffened plates. Sample comparisons between the proposed analytical models and some test results were made to verify the validity of the models.

A numerical method of analysis for determining the axial load-shortening relationship for grillages was also developed. This method provides load-shortening curves which can be used for generating data to develop an analytical model similar to the models proposed for plates and stiffened plates. The method transforms the grillage to a grid of longitudinals and transverses and it employs a large-deformation analysis (using integration procedures) for the longitudinals and an elasto-plastic beam analysis for the transverses. To overcome the nonlinearity of the load-deformation relationships, two different solutions of the nonlinear problems were used: the secant method for moderately nonlinear cases and the flexible polyhedron search method for highly nonlinear cases. Comparisons between grillages of different geometrical configurations were made including comparisons between sample grillages with rigid transverses and a longitudinally stiffened plate.

7.2 Conclusions

The following main conclusions can be drawn from the results of this study:

1. The models proposed for defining the load-shortening relationship of plates and stiffened plates give satisfactory results for design purposes within the practical range of the parameters given in Sections 3.4 and 4.4. The errors between the proposed models and values of the data base used were 7.0% for plates and 7.8% for stiffened plates.

2. The models are simple in application and are suitable for incorporation into computer programs for hull strength analysis.

3. The proposed stiffened plate model can be used for the determination of the axial load-shortening behavior of grillages when the transverse stiffeners are adequately strong to prevent the overall grillage mode of failure.

4. The numerical method of analysis developed for grillages should be used when the transverse stiffeners are relatively flexible. This conclusion is drawn from the interpretation of the numerical results obtained in this study, that is, as the dimensions of the transverse stiffeners were reduced, a significant reduction of strength was observed. The panel

mode of failure was still observed when the transverses were 0.31 times as deep as the longitudinals. The grillage mode of failure was observed only after the dimensions of the transverses were further reduced. The overall length of the transverse stiffener provides a significant factor in determining the axial rigidity and mode of failure of grillages.

7.3 Recommendations for Future Work

The studies conducted in the course of developing the proposed analytical models show that these models can be improved further. There is also a need for more work on grillages and on the tripping mode of failure of longitudinals.

1 Analytical models for plates and stiffened plates can be readily improved by increasing the data base as more results become available from experimental and/or theoretical work and by experimenting with the composition of the coordinate functions.

2. The numerical method of analysis developed for grillages was based on assumptions some of which are yet to be confirmed experimentally and/or analytically. More information is needed for this purpose. Included would be such information as the effective width of the plate under biaxial loads and the moment curvature behavior of beam-columns exhibiting reduction of strength in the post-ultimate range.

3. As a corollary to the development of an analytical model for grillages, definitive criteria should be established for sizing the transverse stiffeners so that only the interpanel (stiffened plate) mode of failure would be possible. As shown above, this would depend on the configuration of the grillages.

4. In the formulations carried out, it was implicitly assumed that the longitudinals would have adequate torsional resistance in order not to fail in the tripping mode. Research is needed to establish accurate criteria for preventing this mode since current recommendations are often contradictory and have essentially no experimental verification.

TABLES

Table 1 Initial Coefficients for Plates

(Initial imperfection w_0 and residual stress S_r are included as variables)

-20.841	42.915	266.494	-627.046	-531.422	1465.978
54.536	-115.433	-351.038	1149.886	114.987	-2026.729
-34.987	75.431	88.646	-539.374	430.802	569.445
11.810	-24.147	-112.467	297.842	154.602	-612.303
-31.146	65.573	29.132	-402.773	572.117	206.705
20.390	-43.062	76.499	117.550	-726.563	393.256
4.286	-10.694	-253.057	372.515	778.753	-1104.590
-9.147	26.246	793.525	-1156.175	-2439.203	3429.730
5.190	-15.140	-539.026	779.563	1644.153	-2310.563
-1.909	5.353	233.566	-334.772	-726.206	1008.745
3.751	-12.124	-744.313	1063.581	2300.311	-3198.652
-1.937	6.486	511.623	-728.623	-1569.661	2186.577
26.031	-52.487	-261.286	737.233	516.147	-1770.348
-60.147	130.053	166.336	-1281.960	396.597	2398.761
38.624	-84.389	113.467	546.326	-975.434	-604.696
-16.063	31.715	136.372	-409.430	-202.765	903.925
38.536	-80.298	0.683	621.632	-701.041	-774.108
-24.477	51.777	-146.032	-213.232	938.792	-143.932
-14.561	32.771	378.814	-804.122	-1179.520	2362.669
23.901	-61.333	-897.101	2201.617	2917.499	-6613.666
-9.272	32.552	450.177	-1348.287	-1569.922	4136.598
11.216	-22.676	-470.074	847.247	1406.045	-2479.139
-21.214	46.433	1328.887	-2517.865	-4032.817	7467.301
9.179	-24.964	-812.067	1634.838	2512.790	-4902.992

Table 2 Constants and Functions for Ultimate Strength of Plates

i	c_i	f_i
1	0.2770	$1/B$
2	-0.0524	A/B
3	0.7318	A^2/B
4	0.0219	$1/B^2$
5	0.1040	A/B^2
6	-0.3817	$(A/B)^2$

Table 3 Constants and Functions
for Ultimate Strength of Stiffened Plates

i	c_i	f_i
1	1.39245	$1/B$
2	-0.70797	$1/B^{1.5}$
3	-0.08964	L^3/B
4	0.05749	$L^3/B^{1.5}$
5	0.00840	R/B
6	0.02572	$R/B^{1.5}$
7	0.43471	RL^3/B
8	-0.40420	$RL^3/B^{1.5}$
9	-0.39092	G/B
10	0.29638	$G/B^{1.5}$
11	-0.14615	GL^3/B
12	0.11133	$GL^3/B^{1.5}$
13	2.04053	RG/B
14	-1.63433	$RG/B^{1.5}$
15	0.25601	RGL^3/B
16	0.00054	$RGL^3/B^{1.5}$

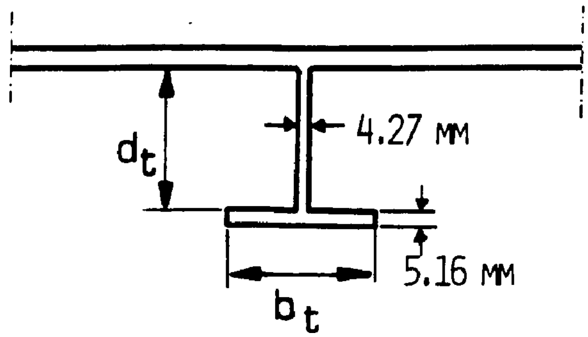

Table 4 Dimensions of Transverse Stiffeners

Sample	Number of Stiffener Longitudinal	Transverse	d_t (mm)	b_t (mm)
G11-A	2	2	74.17	99.82
G11-B	2	2	23.37	23.62
G11-C	2	2	20.83	21.08
G11-D	2	2	18.29	18.54
G11-E	2	2	15.75	16.00
G11-F	2	2	5.59	5.84
G21-B	4	2	23.37	23.62
G12-F	2	4	5.59	5.84

FIGURES

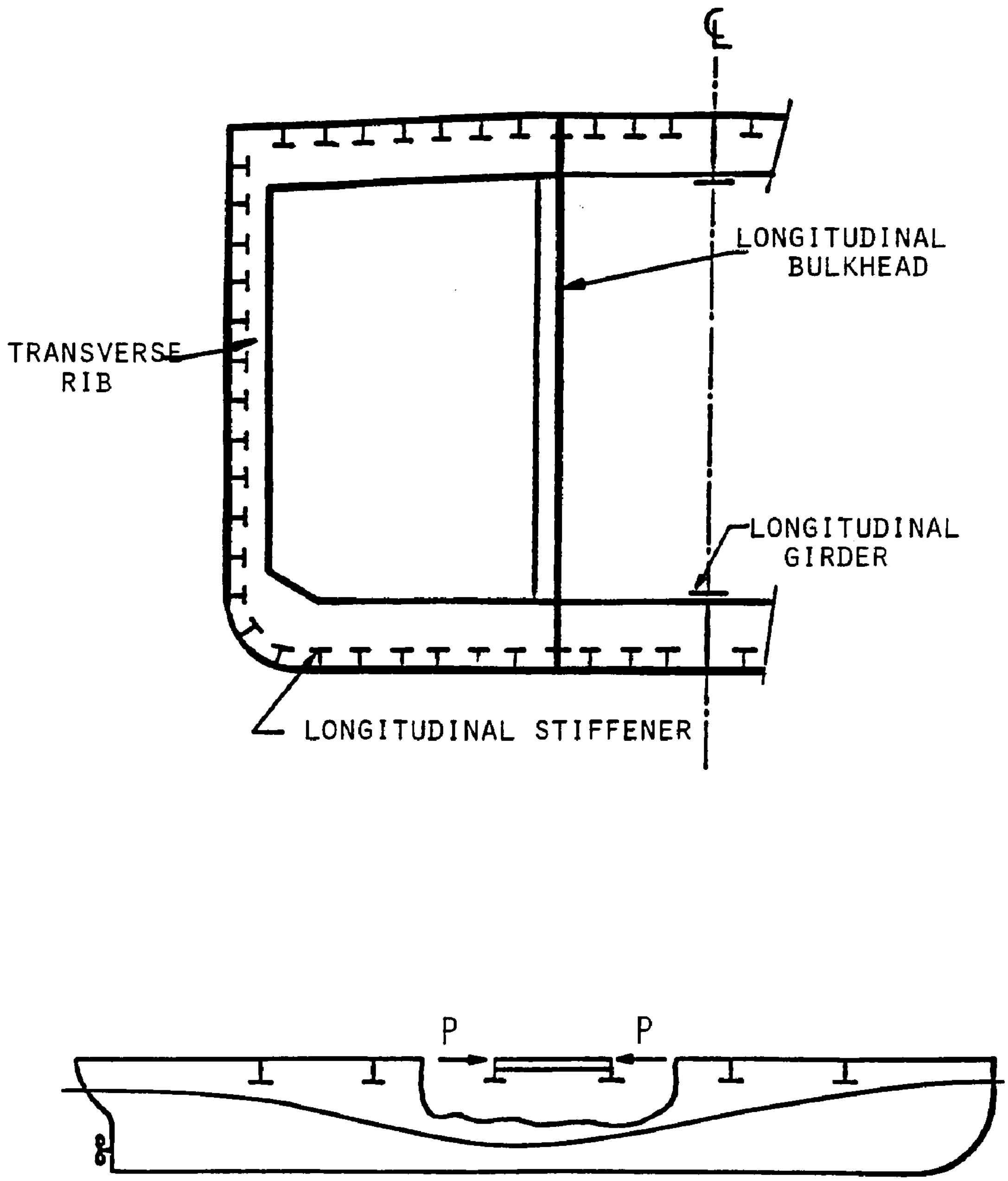

Fig. 1 Typical Cross Section and Component Element of Ship Hull

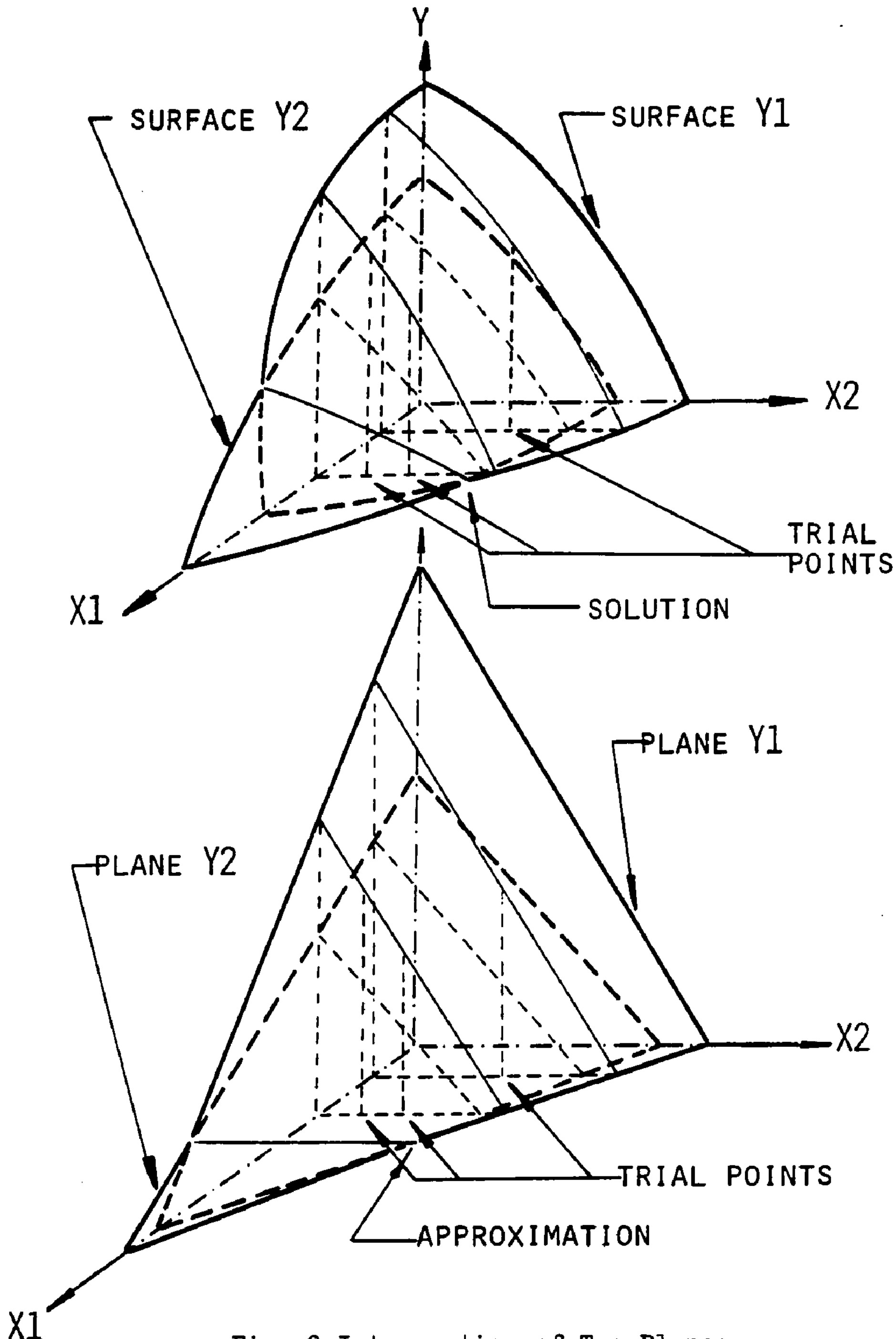

Fig. 2 Intersection of Two Planes

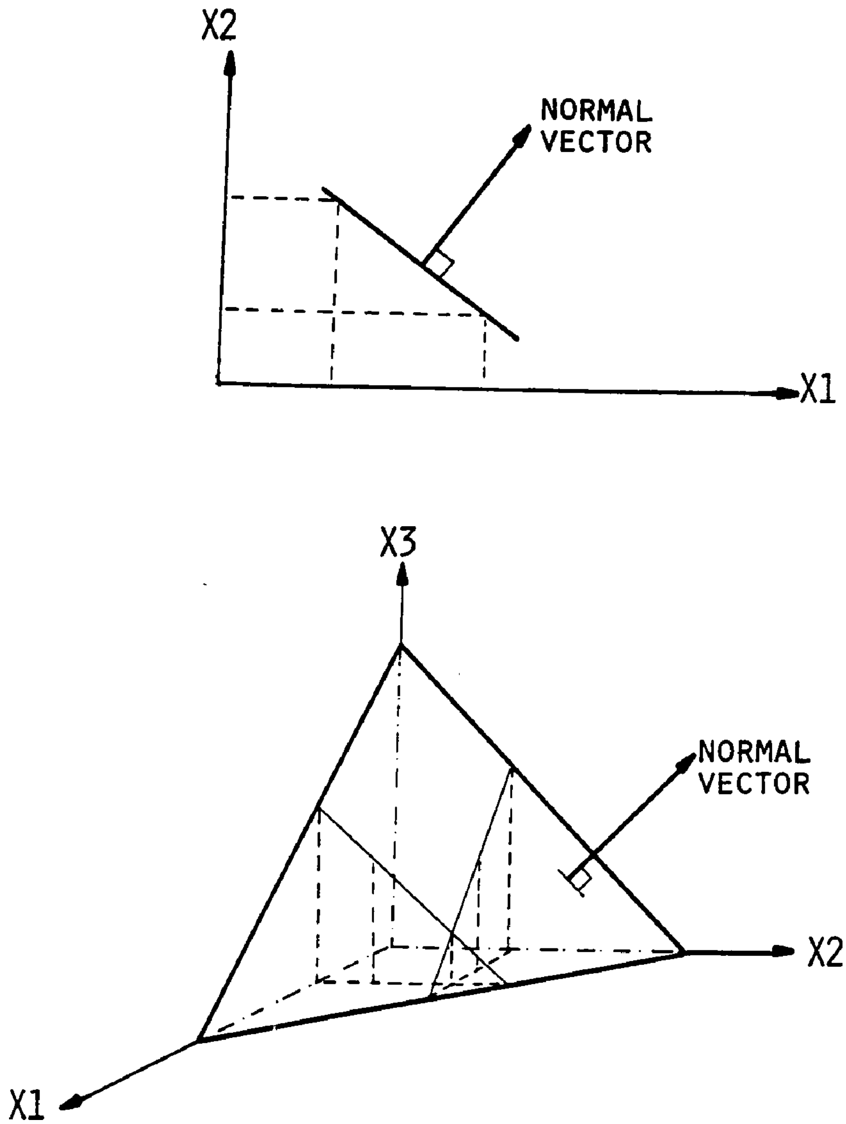

Fig. 3 Two- and Three-Dimensional Subspaces

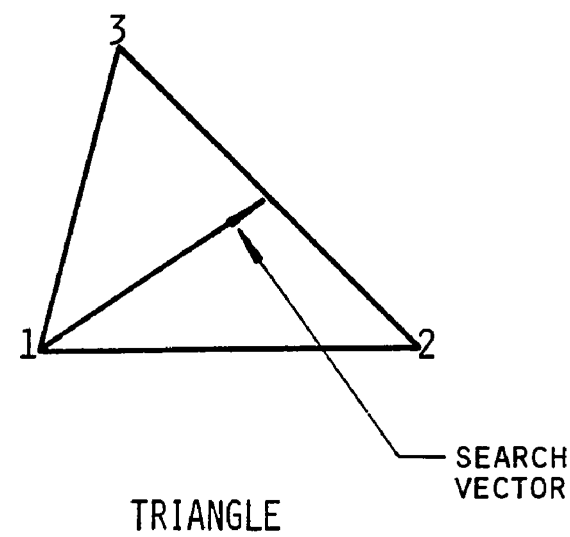

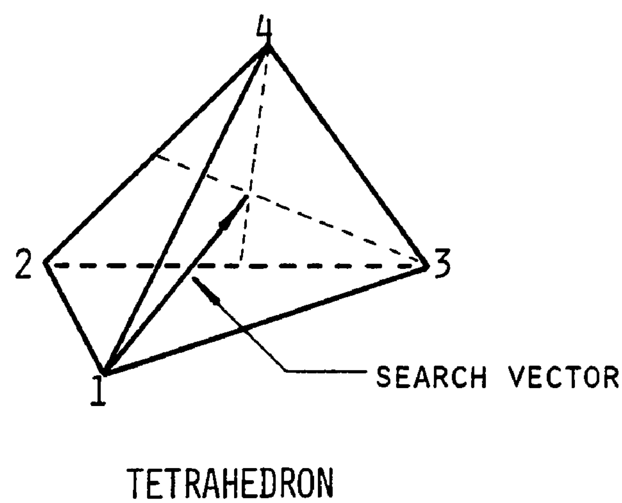

Fig. 4 Polyhedron

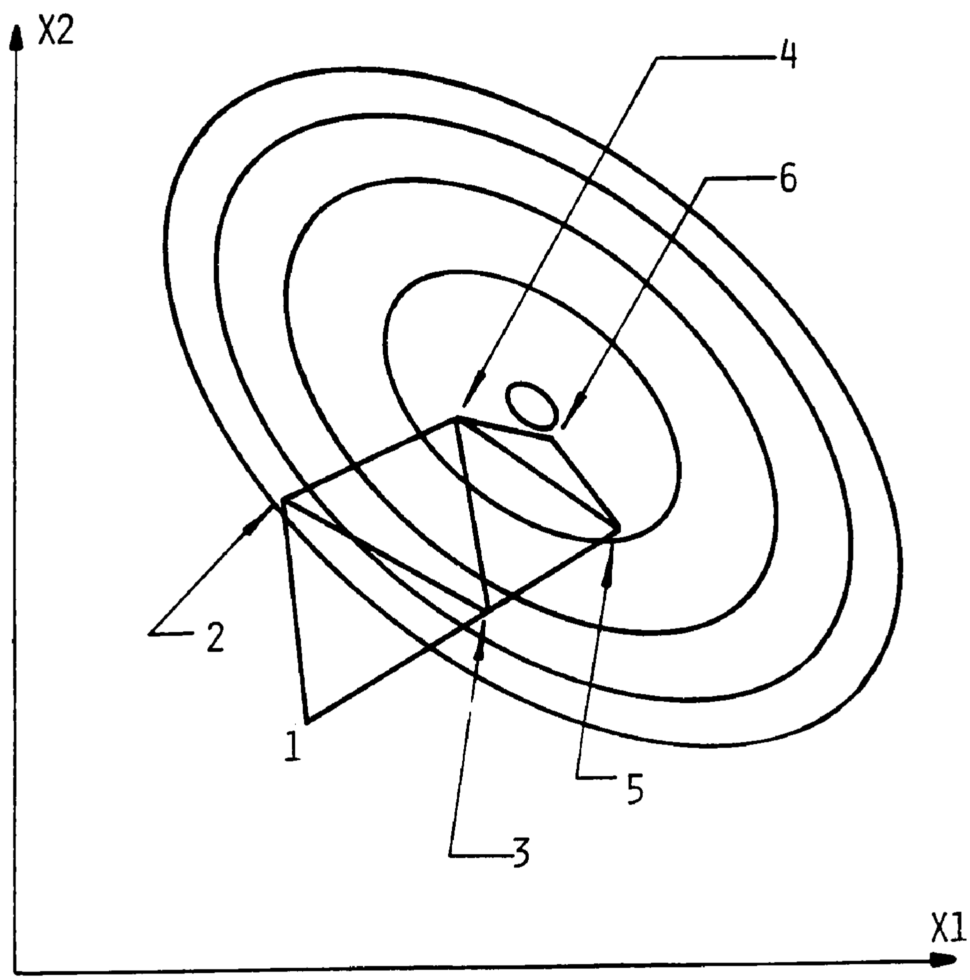

Fig. 5 Two Dimensional Polyhedron Search (Triangle)

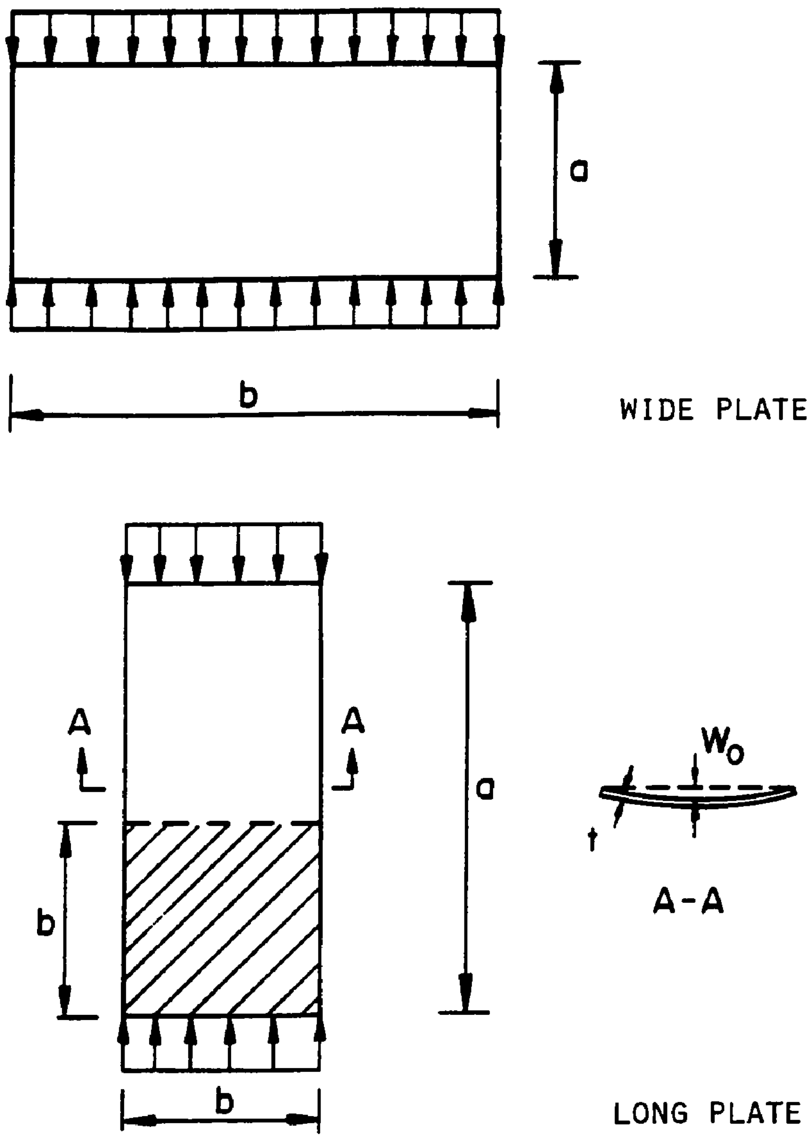

Fig. 6 Wide and Long Plates

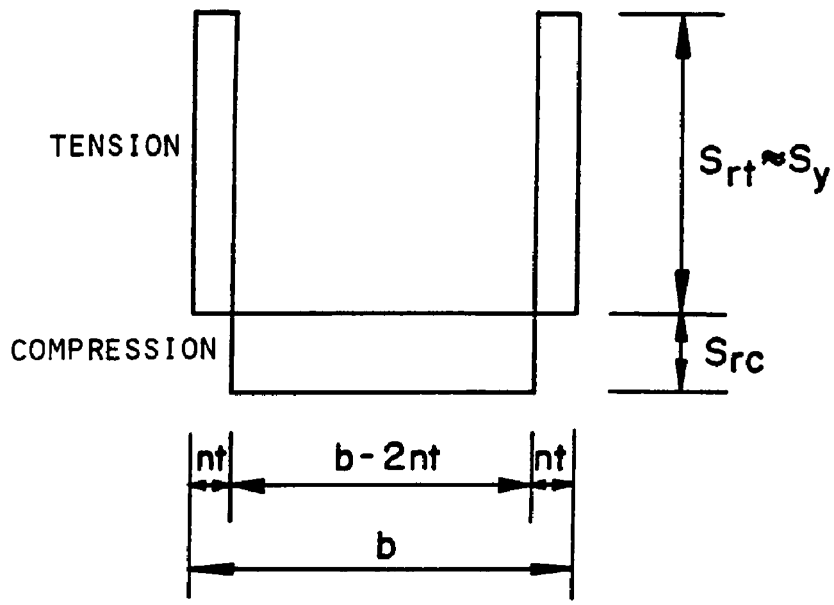

Fig. 7 Typical Residual Stress Pattern

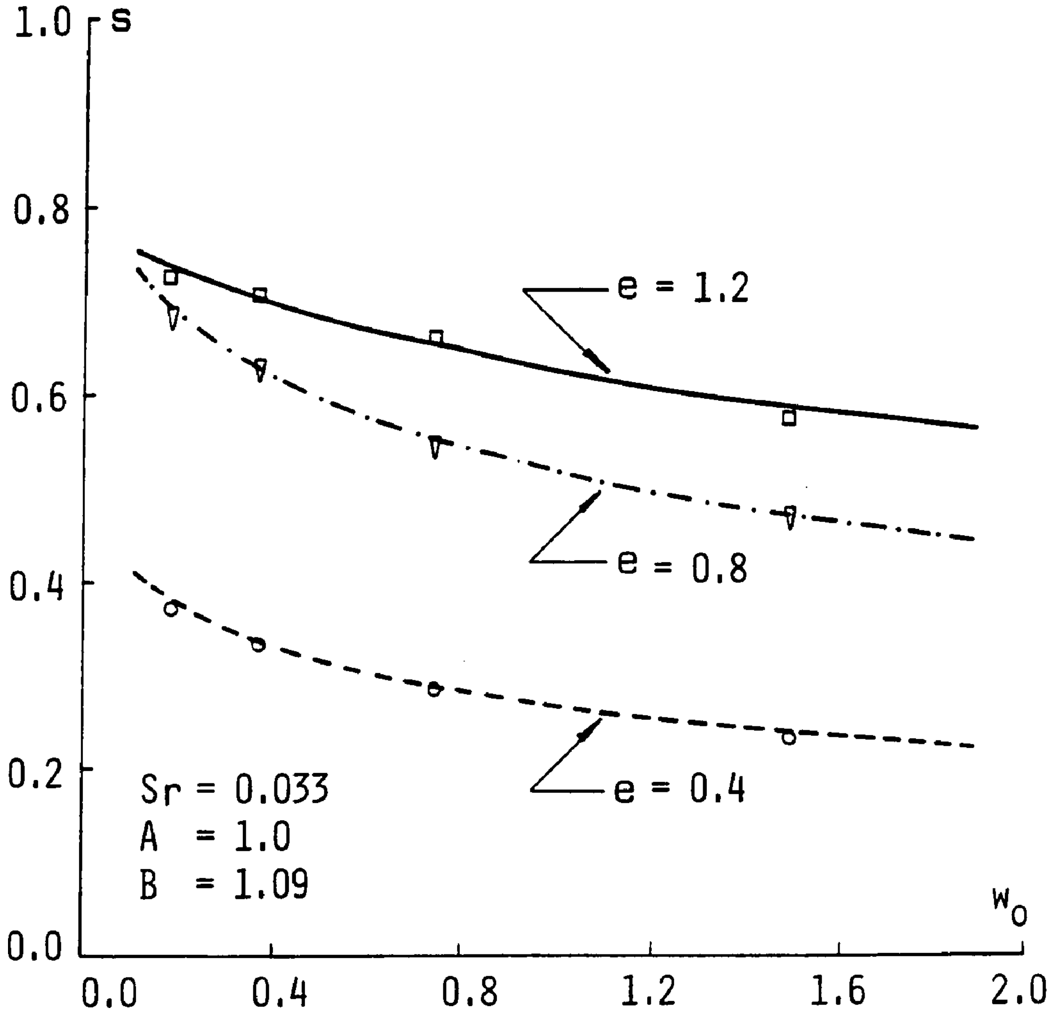

Fig. 8 Parametric Study for Stress-Strain of Plates
(Effect of Initial Deformation)

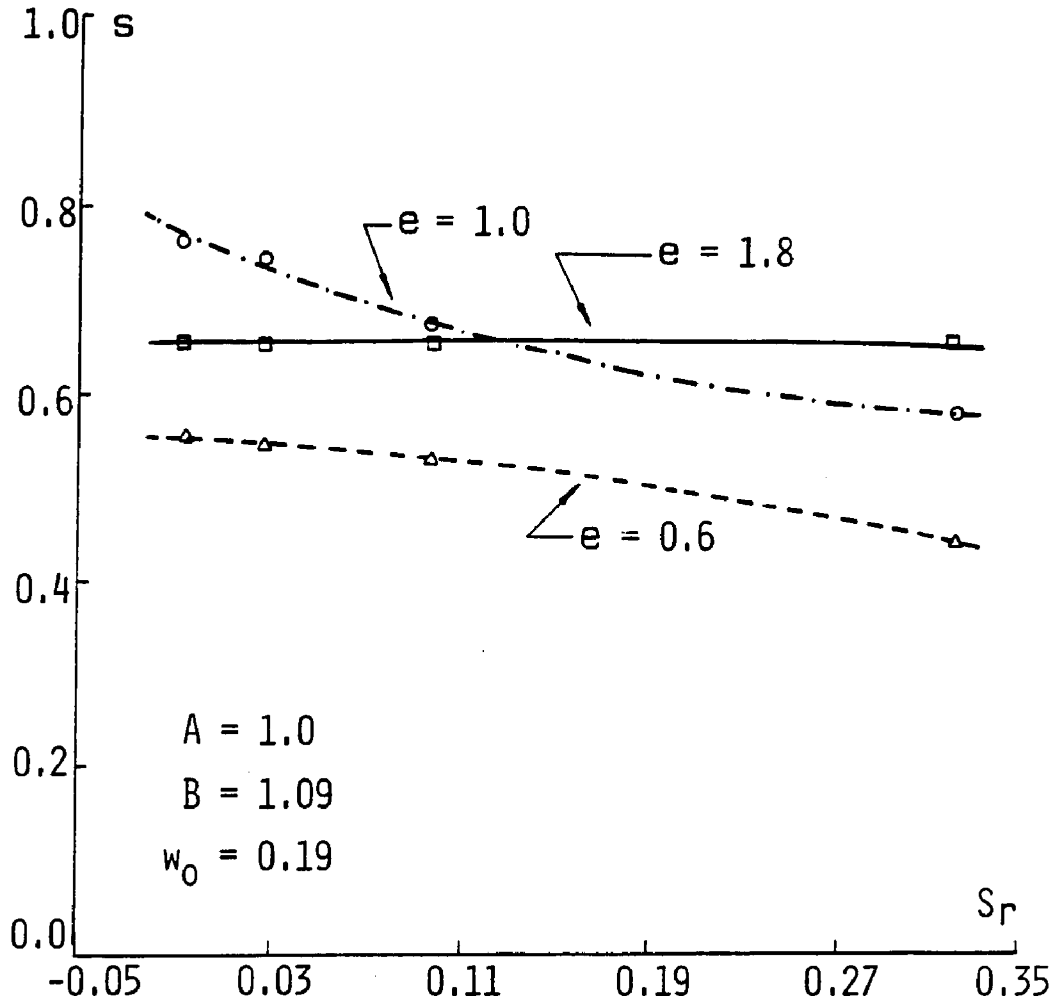

Fig. 9 Parametric Study for Stress-Strain of Plates
(Effect of Residual Stress)

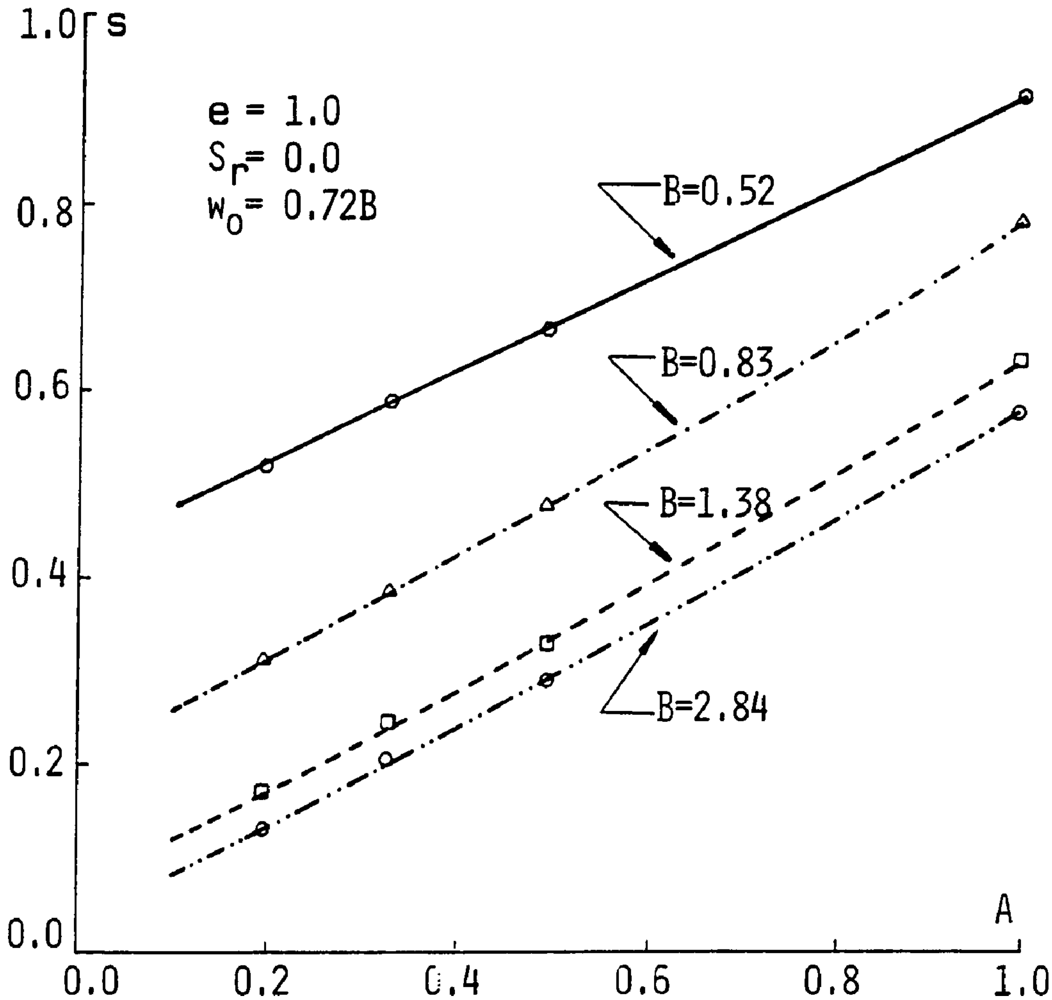

Fig. 10 Parametric Study for Stress-Strain of Plates
(Effect of Aspect Ratio)

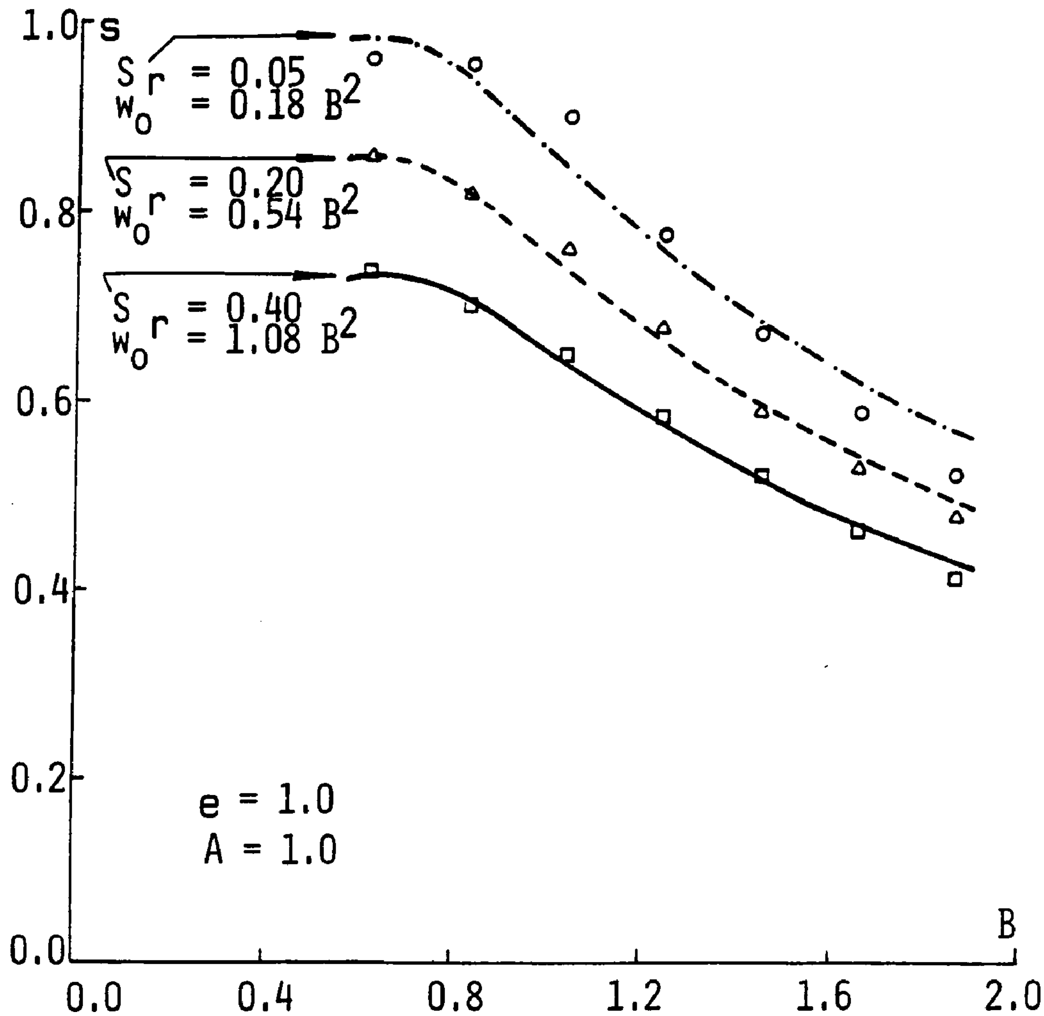

Fig. 11 Parametric Study for Stress-Strain of Plates
(Effect of slenderness Ratio)

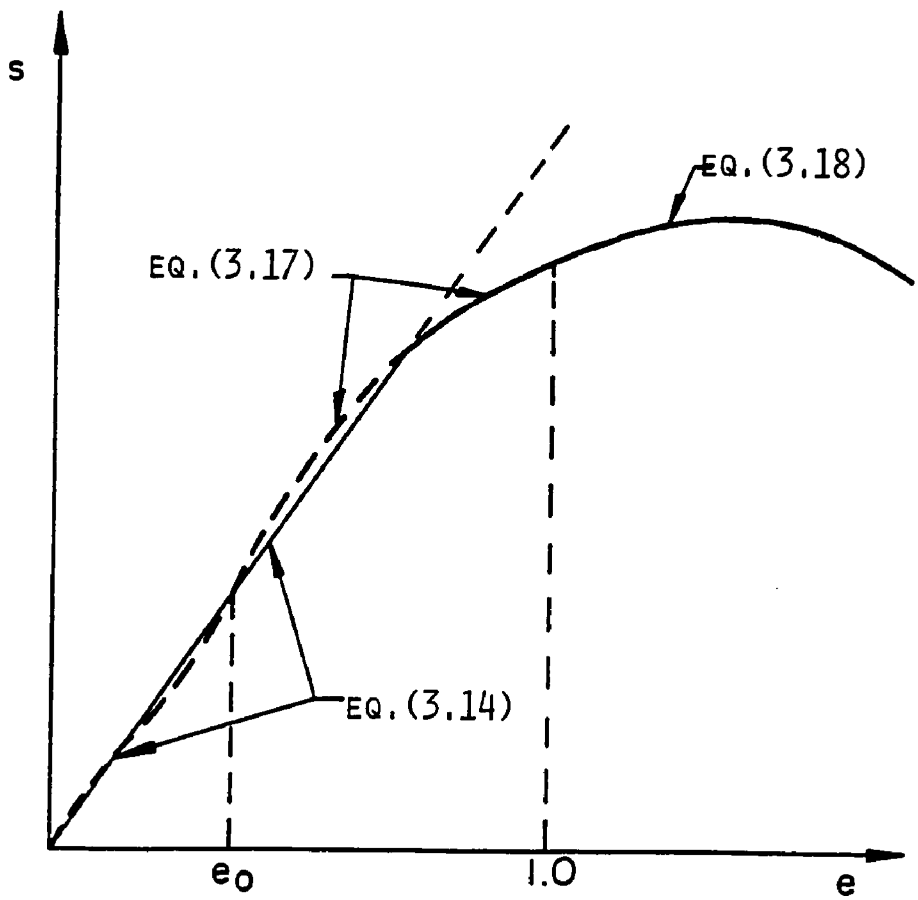

Fig. 12 Stress-Strain Curve for Plates
(Range of Application for Various Strain Levels)

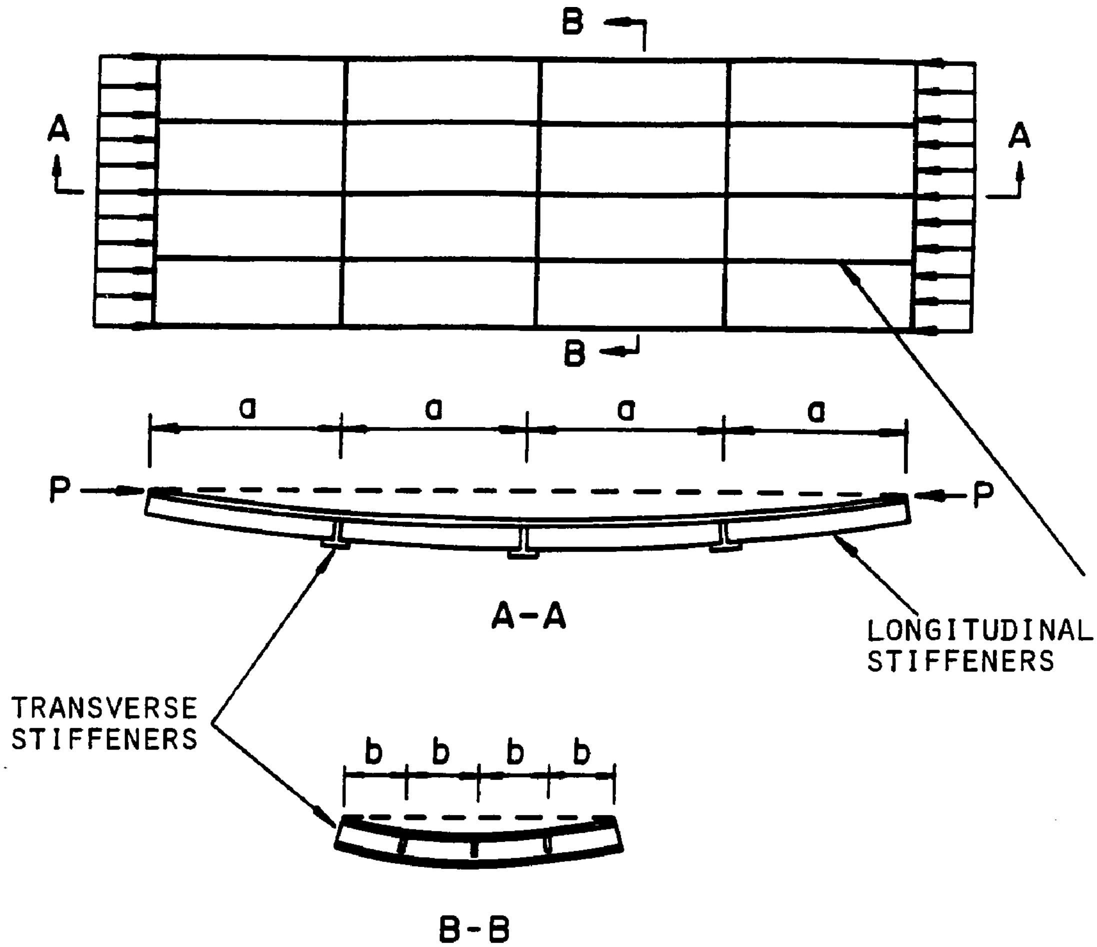

Fig. 13 Grillage

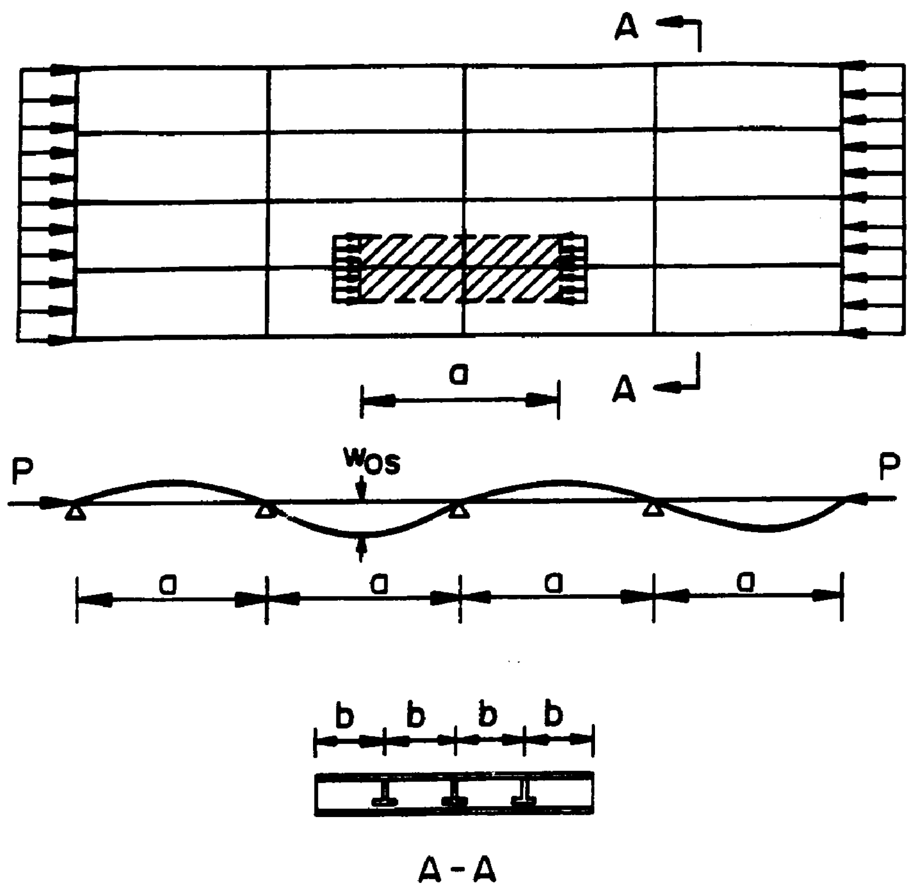

Fig. 14 Stiffened Plate

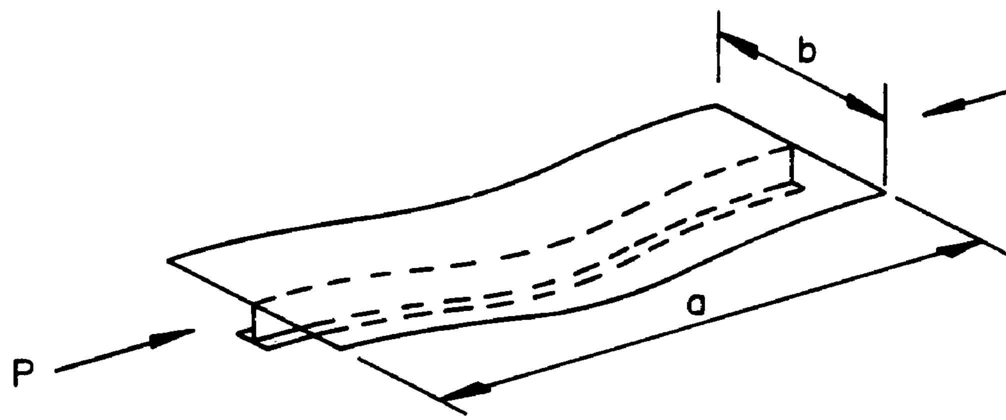

Fig. 15 Stiffened Plate Idealization

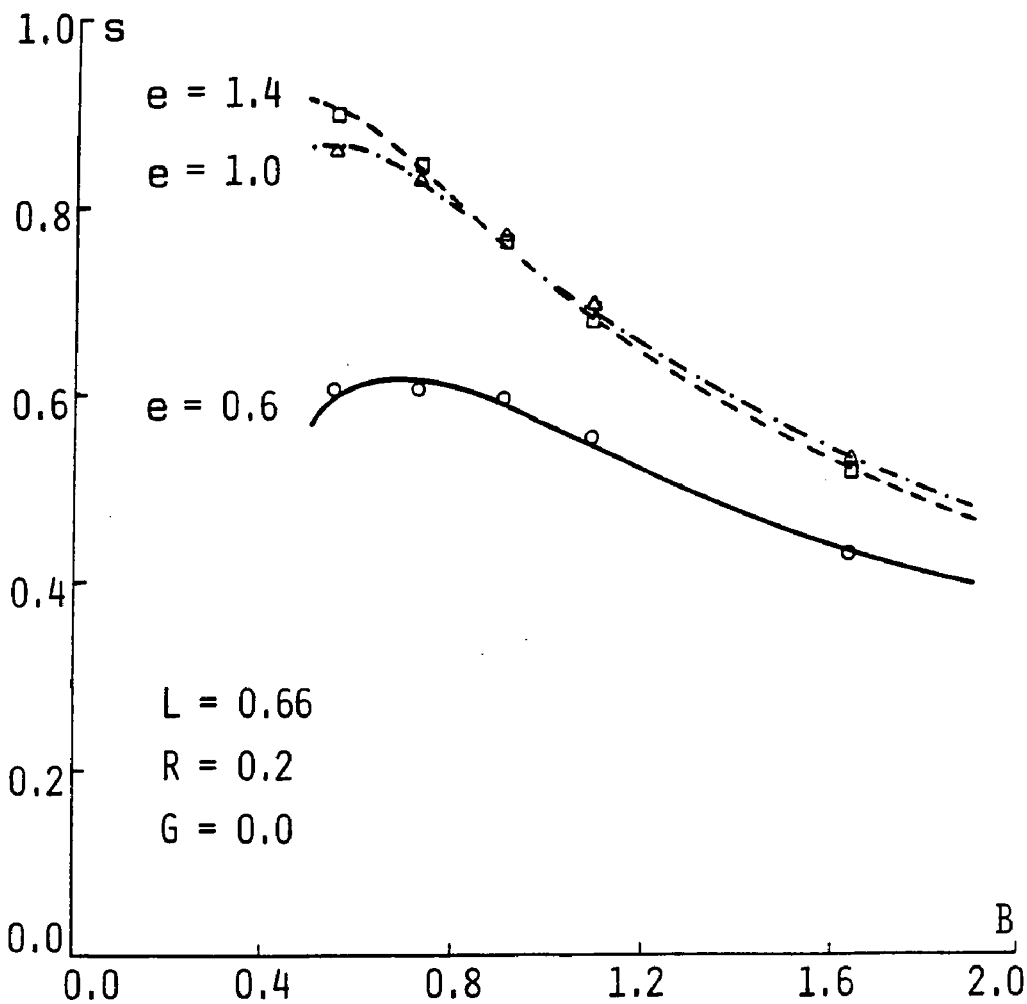

Fig. 16 Parametric Study for Stress-Strain of Stiffened Plates
(Effect of Plate Slenderness Ratio)

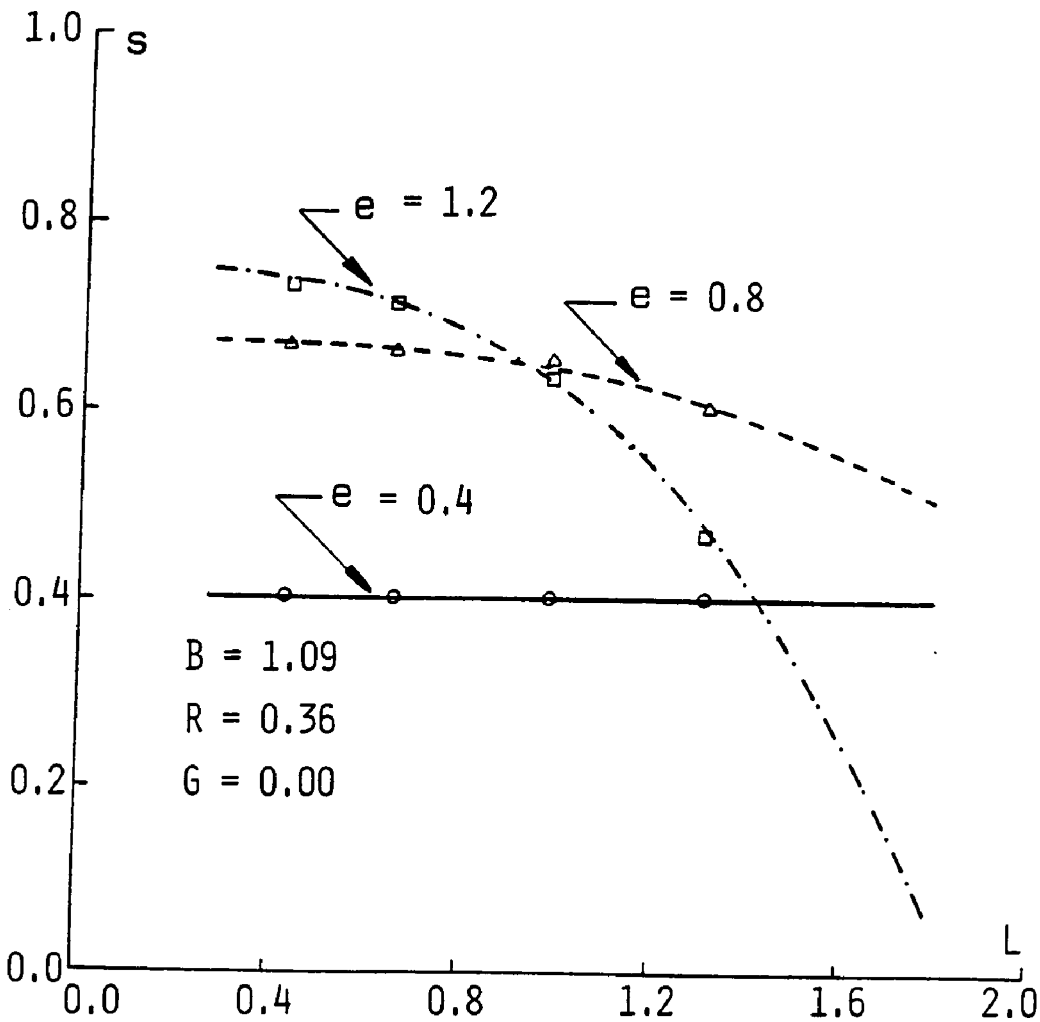

Fig. 17 Parametric Study for Stress-Strain of Stiffened Plates
(Effect of Panel Slenderness Ratio)

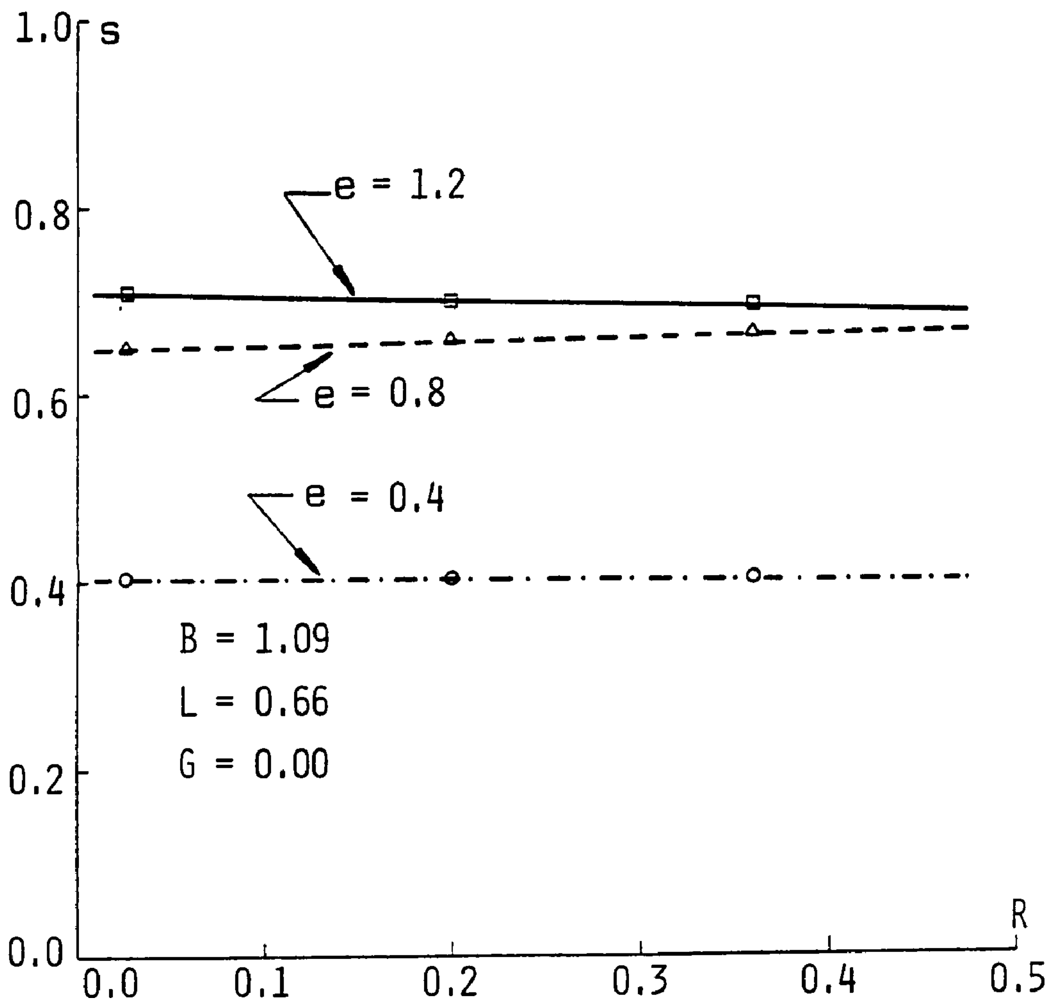

Fig. 18 Parametric Study for Stress-Strain of Stiffened Plates
(Effect of Stiffener-Plate Area Ratio)

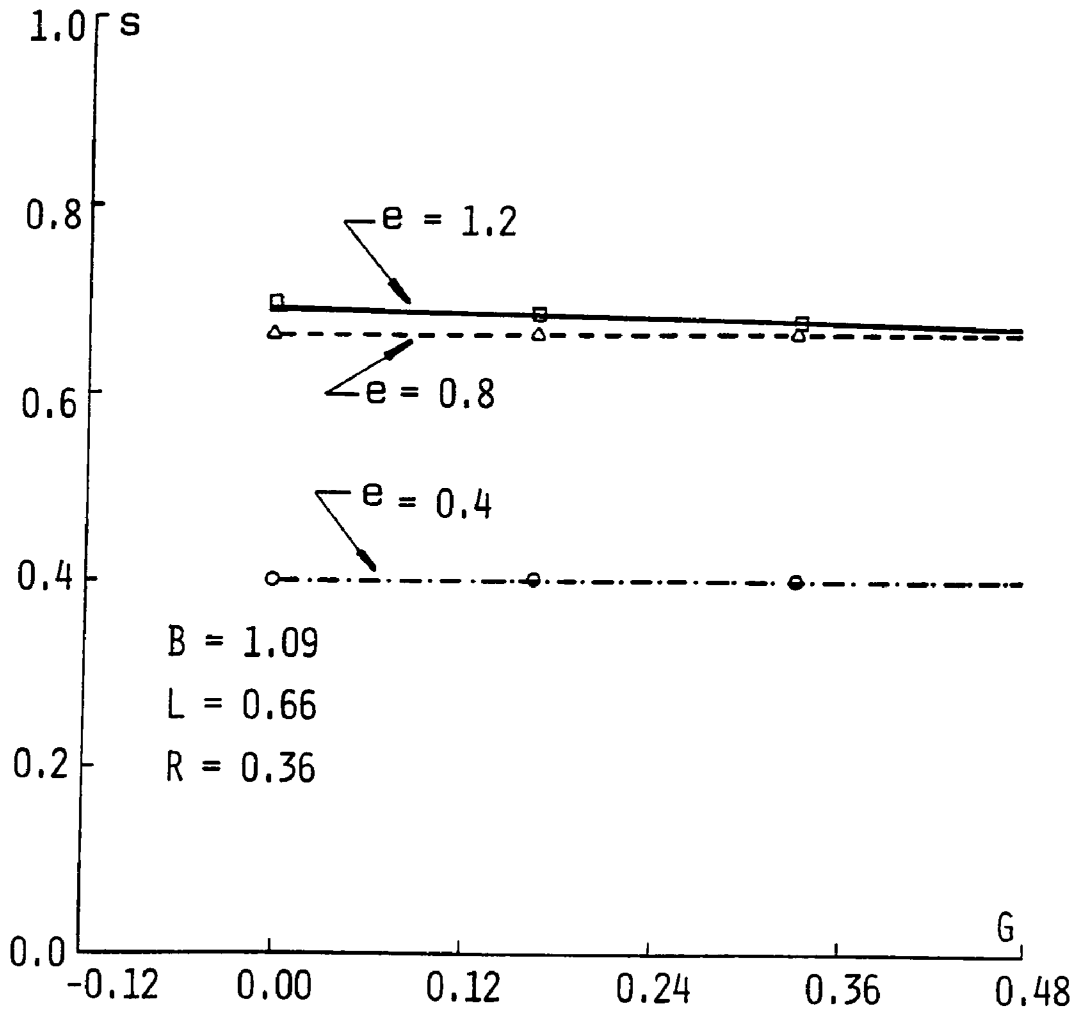

Fig. 19 Parametric Study for Stress-Strain of Stiffened Plates
(Effect of Flange-Web Area Ratio)

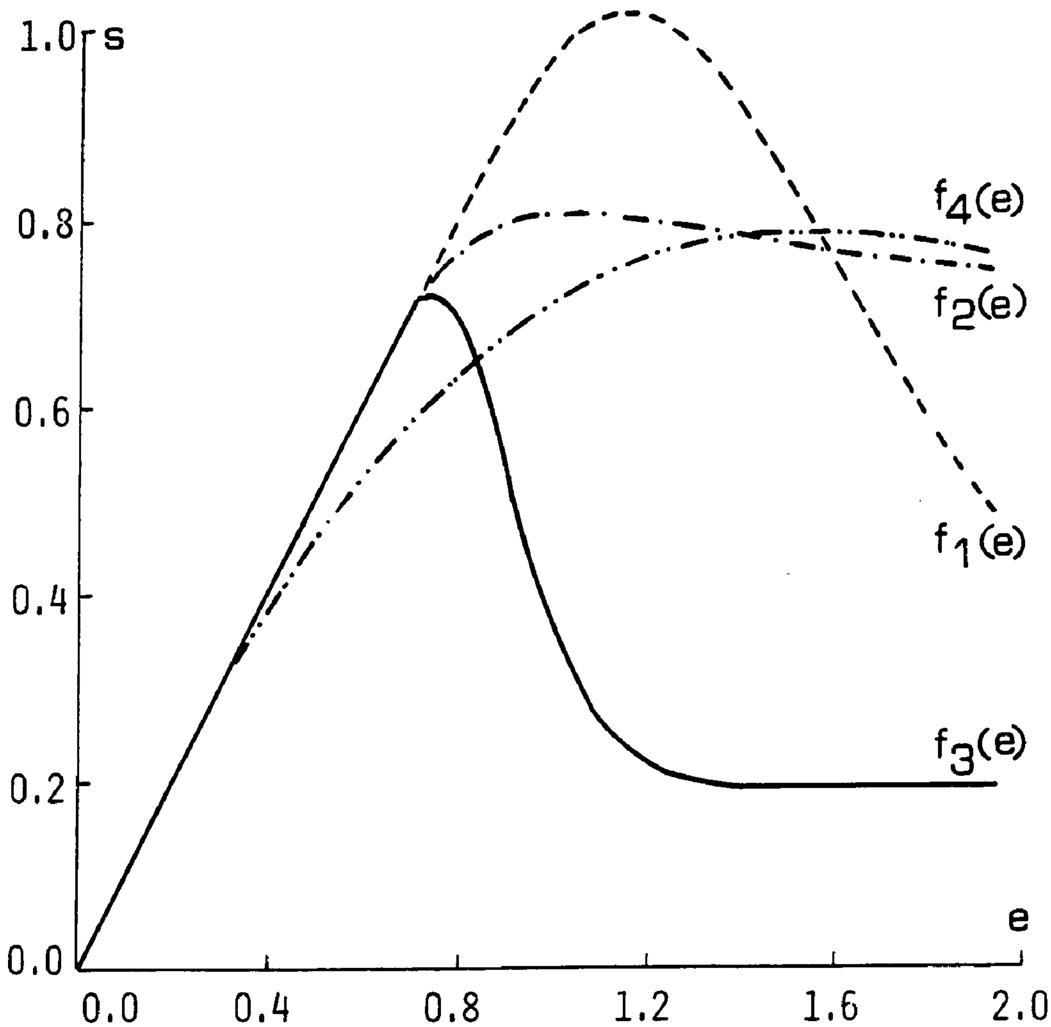

Fig. 20 Individual Functions of Relative Strain e for Stiffened Plates

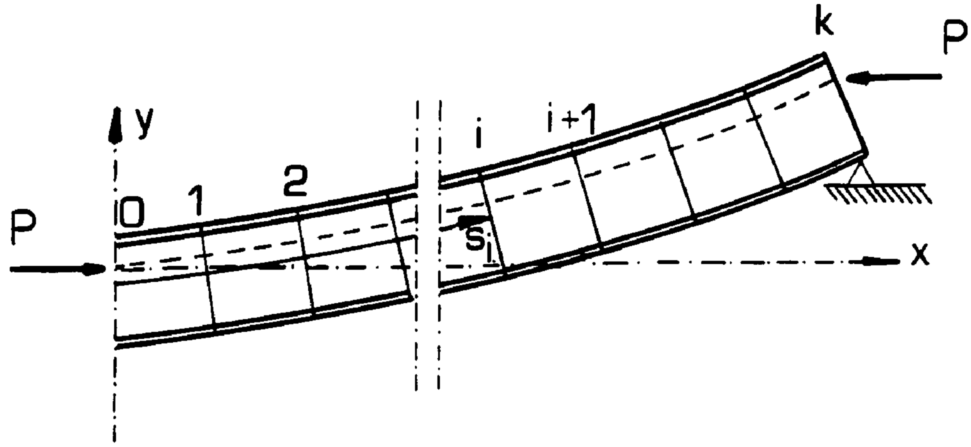

LONGITUDINAL SEGMENTS

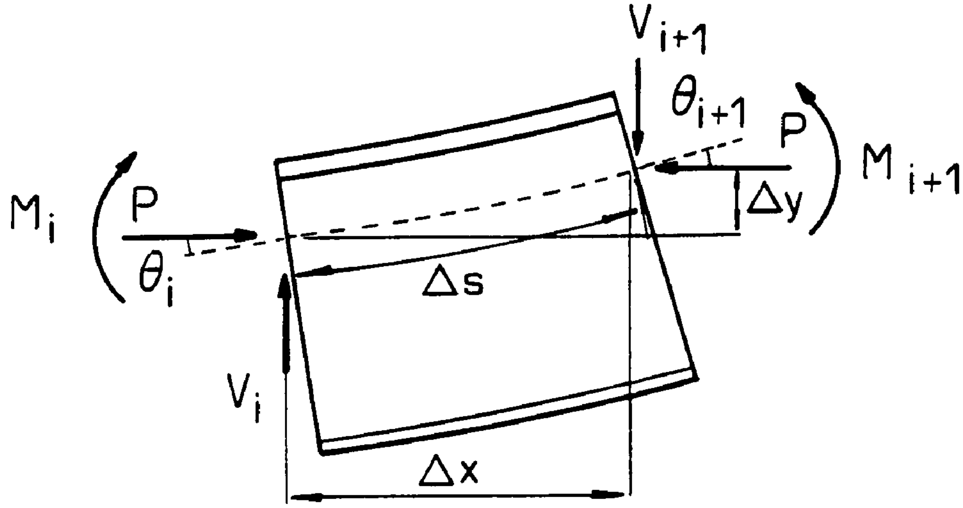

POSITIVE DIRECTIONS

Fig. 21 Segments of the Longitudinal Stiffener

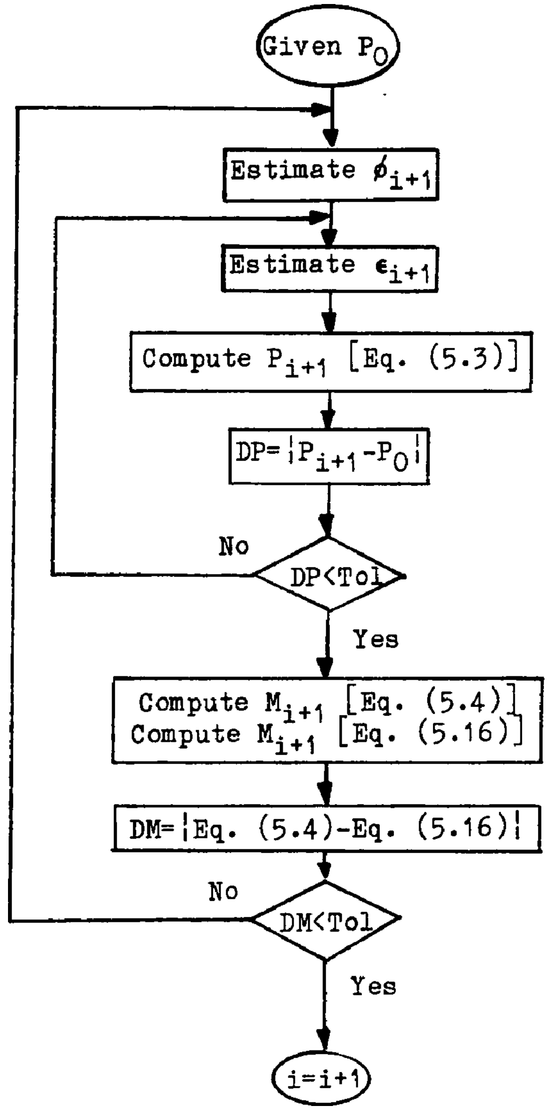

Fig. 22 Iteration to Impose Equilibrium in the Longitudinal Segments

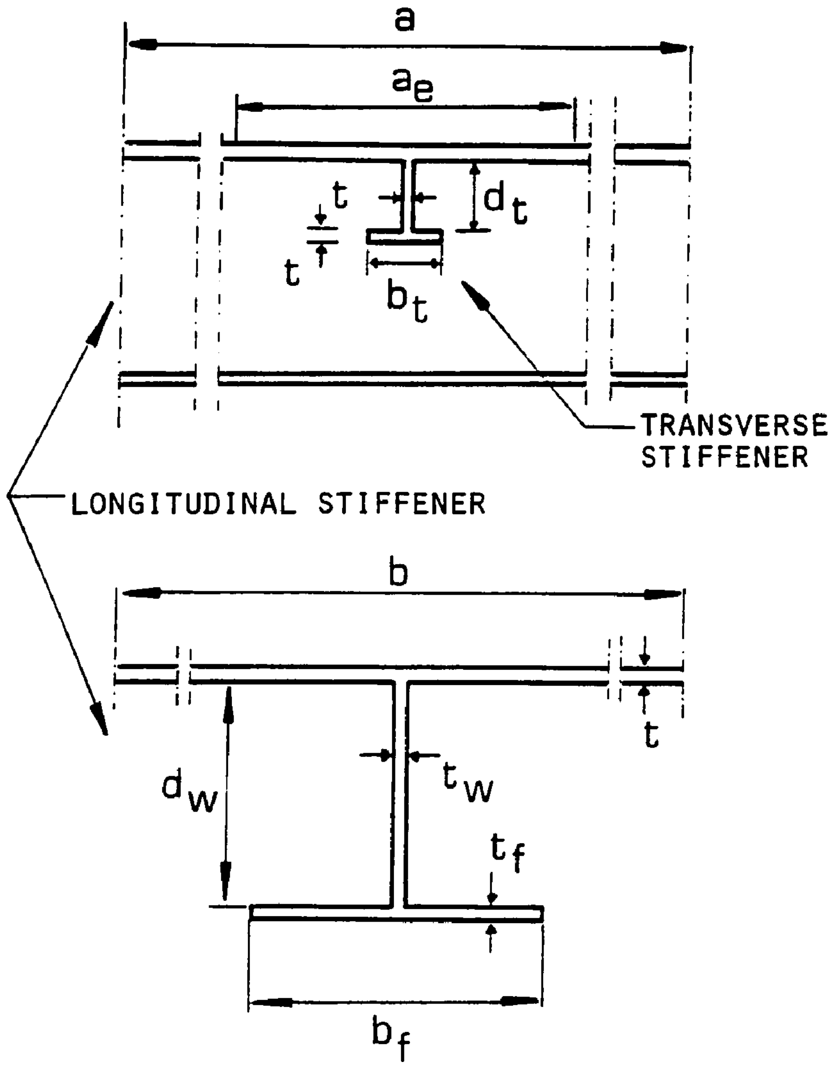

Fig. 23 Cross Section of Stiffeners

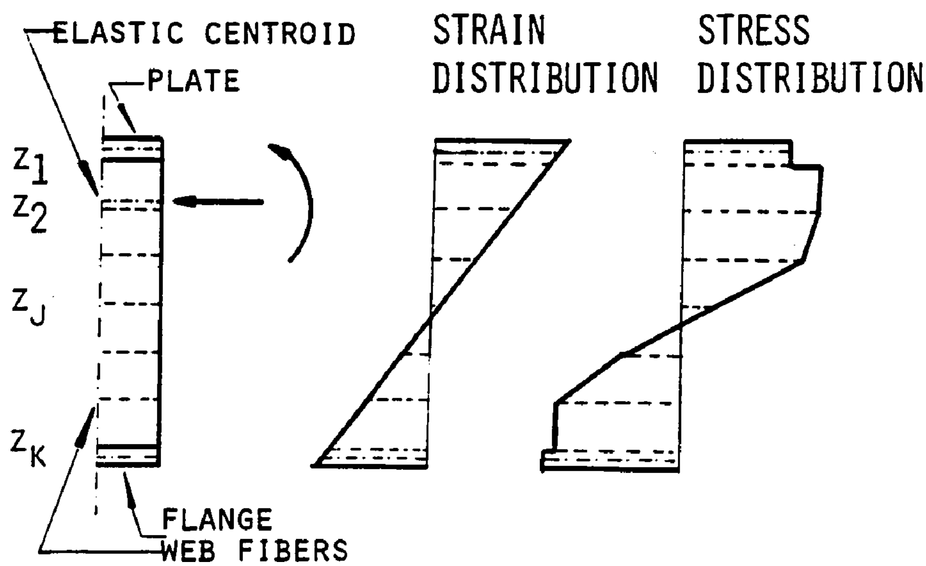

Fig. 24 Stress Distribution in a Longitudinal Cross Section

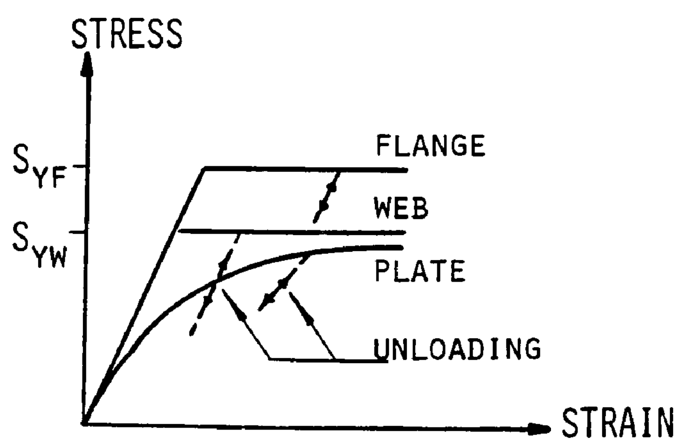

Fig. 25 Material Stress-Strain Curves

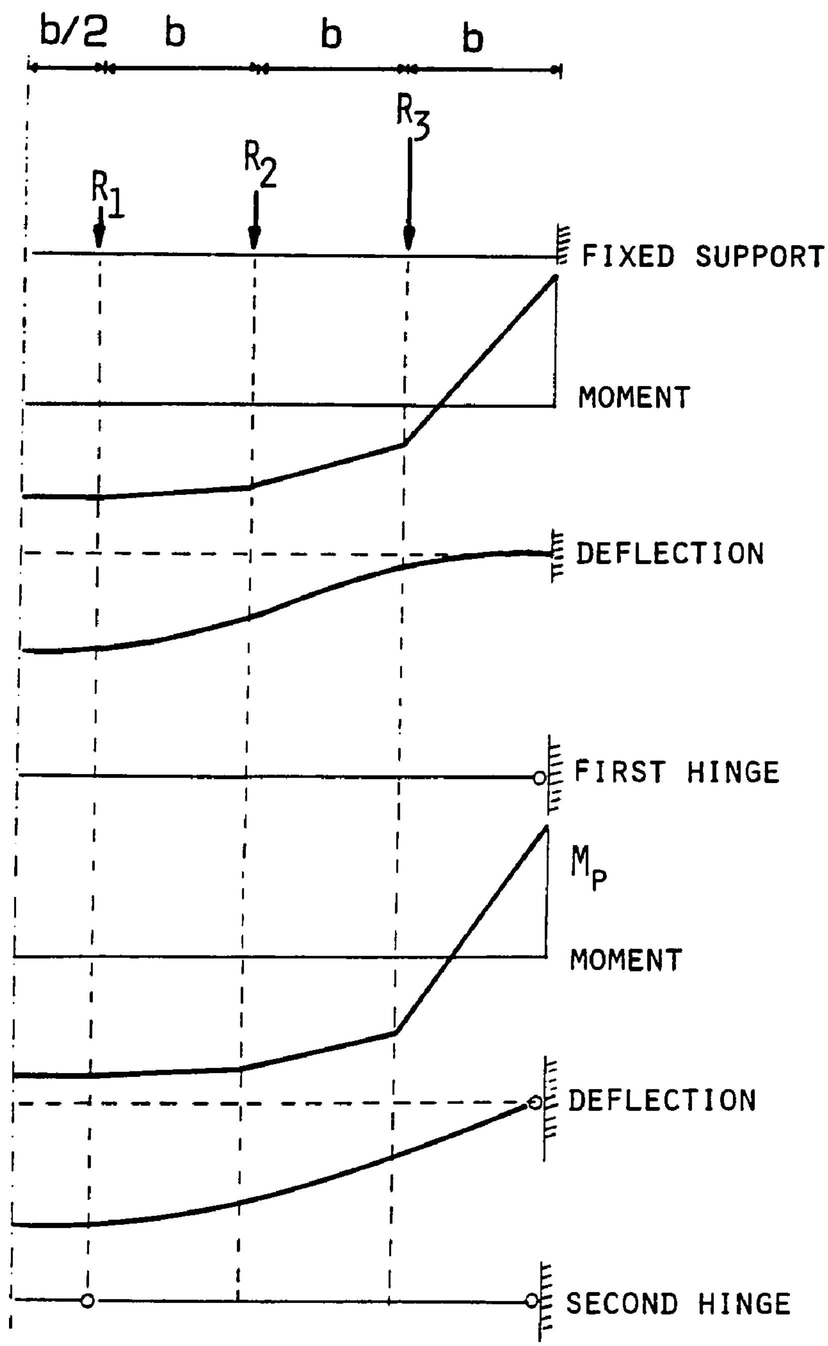

Fig. 26 Transverse Stiffener

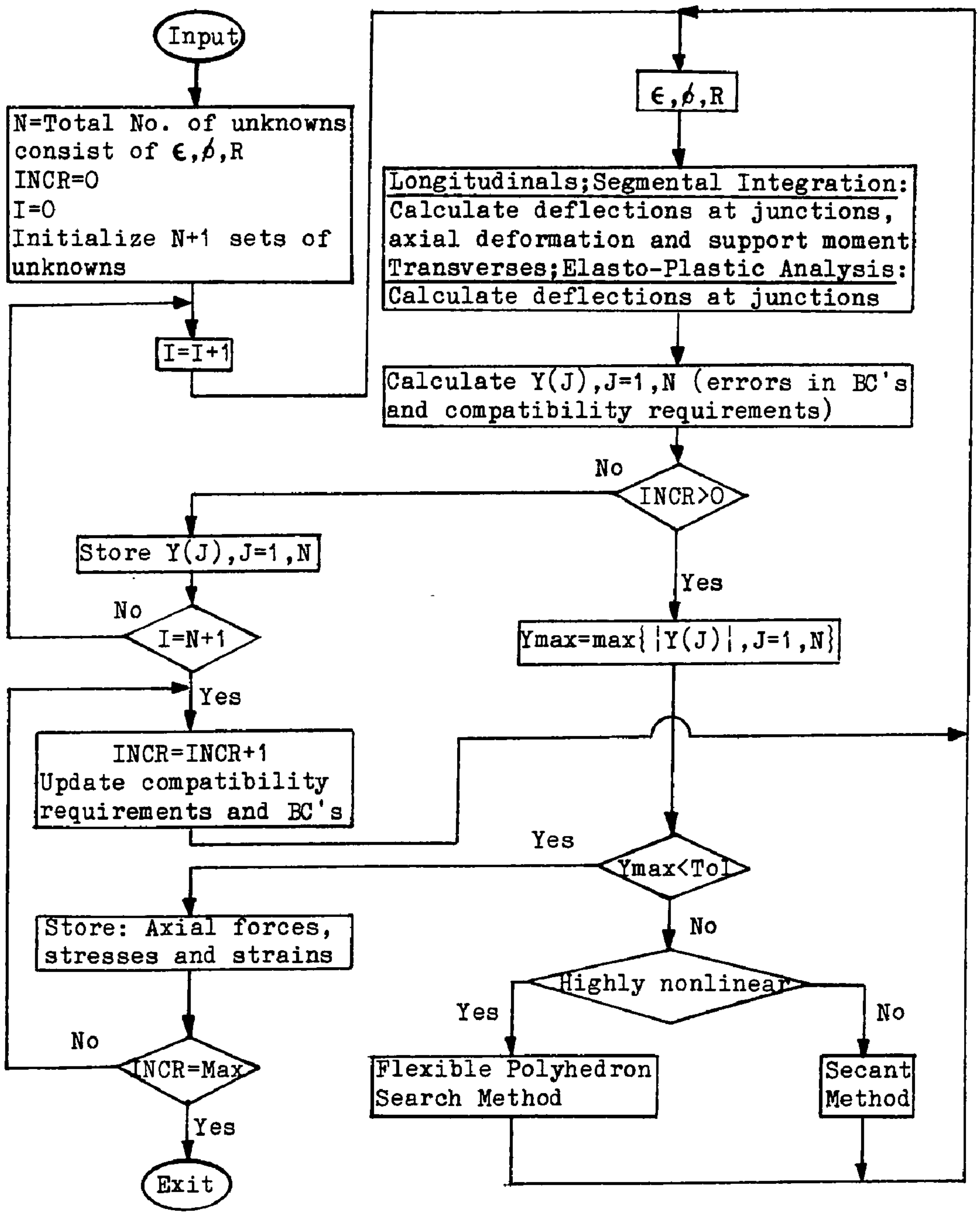

Fig. 27 Flowchart of the Computer Program for Grillage

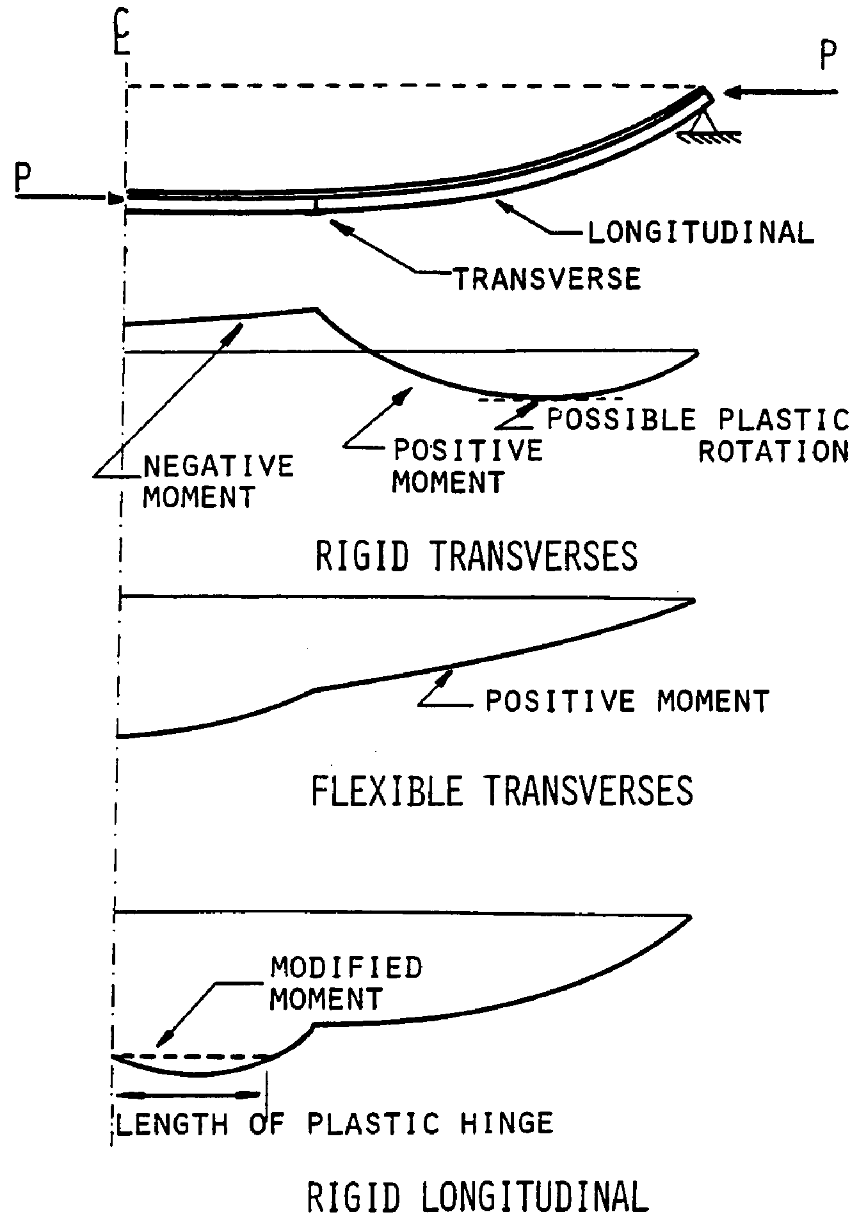

Fig. 28 Bending Moment Diagram Along a Longitudinal Stiffener

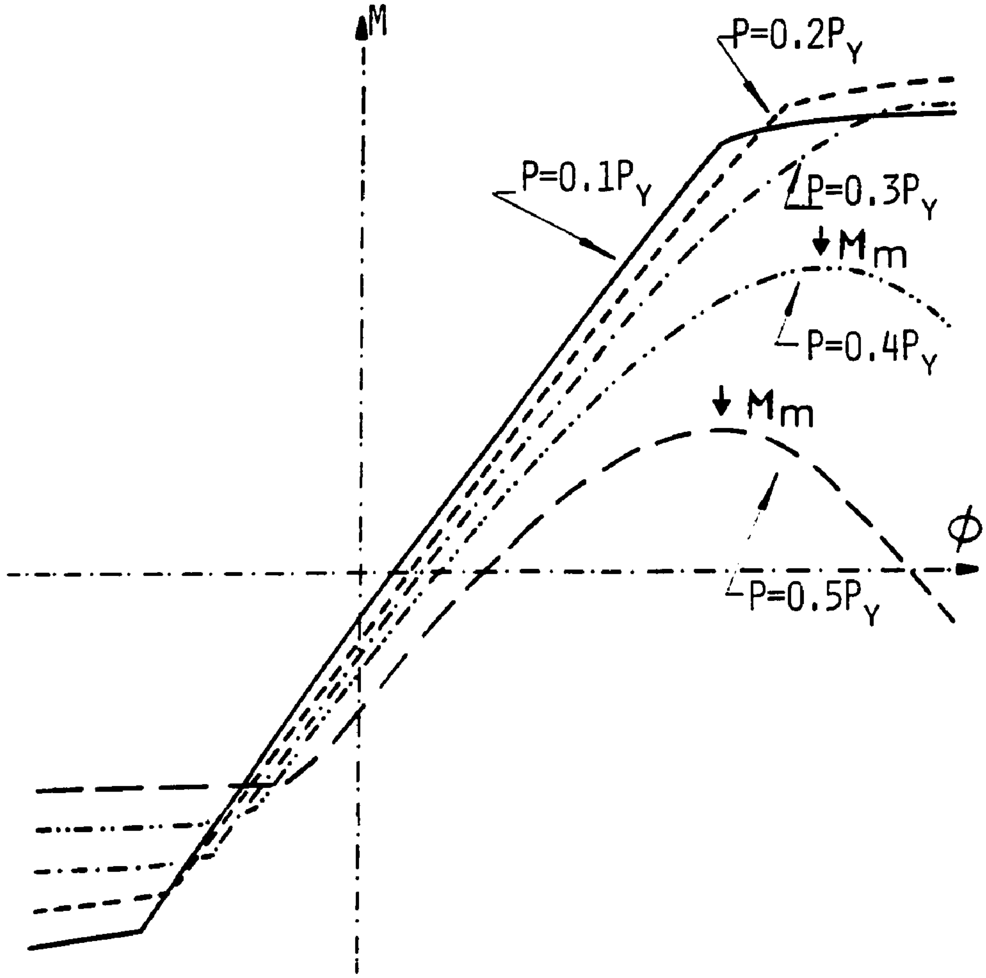

Fig. 29 Moment-Curvature Relationship

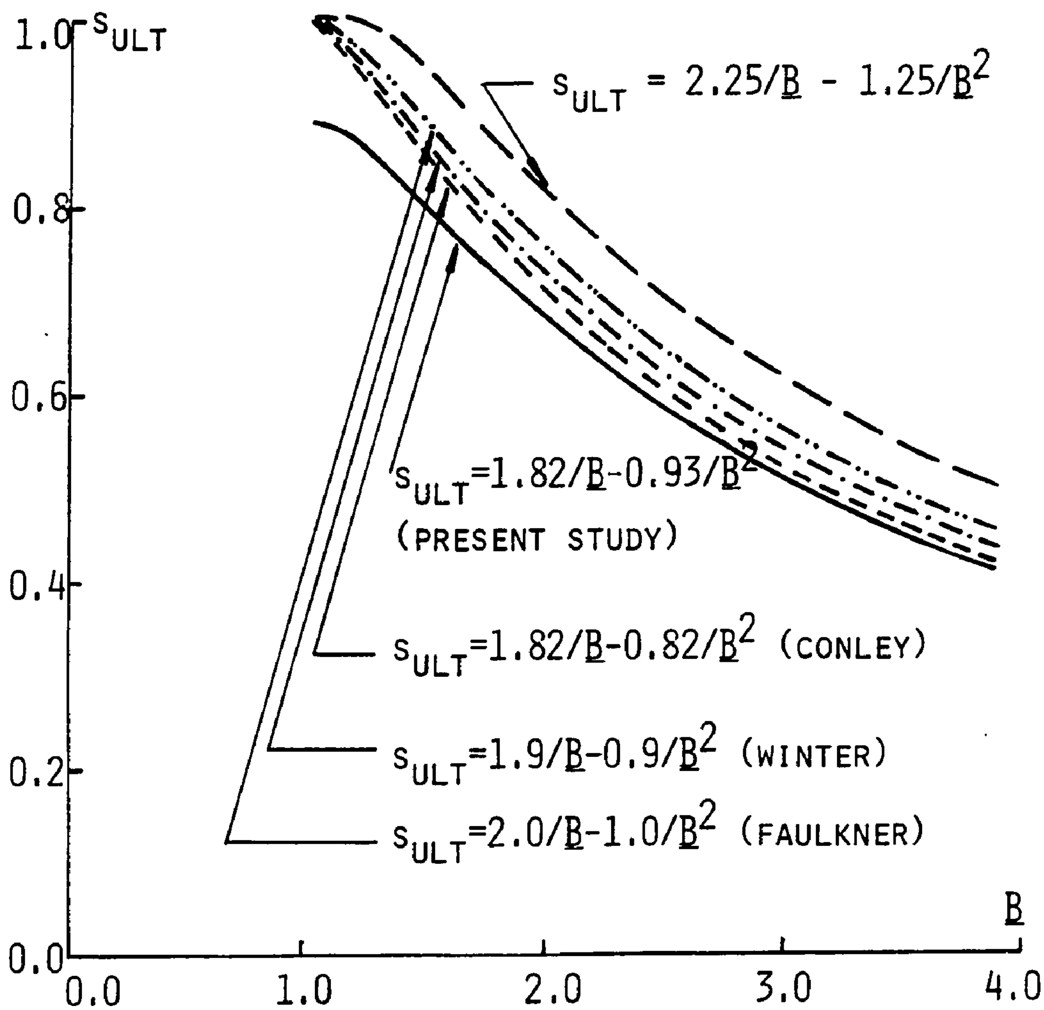

Fig. 30 Design Ultimate Strength Curves
(For square and long plates)

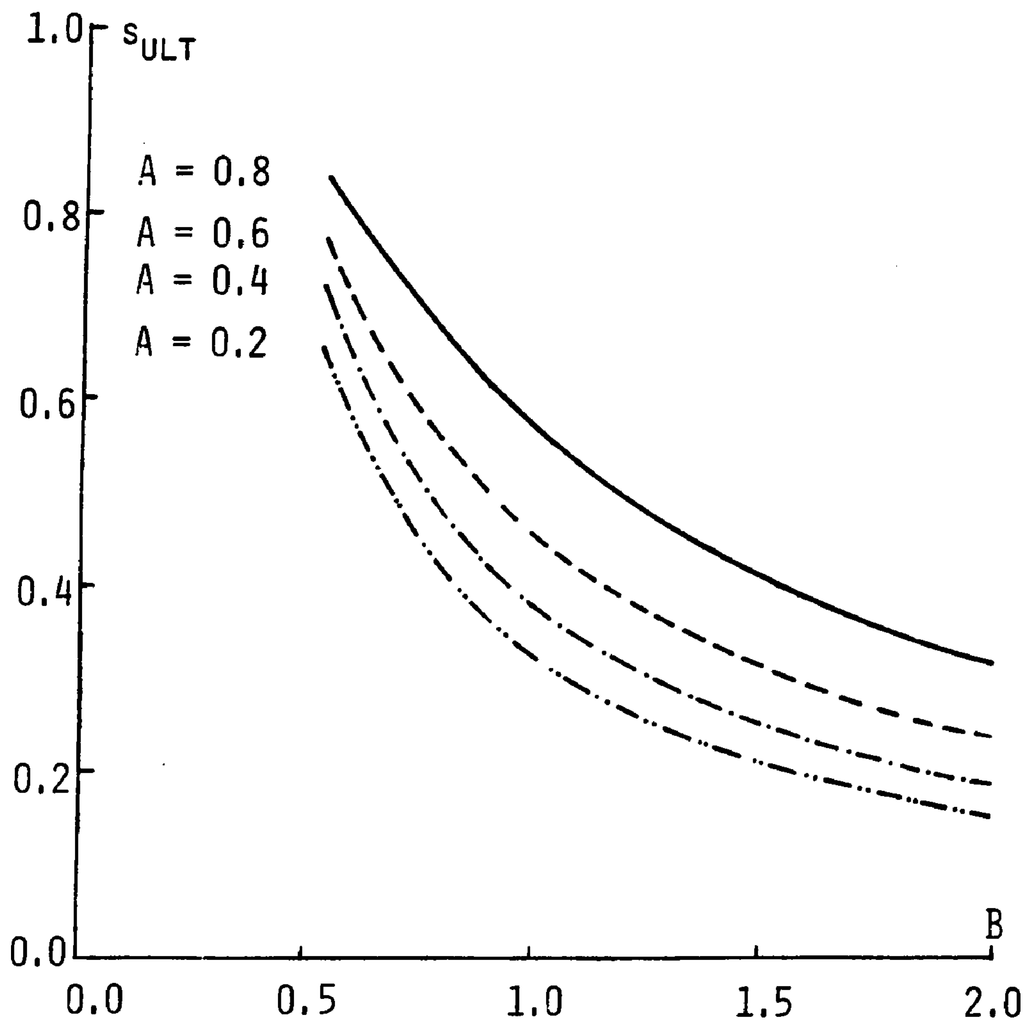

Fig. 31 Ultimate Strength of Wide Plates

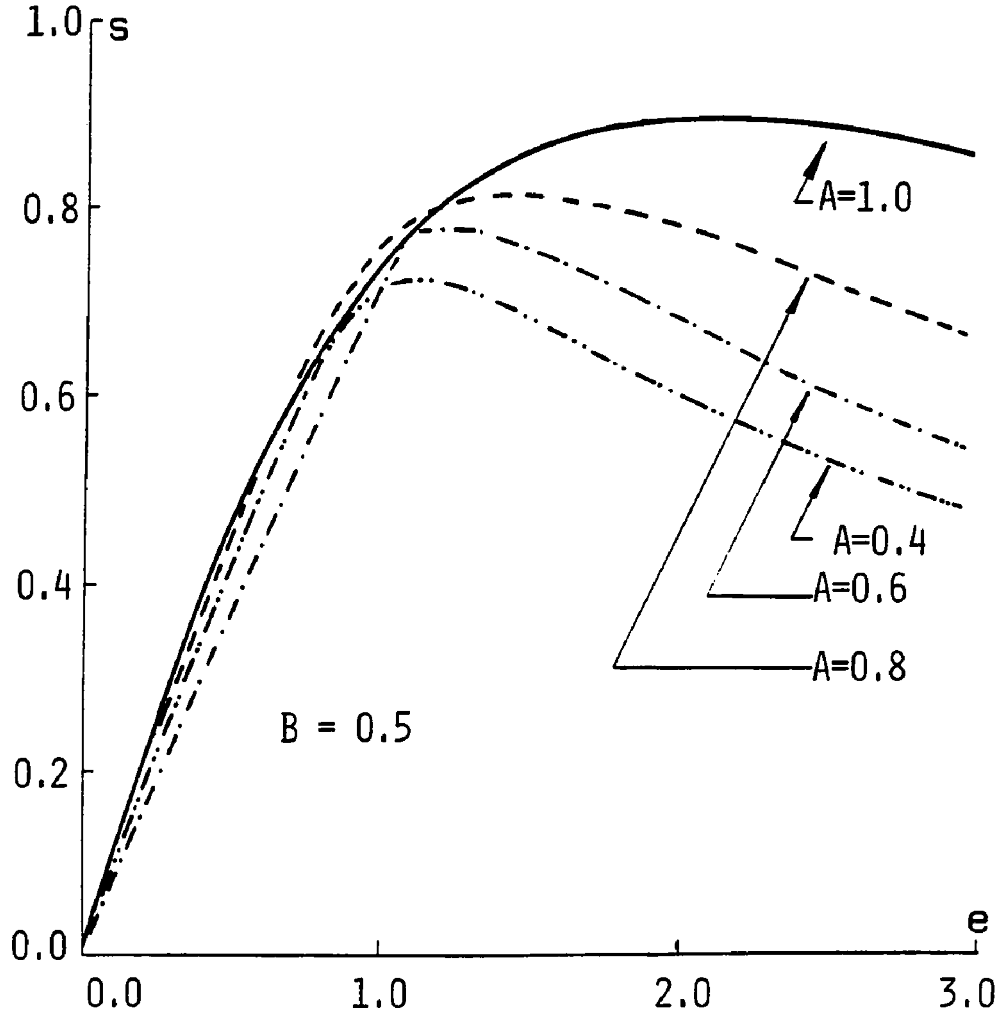

Fig. 32 Relative Stress-Strain Curve for Plates
(Effect of aspect ratio, A)

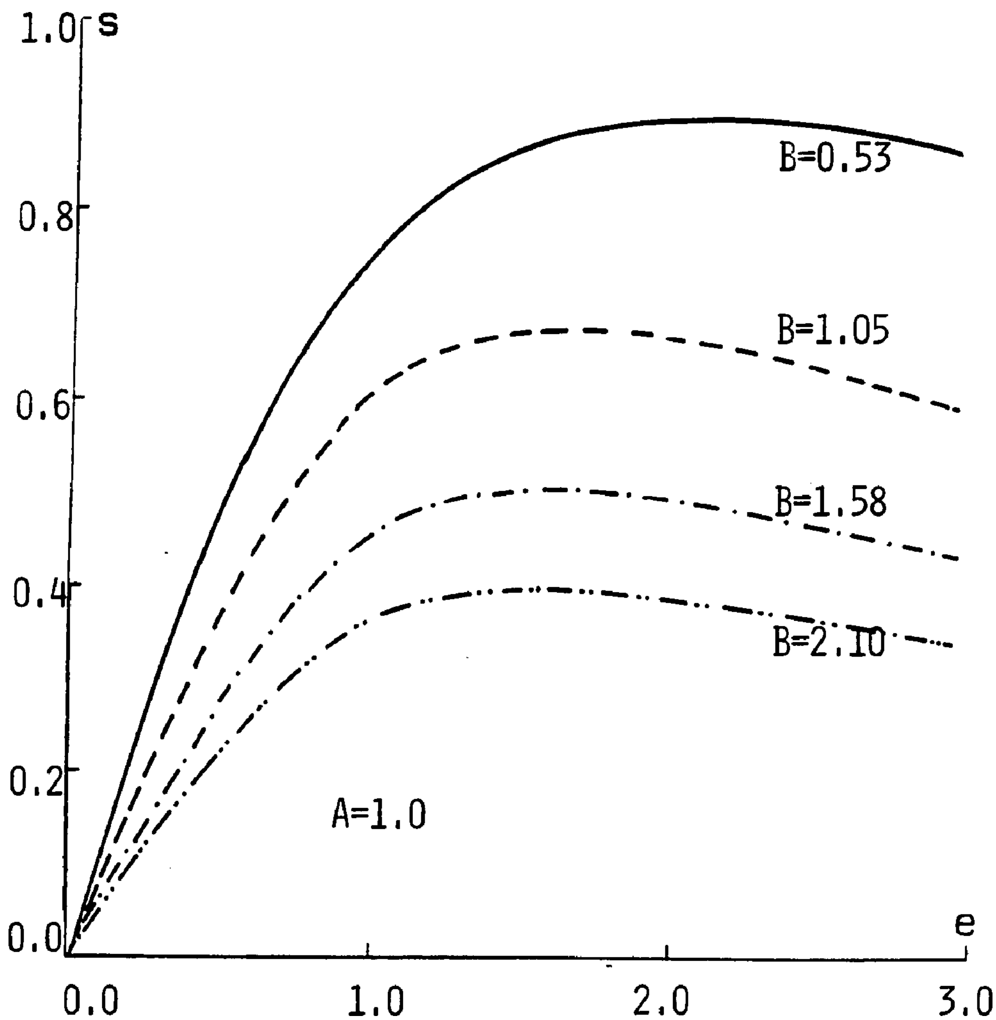

Fig. 33 Relative Stress-Strain Curve for Plates
(Effect of slenderness ratio, B)

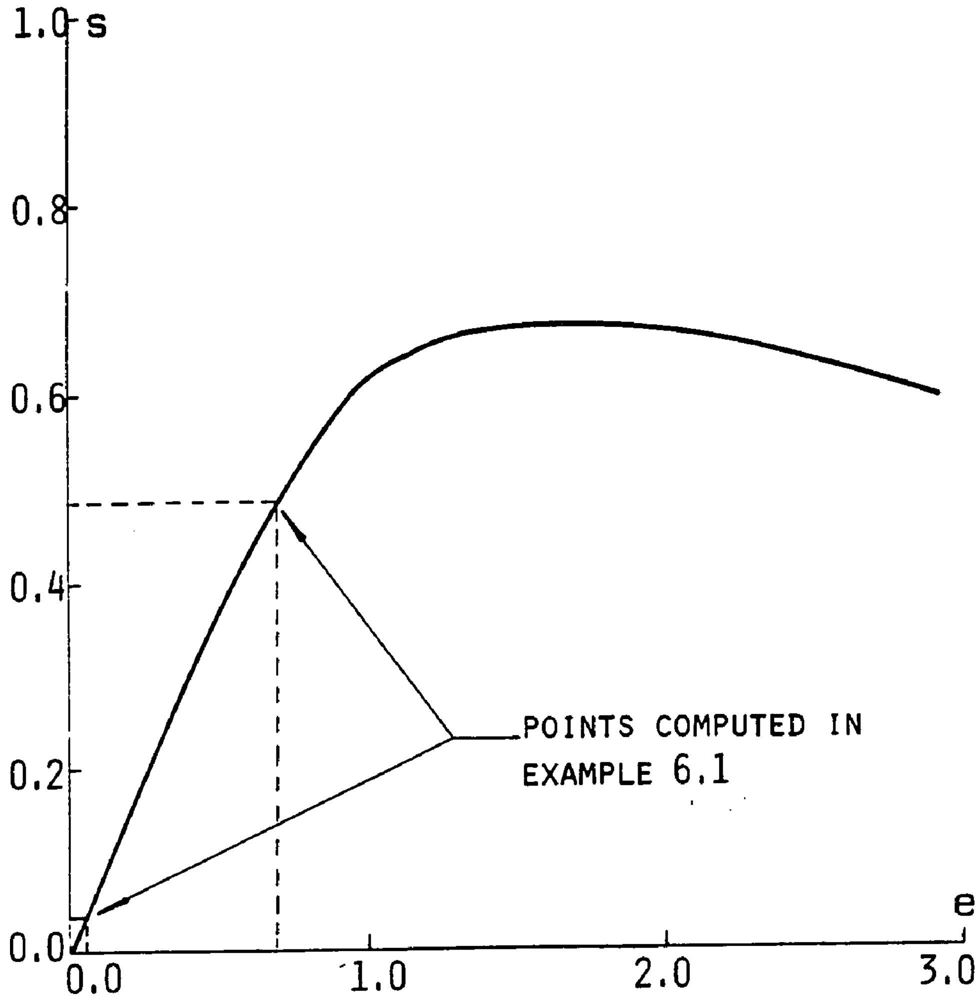

Fig. 34 Stress-Strain Relationship for a Plate
(Example 6.1)

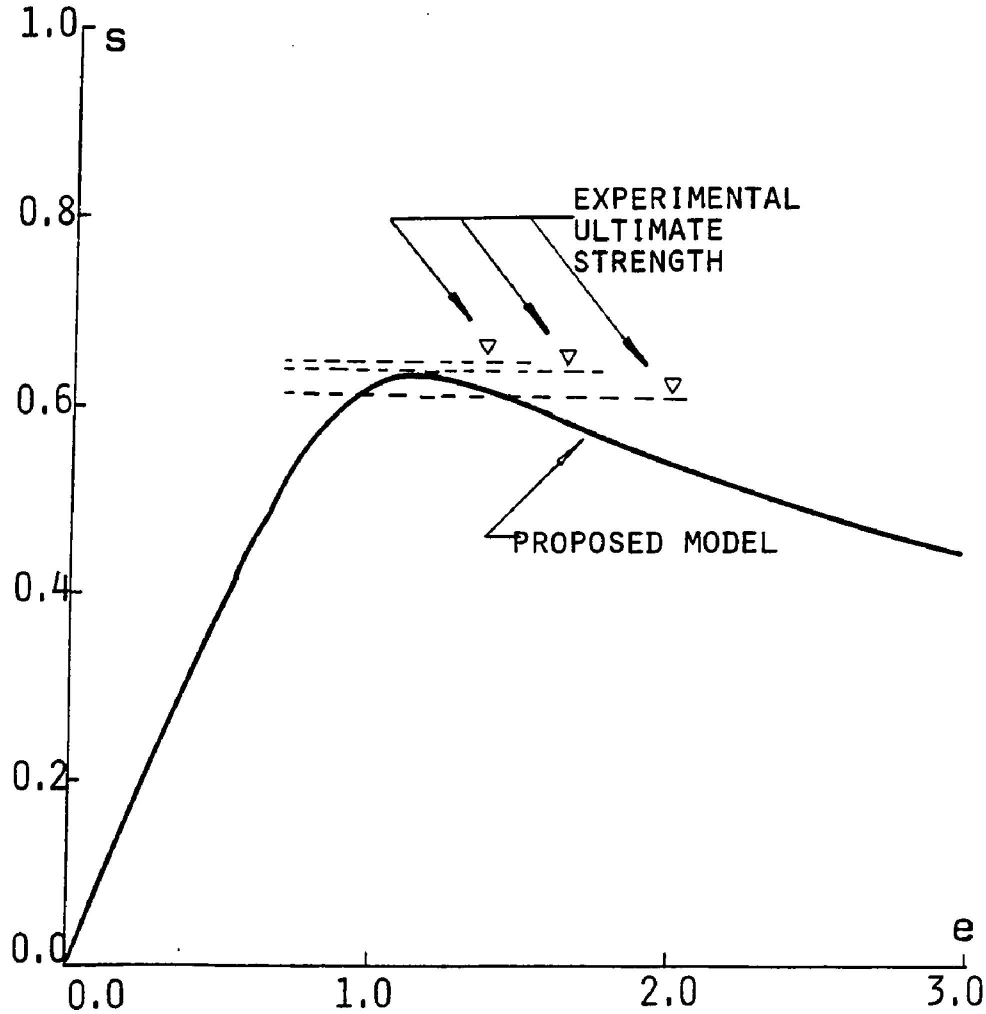

Fig. 35 Test and Theory -- Plate Specimen HTS [7]

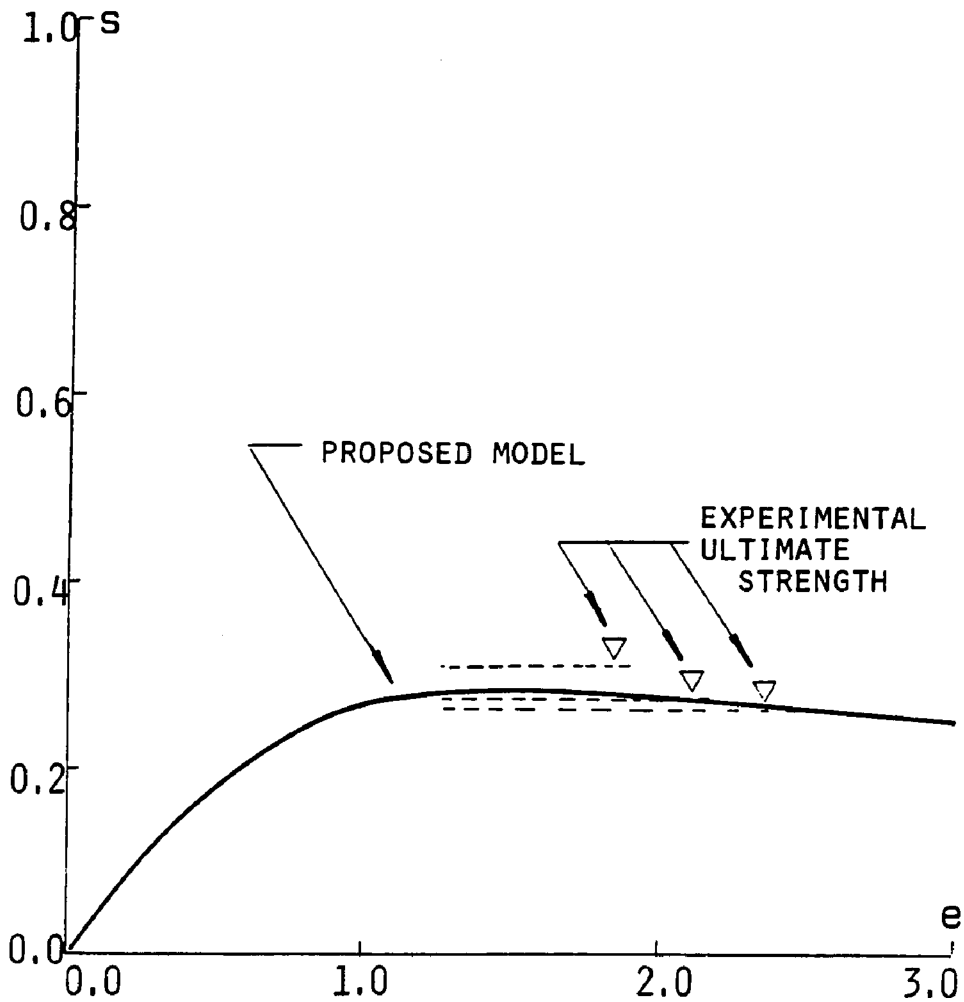

Fig. 36 Test and Theory -- Plate Specimen HY-80 [7]

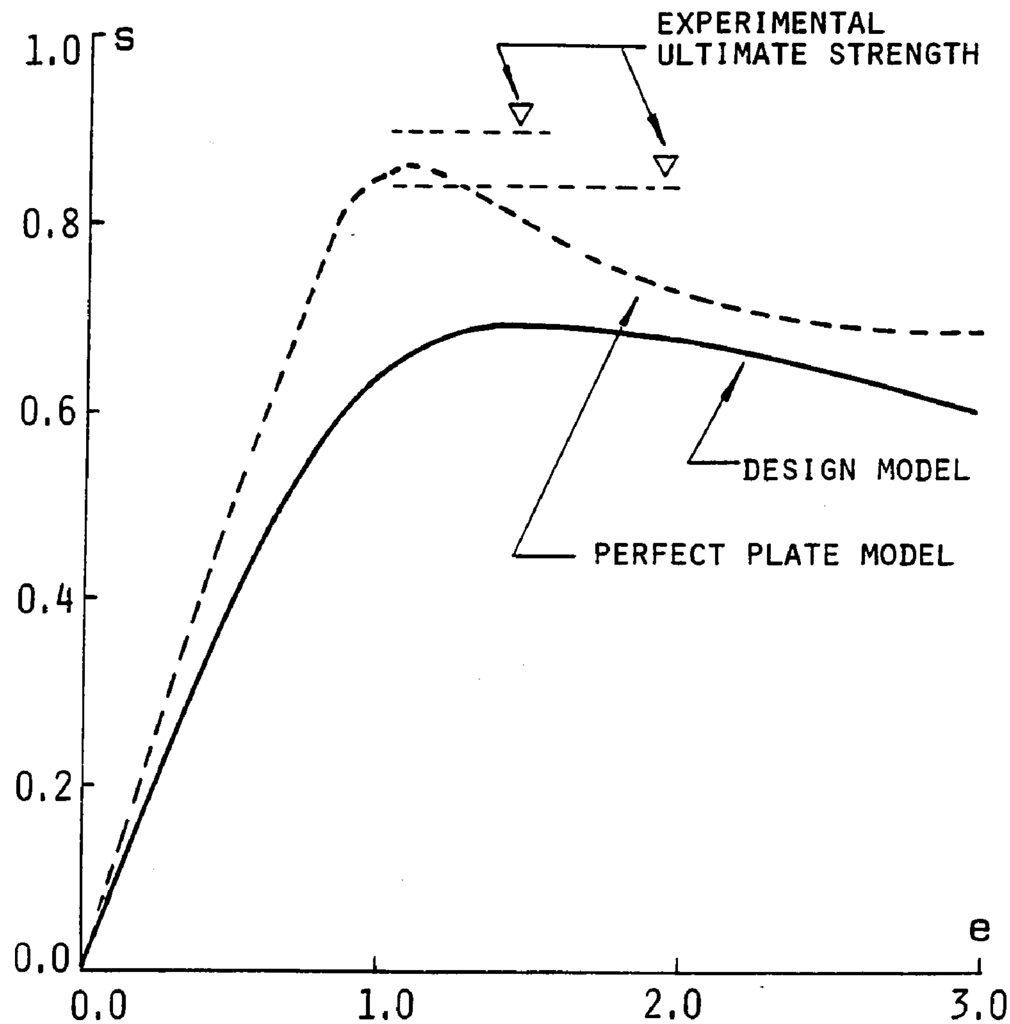

Fig. 37 Test and Theory -- Plate Specimen A=0.875 and B=0.815 [43]

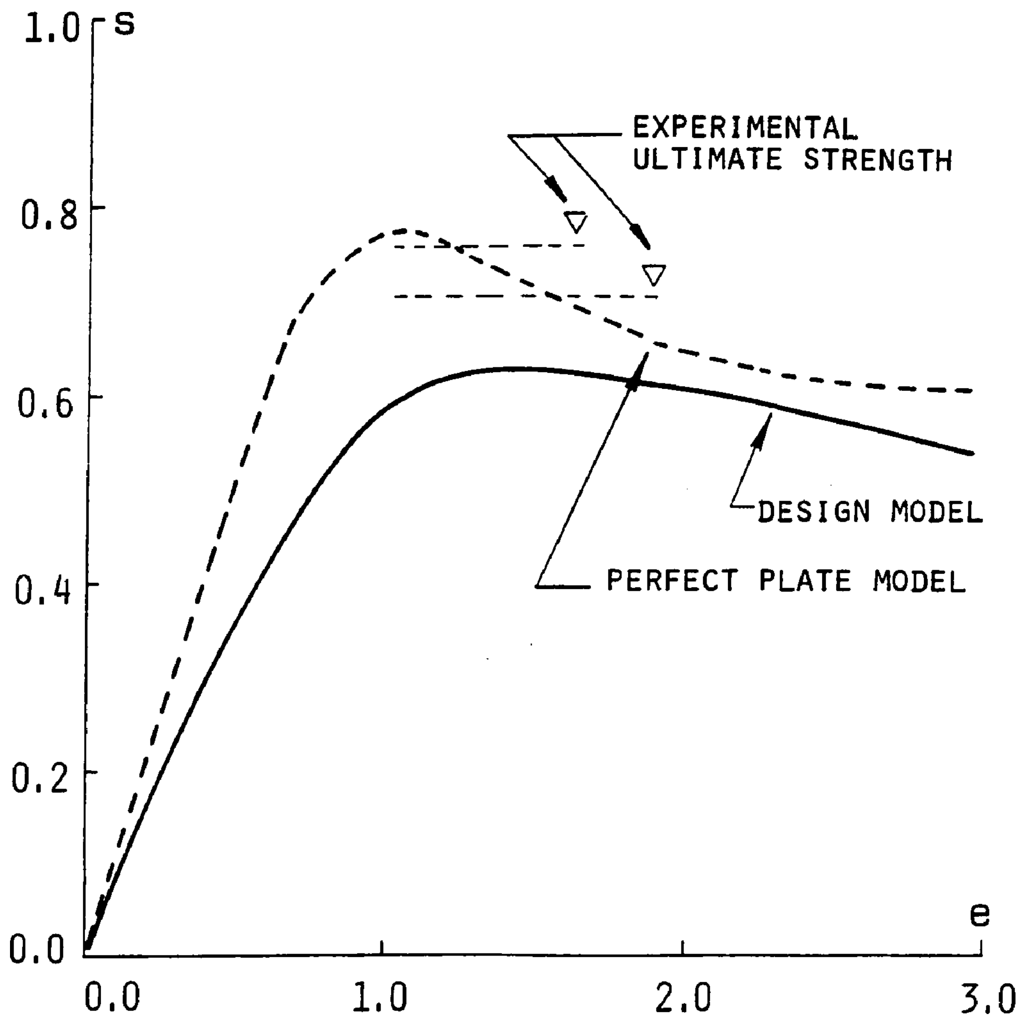

Fig. 38 Test and Theory -- Plate Specimen A=0.875 and B=1.005 [43]

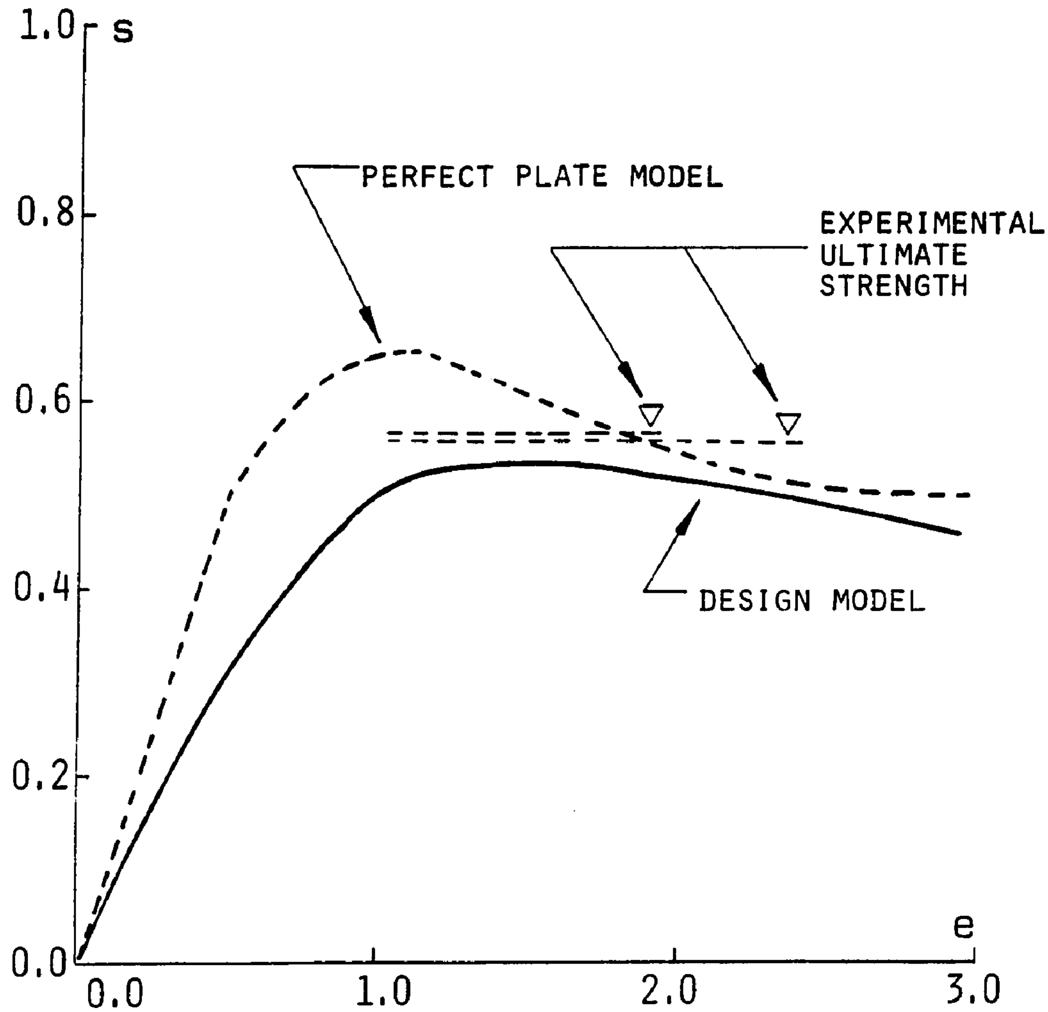

Fig. 39 Test and Theory -- Plate Specimen A=0.875 and B=1.189 [43]

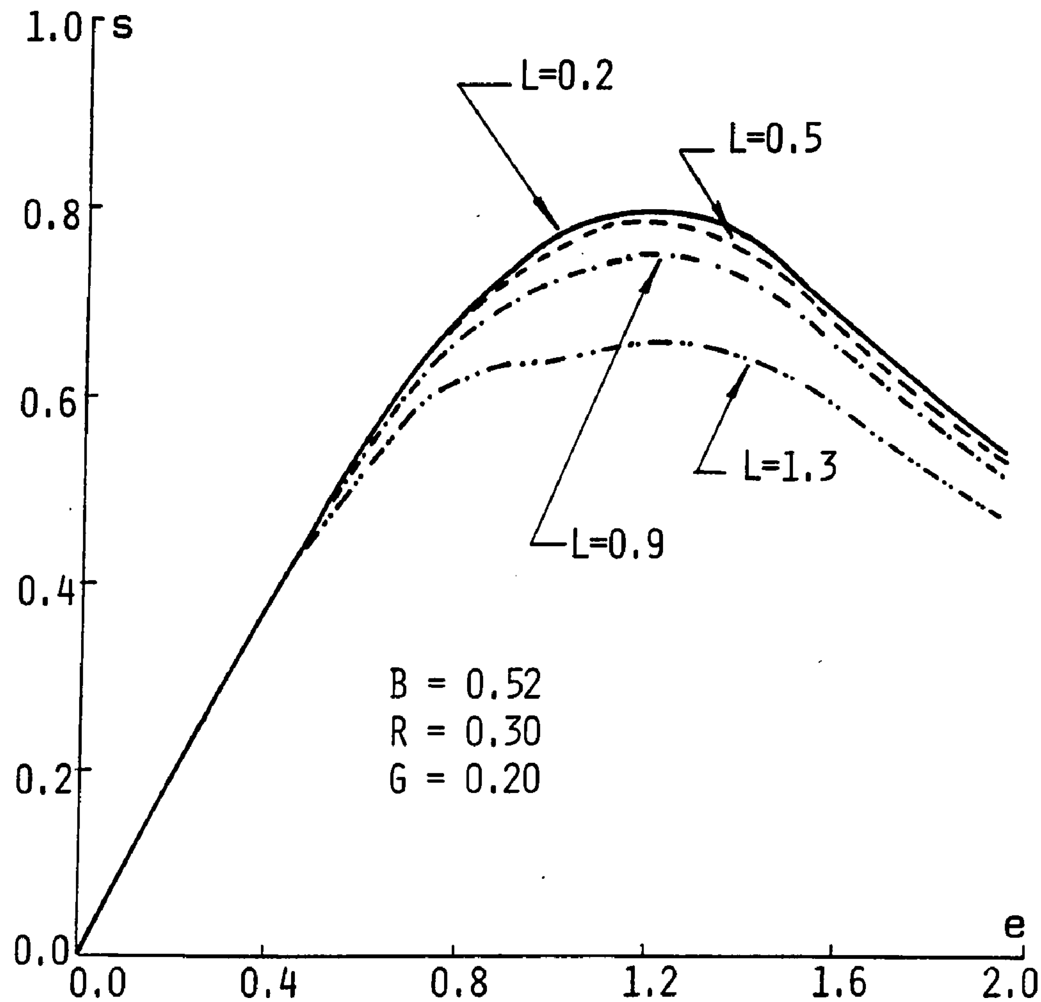

Fig. 40 Relative Stress-Strain Curves for Stiffened Plates
(Effect of plate slenderness, B)

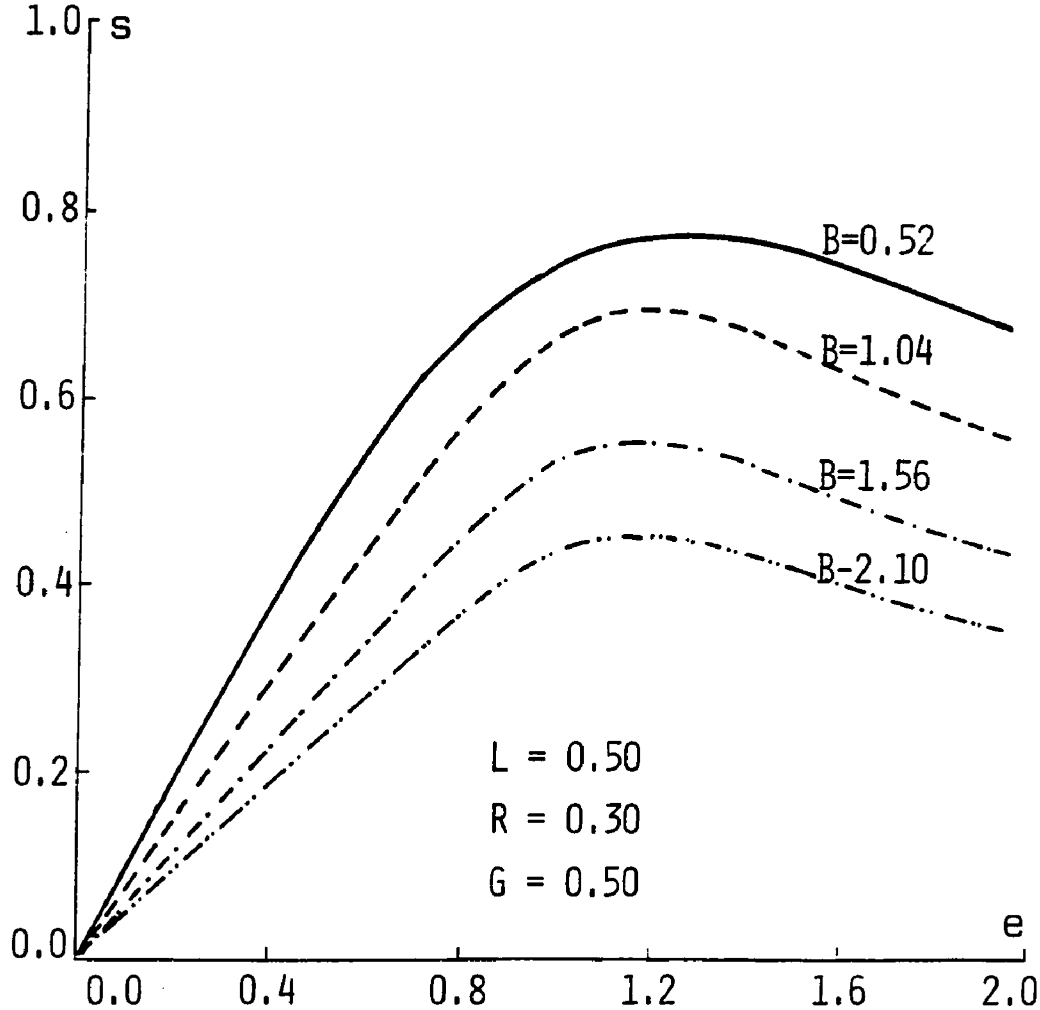

Fig. 41 Relative Stress-Strain Curves for Stiffened Plates
(Effect of panel slenderness, L)

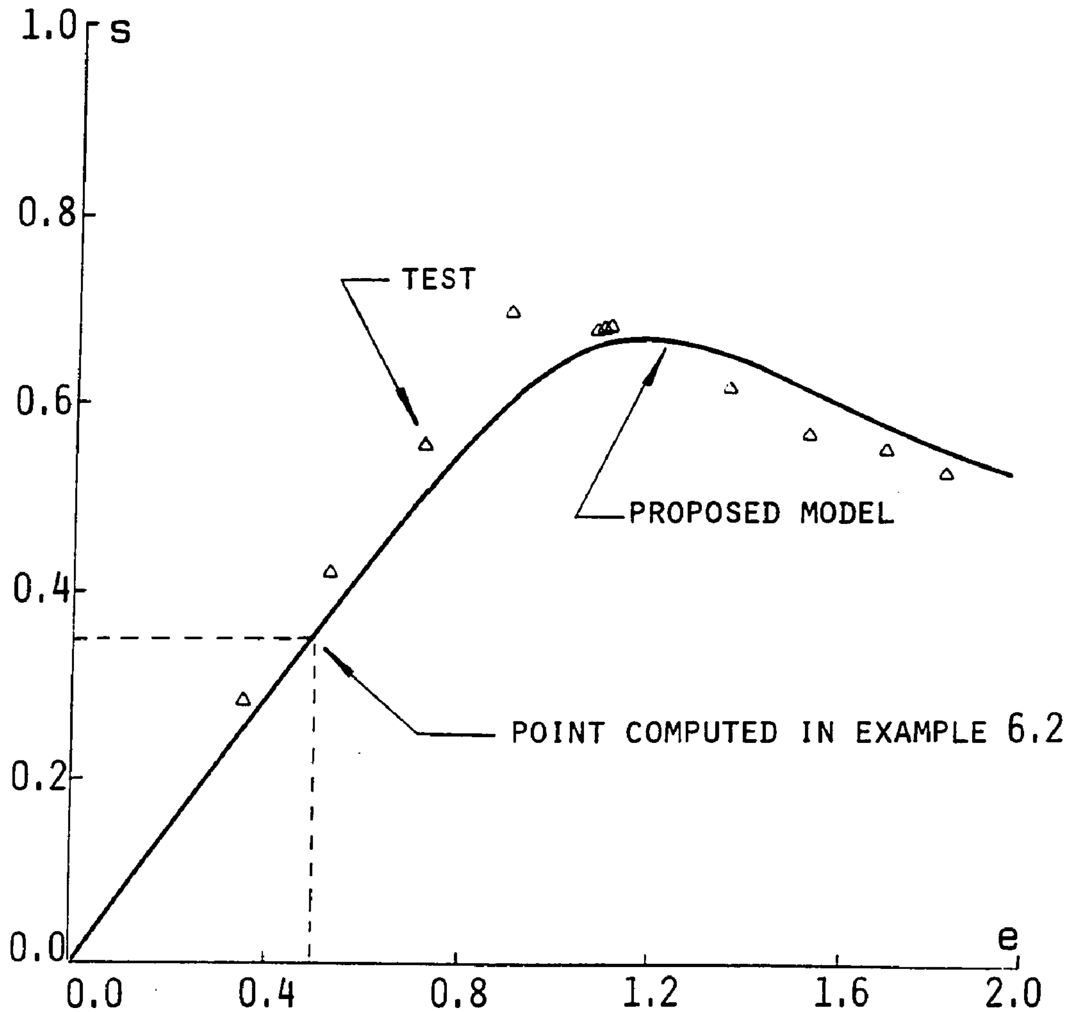

Fig. 42 Stress-Strain Relationship for a Stiffened Plate
(Example 6.2)

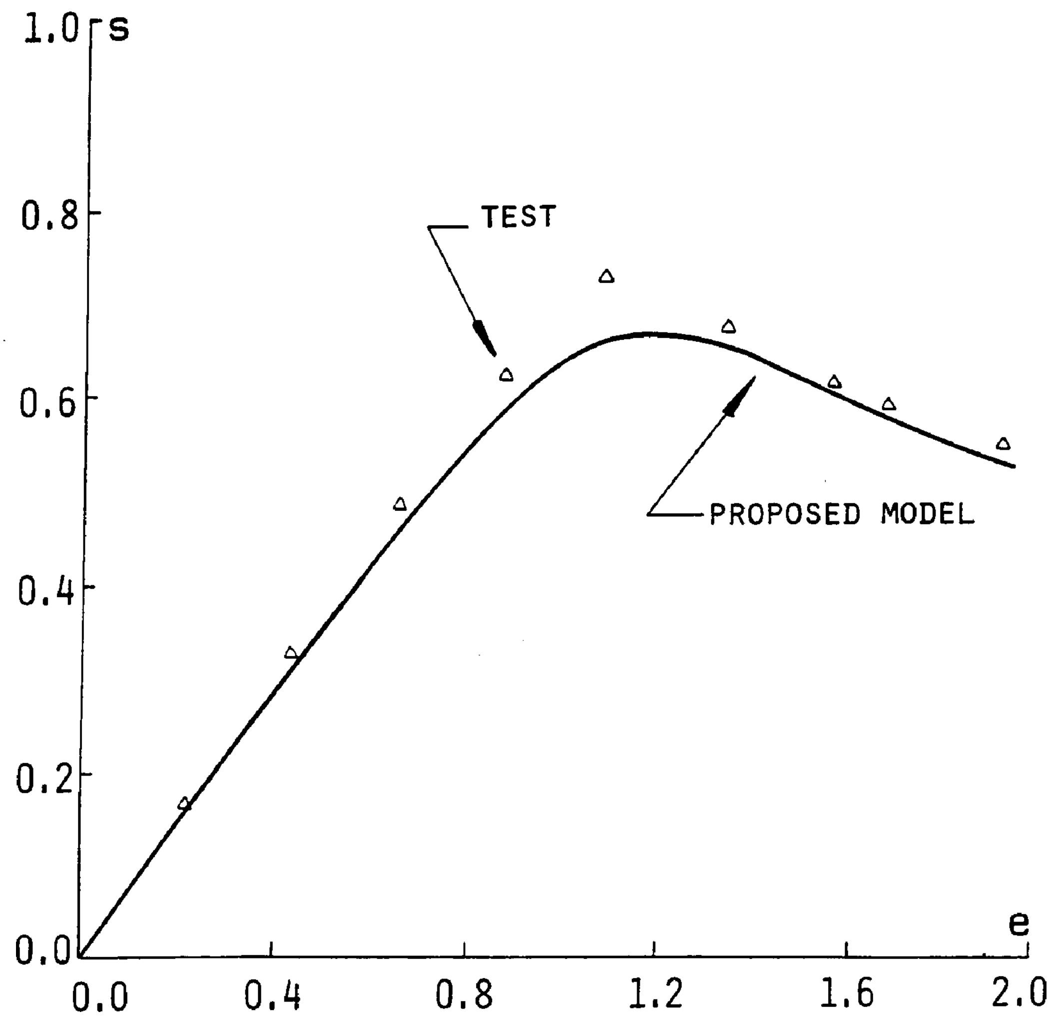

Fig. 43 Test and Theory -- Stiffened Plate Specimen T-7 [32]
(Specimen not annealed)

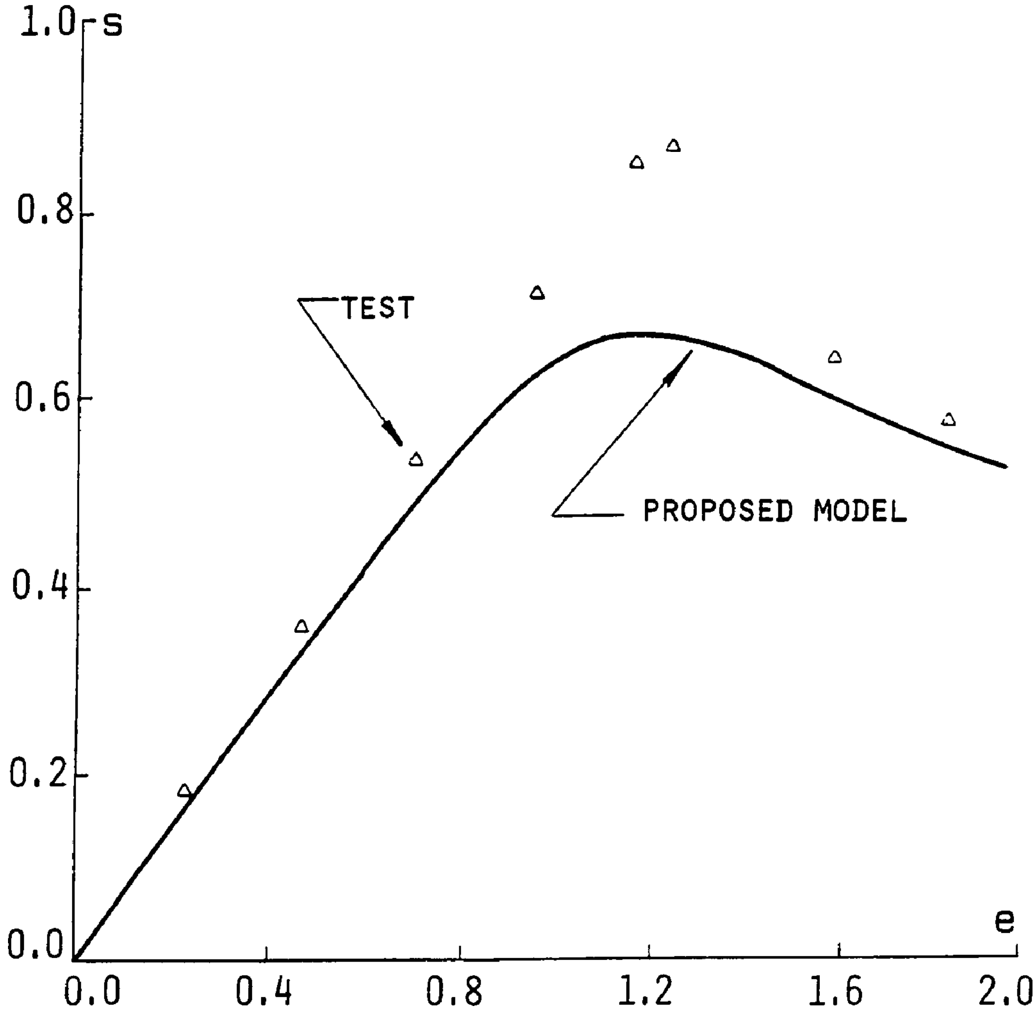

Fig. 44 Test and Theory -- Stiffened Plate Specimen T-8 [32]
(Specimen annealed after welding)

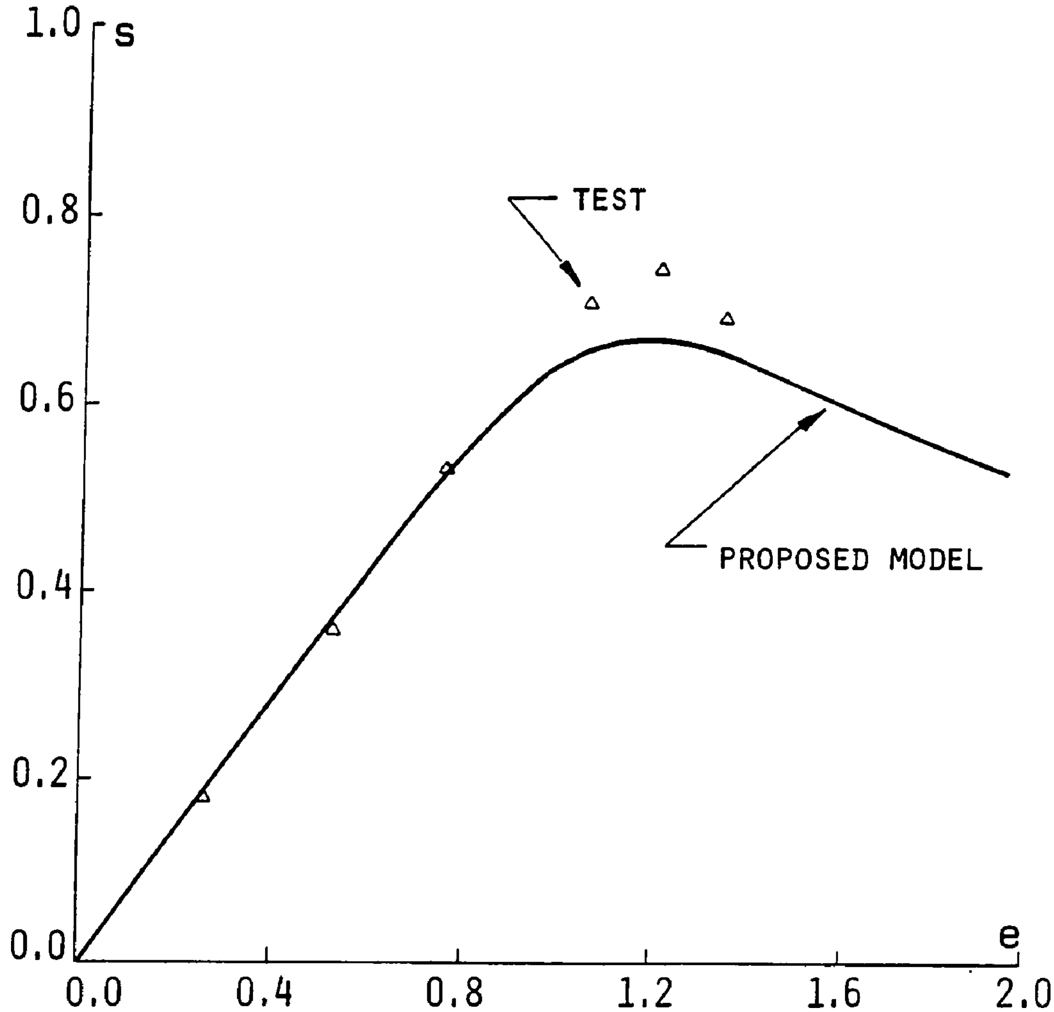

Fig. 45 Test and Theory -- Stiffened Plate Specimen T-9 [32]
(Specimen components annealed then welded)

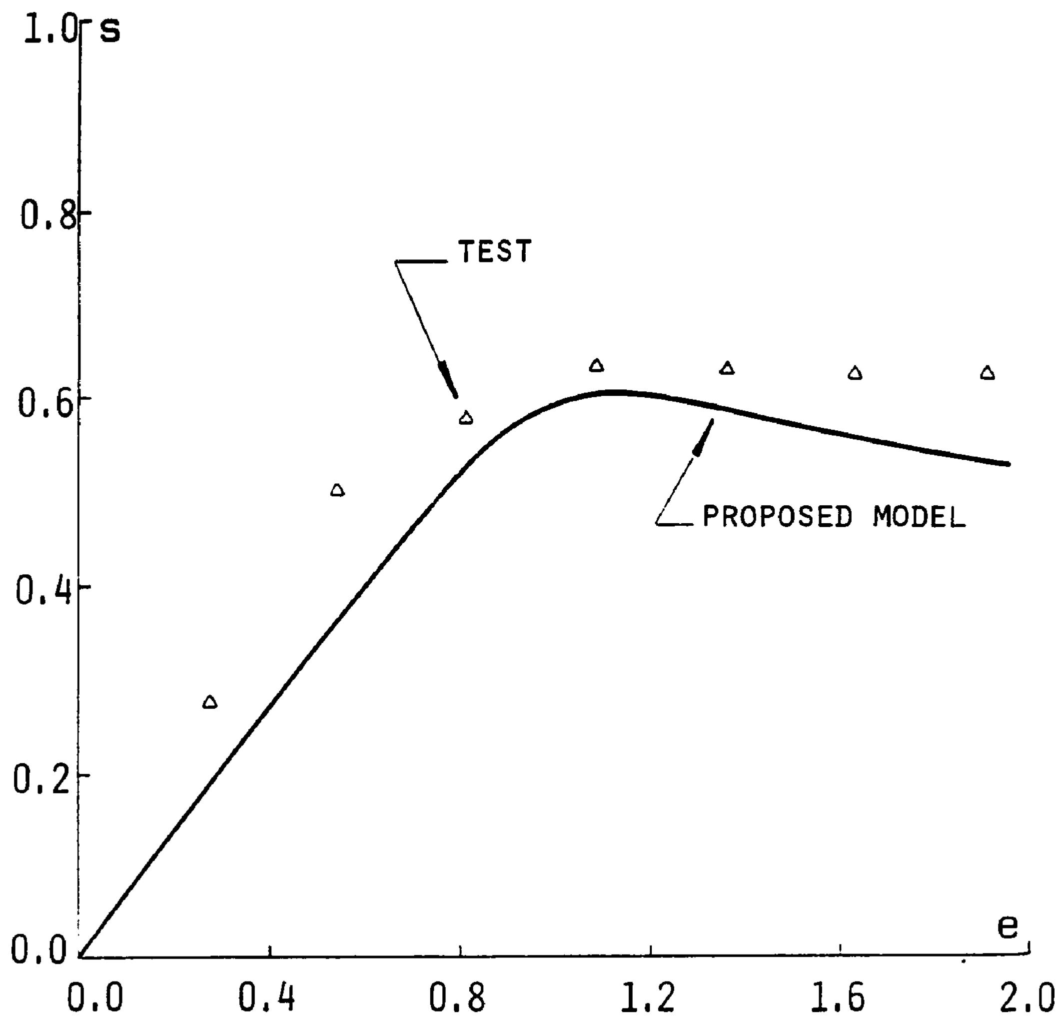

Fig. 46 Test and Theory -- Stiffened Plate Specimen M-1 [28]

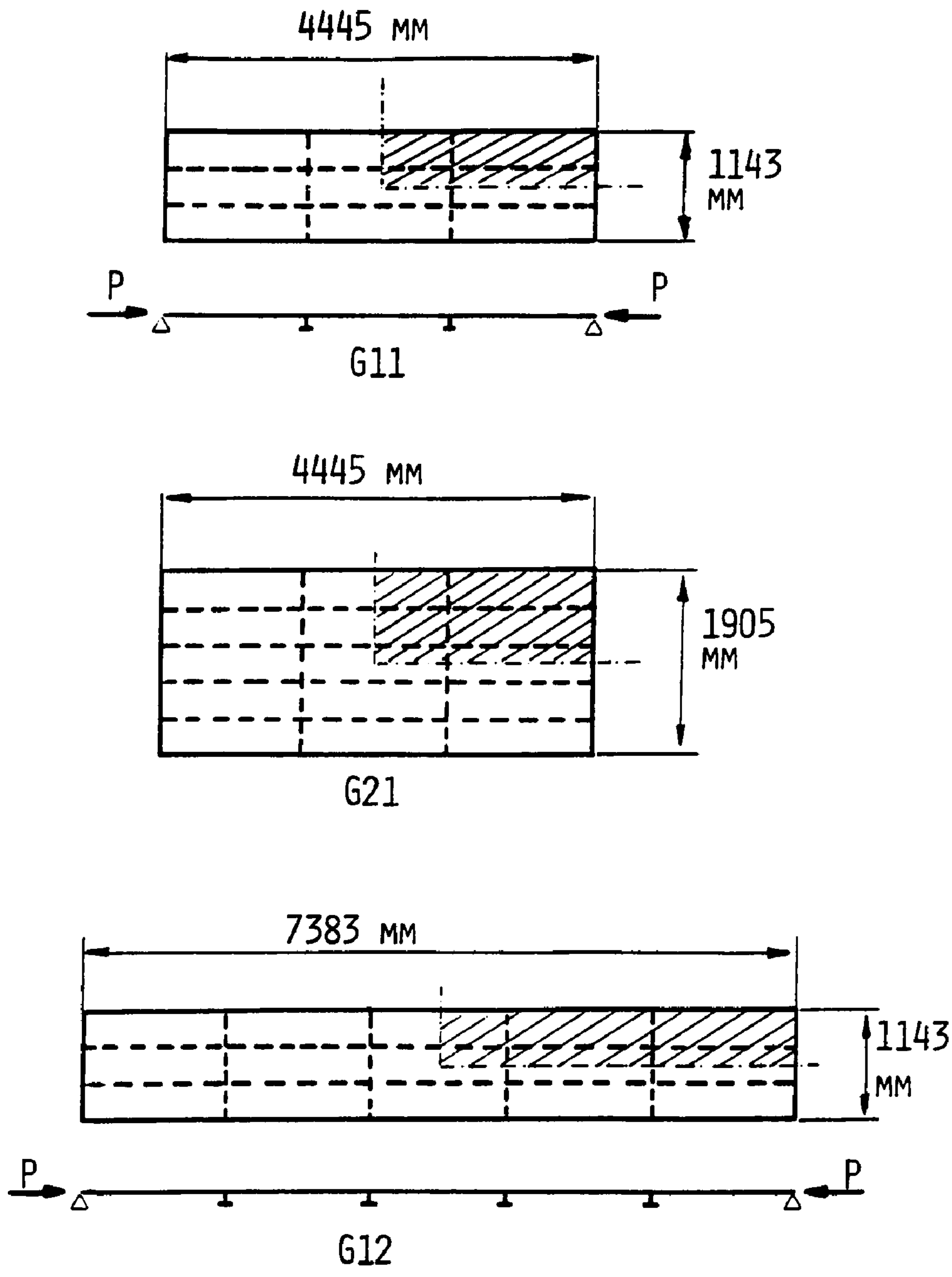

Fig. 47 Samples of Grillages

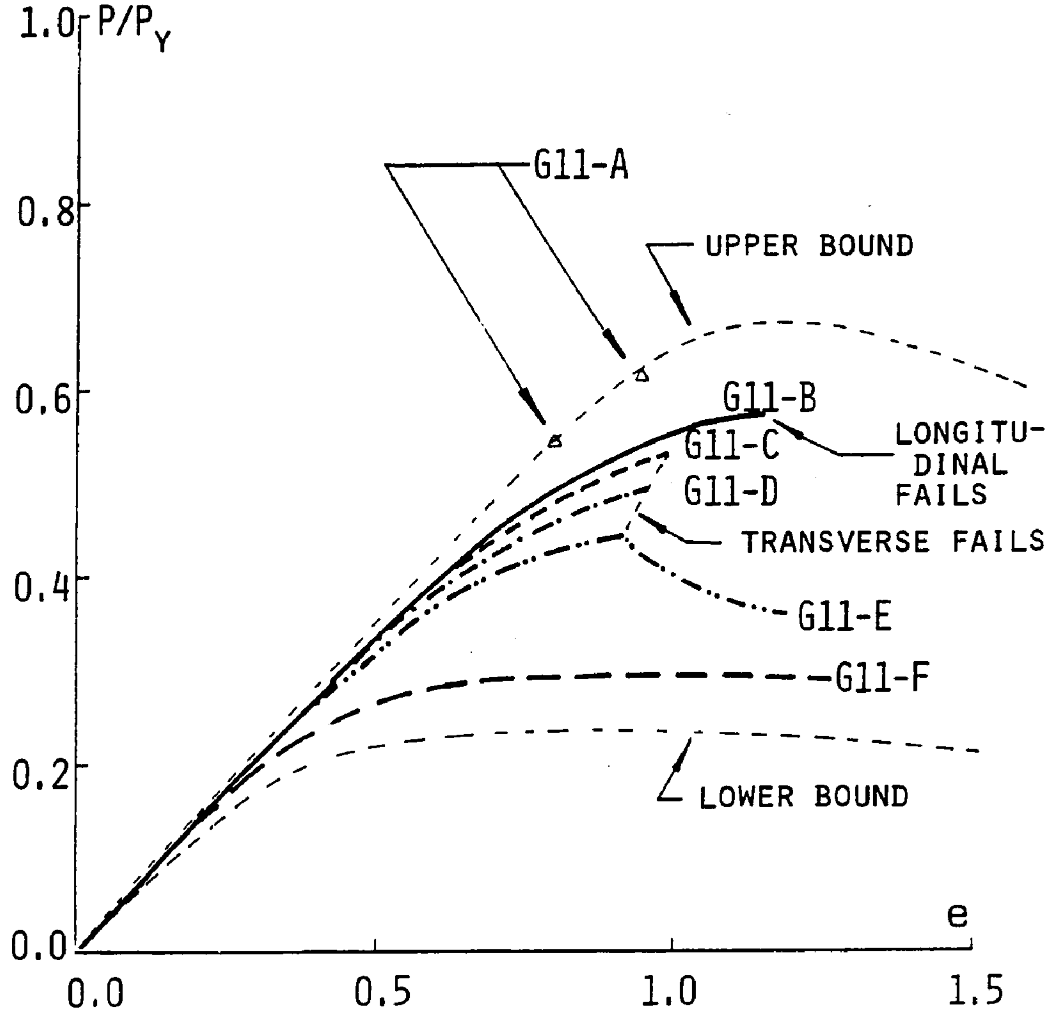

Fig. 48 Relative Stress-Strain Curves for Grillages
(Effect of transverse dimensions)

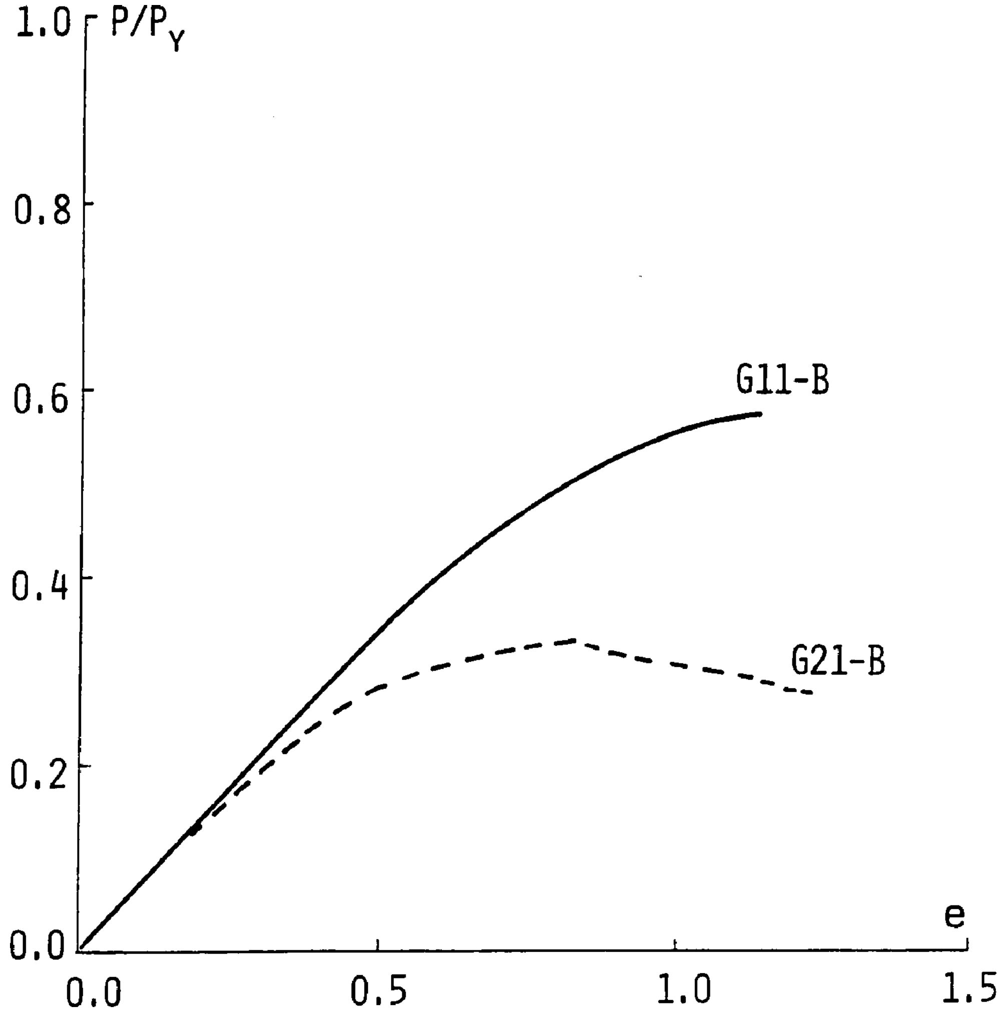

Fig. 49 Relative Stress-Strain Curves for Grillages
(Effect of number of longitudinals)

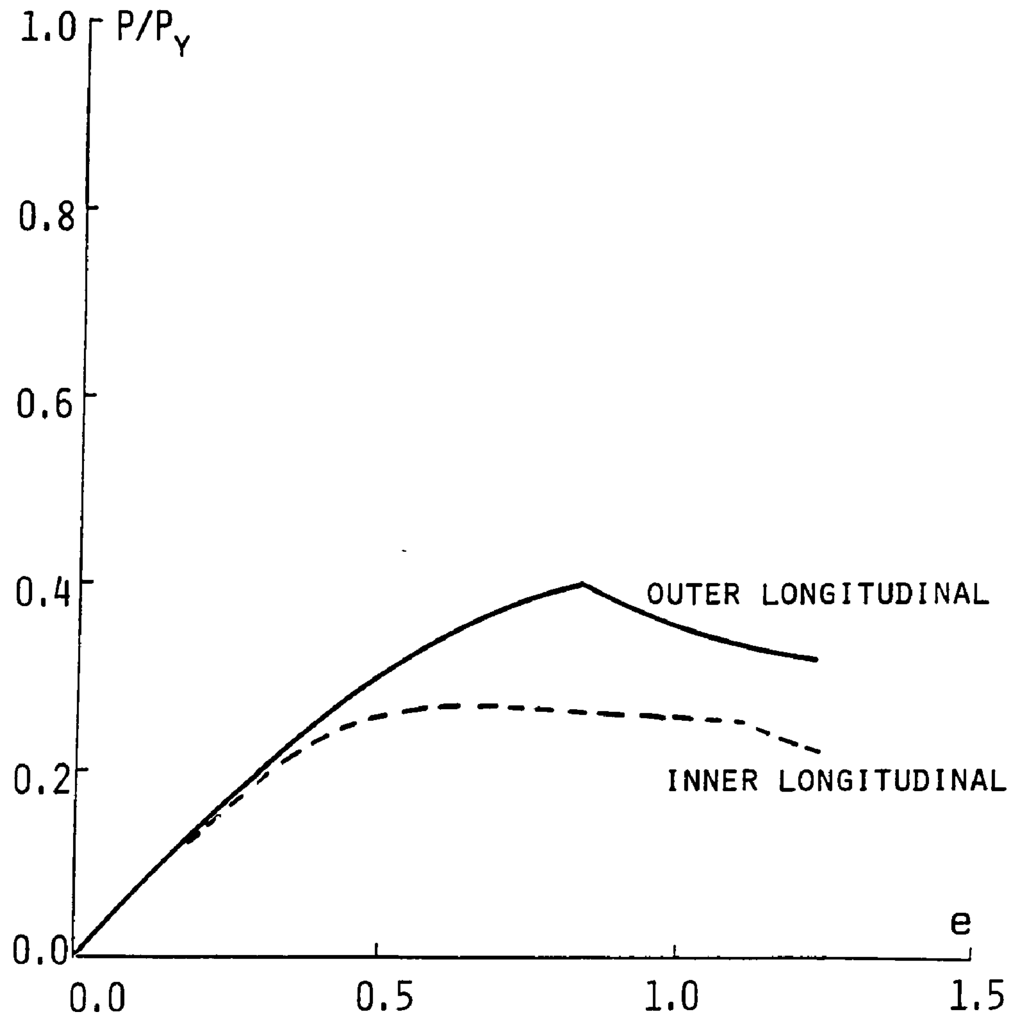

Fig. 50 Relative Stress-Strain Curves for Grillage G21-B
(Distribution of axial forces)

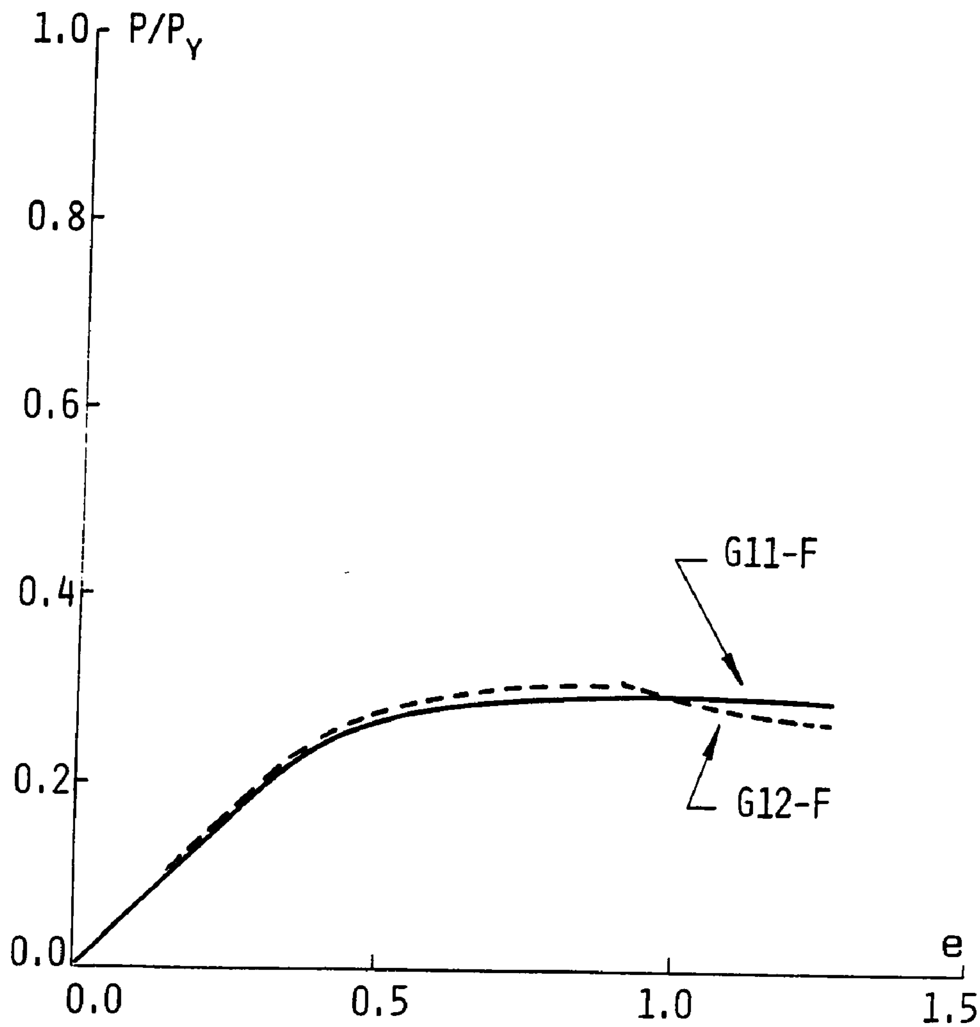

Fig. 51 Relative Stress-Strain Curves for Grillages
(Effect of number of transverses)

BIBLIOGRAPHY

[1] Avriel, M.
Prentice-Hall Series in Automatic Computation: Nonlinear Programming: Analysis and Methods.
Prentice-Hall Inc., Englewood Cliffs, New Jersey, 1976.

[2] Barbre, R., Schmidt, H., Riemann, S.
Ultimate Load Tests on Plates, Longitudinally Stiffened with Welded Bulb Flats, with Unsupported Longitudinal Edges (in German: Traglastversuche an laengsgestauchten, durch Wulstflachstaehle versteiften Blechen mit freien Laengsraendern).
Der Stahlbau 51(11):321-331, November, 1982.

[3] Becker, H.
Instability Strength of Polyaxially Loaded Plates and Relation to Design.
In Dowling, P.J., Harding, J.E., and Frieze, P.A. (editor), Steel Plated Structures, pages 559-580. Crosby Lockwood Staples, London, 1977.
(Proceedings of the International Conference held at Imperial College, London, on July 6-9, 1976).

[4] Billingsley, D.W.
Hull Girder Response to Extreme Bending Moments.
The Society of Naval Architects and Marine Engineers :51-63, June, 1980.
Discussions by P.Y. Chang (Chang 1980), J.B. O'Brien and W.P. Glennie (O'Brien 1980), J.C. Adamchak (Adamchak 1980), D.G. Faulkner (Faulkner 1980), and S.G. Stiansen (Stiansen 1980).

[5] Caldwell, J.B.
Ultimate Longitudinal Strength.
In Proceedings, Vol. 107, pages 411-418. Royal Institution of Naval Architects, London, 1965.

[6] Clarkson, J.
Cambridge Engineering Series: The Elastic Analysis of Flat Grillages.
University Press, Cambridge, 1965.
(With Particular Reference To Ship Structures).

[7] Collier, J.S.
Ultimate Strength of Plating Loaded in Edge Compression - Effect of Adjacent Panels.
NSRDC 760-95, Naval Ship Research and Development Center,Department of the Navy, April, 1967.

[8] Conley, W.F., Becker, L.A., and Allnutt, R.A.
Buckling and Ultimate Strength of Plating Loaded in Edge Compression.
Technical Report 1682, David Taylor Model Basin, Department of the Navy, May, 1963.
Progress Report 2 - Unstiffened Panels.

[9] Crisfield, M.A.
Full Range Analysis of Steel Plates and Stiffened Plating under Uniaxial Compression.
Proceedings of Instn. Civ. Engrs. Part 2(59):595-624, December, 1975.

[10] Crisfield, M.A.
A Computer Program to Generate Load/Shortening Relationships for Simply Supported Steel Plates.
Transport and Road Research Laboratory Report 683, Department of the Environment, 1975.

[11] Det Norske Veritas.
Ultimate Capacity of Plates in Transverse Compression.
VERITAS 79-0104, Det Norske Veritas, February, 1979.

[12] Dow, R.S., Hugill, R.C., Clark, J.D., and Smith, C.S.
Evaluation of Ultimate Ship Hull Strength.
In Extreme Loads Response Symposium, pages 133-148. Society of Naval Architects and Marine Engineers, New York, October, 1981.
Proceedings of the SSC-SNAME Symposium held in Arlington, VA, on October 19-20, 1981.

[13] Dowling, P.J., Frieze, P.A., Slatford, J.E., and Dier, A.
Strength of Ships Plating.
CESLIC Report SP3, Imperial College, London, June, 1978.
A Second Interim Report for the Admiralty Marine Technology Establishment.

[14] Dwight, J.B., and Moxham, K.E.
Welded Steel Plates.
The Structural Engineer 47(2):49-66, February, 1969.

[15] Dwight, J.B.
Collapse of Steel Compression Panels.
In Rockey, K.C., Bannister, J.L., and Evans, H.R. (editor), Developments in Bridge Design and Construction, pages 519-539. Crosby Lockwood, London, 1971.

[16] Dwight, J.B., and Little,G.H.
Stiffened Steel Compression Flanges - Theoretical Failure Analysis.
The Structural Engineer 54(12):489-500, December, 1976.

[17] Faulkner, D.G.
(Discussion of "Hull Girder Response to Extreme Bending Moments" by D.W. Billingsley).
The Society of Naval Architects and Marine Engineers 4:12-14, June, 1980.

[18] Frankland, J.M.
The Strength of Ship Plating Under Edge Compression.
Technical Report 469, U.S. Experimental Model Basin, May, 1940.

[19] Frey, F.
Nonlinear Structure Analysis by the Method of Finite Elements and its Application to Steel Structures (in French:L'Analyse Statique Non Lineaire Des Structures Par La Methode Des Elements Finis Et Son Application A La Construction Metallique).
PhD thesis, Faculte des Sciences, Universite de Liege, 1978.

[20] Frieze, P.A., Dowling, P.J., and Hobbs, R.E.
Parametric Study on Plates in Compression.
CESLIC Report BG39, Imperial College, London, January, 1975.

[21] Harding, J. E., Hobbs, R. E., and Neal, B. G.
Ultimate Load Behavior of Plates Under Combined Direct and Shear In-Plane Loading.
In Dowling, P.J., Harding, J.E., and Frieze, P.A. (editor), Steel Plated Structures, pages 369-403. Crosby Lockwood Staples, London, 1977.
(Proceedings of the International Conference held at Imperial College, London, on July 6-9, 1976).

[22] Himmelblau, D.M.
Applied Nonlinear Programming.
McGraw-Hill Book Company, 1972.

[23] Horne, M.R., and Narayanan, R.
Ultimate Capacity of Longitudinally Stiffened Plates Used in Box Girders.
Proc. Instn Civ. Engrs. 61:253-280, June, 1976.
Part 2.

[24] Horne, M.R., and Narayanan, R.
The Strength of Straightened Welded Steel Plates.
The Structural Engineer 54(11):437-443, November, 1976.

[25] Horne, M. R., and Narayanan, R.
Ultimate Strength of Stiffened Panels Under Uniaxial Compression.
In Dowling, P.J., Harding, J.E., and Frieze, P.A. (editor), Steel Plated Structures, pages 1-23. Crosby Lockwood Staples, London, 1977.
(Proceedings of the International Conference held at Imperial College, London, on July 6-9, 1976).

[26] Jeeves, T.A.
Secant Modification of Newton's Method.
Communications of the Association for Computing Machinery 1(8):9-10, August, 1958.

[27] Kerfoot, R.P.
Analysis of Grillages Subjected to Combined Loads.
PhD thesis, Lehigh University, September, 1972.
Available from University Microfilms, Ann Arbor, MI.

[28] Kmiecik, M.
The Load-Carrying Capacity of Axially Loaded Longitudinally Stiffened Plate Panels Having Initial Deformations.
Technical Report R 80, Skipsteknisk Forskningsinstitutt, May, 1970.

[29] Kmiecik, M.
Behaviour of Axially Loaded Simply Supported Long Rectangular Plates Having Initial Deformations.
Technical Report R 84, Skipsteknisk Forskningsinstitutt, Sept., 1971.

[30] Komatsu, S., Ushio M., and Kitada T.
An Experimental Study on the Ultimate Strength of Stiffened Plates (in Japanese).
Proc. of JSCE (255):47-61, November, 1976.

[31] Komatsu, S., Nara, S., and Kitada, T.
Elasto-Plastic Analysis of Orthogonally Stiffened Plates with Initial Imperfections under Uniaxial Compression.
Computers and Structures 11:429-437, 1980.

[32] Kondo, J., and Ostapenko, A.
Tests on Longitudinally Stiffened Plate Panels with Fixed Ends -- Effect of Lateral Loading.
Fritz Engineering Laboratory Report No. 248.12, Lehigh University, July, 1964.

[33] Kondo, J.
Ultimate Strength of Longitudinally Stiffened Plate Panels Subjected to Combined Axial and Lateral Loading.
Fritz Engineering Laboratory Report No. 248.13, Lehigh University, 1965.

[34] LaFara, R.L.
Computer Methods for Science and Engineering.
Hayden Book Company, Inc., Rochelle Park, New Jersey, 1973.

[35] Lee, T.
Elastic-Plastic Analysis of Simply Supported Rectangular Plates Under Combined Axial and Lateral Loading.
Fritz Engineering Laboratory Report No. 248.7, Lehigh University, 1961.

[36] Little, G.H.
Stiffened Steel Compression Panels - Theoretical Failure Analysis.
The Structural Engineer 54(12):489-509, December, 1976.

[37] Little, G.H.
Rapid Analysis of Plate Collapse by Live-Energy Minimisation.
International Journal of Mechanical Sciences 19(12):725-744, 1977.

[38] Little, G.H.
Stiffened Steel Compression Panels -- Plate Failure Results for Plain Flat Stiffeners and T-Section Stiffeners.
Technical Report, Birmingham University, Jul, 1977.
Unpublished Preliminary Report.

[39] Little, G.H.
The Collapse of Rectangular Steel Plates under Uniaxial Compression.
The Structural Engineer 58B(3):45-61, September, 1980.

[40] Mansour, A.E.
Charts for the Buckling and Post-Buckling Analysis of Stiffened Plates under Combined Loading.
Technical Research Bulletin 2-22, Society of Naval Architects and Marine Engineers, July, 1976.

[41] Moolani, F.M., and Dowling, P.J.
Ultimate Load Behaviour of Stiffened Plates in Compression.
In Dowling, P.J., Harding, J.E., and Frieze, P.A. (editor), Steel Plated Structures, pages 51-88. Crosby Lockwood Staples, London, 1977.

[42] Moxham, K.E.
Theoretical Prediction of the Strength of Welded Plates in Compression.
Technical Report CUED/C-Struct/TR.2, University of Cambridge, 1971.

[43] Moxham, K.E.
Buckling Tests on Individual Welded Steel Plates in Compression.
Technical Report CUED/C Struct/TR.3, University of Cambridge, 1971.

[44] Ostapenko, A., and Lee, T.T.
Tests on Longitudinally Stiffened Plate Panels Subjected to Lateral and Axial Loading.
Fritz Engineering Laboratory Report No. 248.4, Lehigh University, August, 1960.

[45] Ostapenko, A.
Ultimate Strength Design of Wide Stiffened Plates Loaded Axially and Normally.
In Proceedings of Symposium on Structural Analysis, Non-Linear Behavior and Techniques, Supplementary Report 164 UC, pages 175-180. Transport and Road Research Laboratory, Crowthorne, Berkshire, 1975.

[46] Ostapenko, A., and Vaucher, A.
Ultimate Strength of Ship Hull Girders under Moment, Shear and Torque.
Fritz Engineering Laboratory Report No. 453.6 (MARAD Report MA-RD-940-80077), Lehigh University, July, 1980.

[47] Ostapenko, A., Chen, Y., Vaucher, A., and Moore, T.R.
Computer Program for Ultimate Strength Analysis of Ship Hulls Subjected to Moment, Torque and Shear.
Fritz Engineering Laboratory Report No. 479.4 (MARAD Report No. MA-RD-940-82081), Lehigh University, November, 1982.

[48] Ostapenko, A., and Moore, T.R.
Maximum Strength of Ship Hulls Subjected to Moment, Torque and Shear.
Fritz Engineering Laboratory Report No. 479.5 (MARAD Report No. MA-RD-940-82080), Lehigh University, November, 1982.

[49] Parsanejad, S., and Ostapenko, A.
Ultimate Strength Analysis of Plate Grillages under Combined Loads.
Fritz Engineering Laboratory Report No. 323.11, Lehigh University, 1972.

[50] Puthli, R.S., Bijlaard, F.S.K., and Stol, H.G.A.
Theoretical Background to the Solution of Highly Non-Linear Inelastic Buckling and Collapse Problems in Stiffened Panels.
Technical Report BI-83-42/63.6.0829, IBBC-TNO, Delft, The Netherlands, June, 1983.

[51] Puthli, R.S., Bijlaard, F.S.K., and Stol, H.G.A.
Numerical Study on the Collapse of Simply Supported Longitudinally Stiffened Panels under Uniaxial Compression.
Technical Report B-83-431/63.6.0829, IBBC-TNO, Delft, The Netherlands, July, 1983.

[52] Rutledge, D.R., and Ostapenko, A.
Ultimate Strength of Longitudinally Stiffened Plate Panels (Large and Small b/t, General Material Properties).
Fritz Engineering Laboratory Report No. 248.24, Lehigh University, 1968.

[53] Rutledge, D.R.
Computer Program for Ultimate Strength of Longitudinally Stiffened Panels.
Fritz Engineering Laboratory Report No. 248.23, Lehigh University, 1968.

[54] Saettele, J.M., and Fischer, M.
The Ultimate Strength Curves for Rectangular Plates under Uniaxial Compression with Aspect Ratio (a/b)<1 and with Prescribed Initial Imperfections (In German: Traglastkurven einachsig gedrueckter Rechteckplatten mit Seitenverhaeltnissen (a/b)<1 bei vorgegebenen geometrischen Imperfektionen).
Der Stahlbau 50(7):205-210, July, 1981.

[55] Sherman, D.R.
Inelastic Local Buckling of Circular Tubes.
In Fujita, Y. and Galambos, T.V. (editor), Inelastic Instability of Steel Structures and Structural Elements, pages 122-145. University of Tokyo, Hongo 7-3-1, Bunkyo-ku, Tokyo, Japan, May, 1981.

[56] Smith, C.S.
Compressive Strength of Welded Steel Ship Grillages.
In Proceedings, Vol. 117, pages 325-347. Royal Institution of Naval Architects, London, 1975.

[57] Smith, C.S.
Influence of Local Compressive Failure on Ultimate Longitudinal Strength of a Ship's Hull.
In International Symposium on Practical Design in Shipbuilding, pages . , Tokyo, October, 1977.

[58] Smith, C.S., Kirkwood, W.C., McKeeman, J.L.
Evaluation of Ultimate Longitudinal Strength of a Ship's Hull.
AMTE(S) R 671, Admiralty Marine Technology Establishment, November, 1977.

[59] Smith, C.S., and Dow, R.S.
Residual Strength of Damaged Steel Ships and Offshore Structures.
The Journal of Constructional Steel Research 1(4):2-15, Sept, 1981.
Published by Granada.

[60] Soares, C.G.
Survey Methods of Prediction of the Compressive Strength Stiffened Plates.
Technical Report MK/R/57, University of Trondheim, Trondheim, Norway, August, 1981.

[61] Szilard, R.
Book: Theory and Analysis of Plates.
Prentice-Hall, Englewood Cliffs,N.J., 1974.

[62] Tsuiji, T.
Strength of Longitudinally Stiffened Plate Panels with Large b/t.
Fritz Engineering Laboratory Report No. 248.14, Lehigh University, June, 1965.

[63] USN.
Strength of Structural Members.
NAVSEA DDS 100-4, The United States Navy, February, 1979.

[64] Vojta, J.F., and Ostapenko, A.
Ultimate Strength Design Curves for Longitudinally Stiffened Plate Panels with Large b/t.
Fritz Engineering Laboratory Report No. 248.19, Lehigh University, August, 1967.

[65] Walker, A.C., and Davies, P.
An Elementary Study of Non-Linear Buckling Phenomena in Stiffened Plates.
In Proceedings of Symposium on Structural Analysis, Non-Linear Behavior and Techniques, Supplementary Report 164 UC, pages 19-25. Transport and Road Research Laboratory, Crowthorne, Berkshire, 1975.

[66] Wilde, D.J.
Prentice-Hall International Series in the Physical and Chemical Engineering Sciences: Optimum Seeking Method.
Prentice-Hall Inc., Englewood Cliffs, New Jersey, 1964.

[67] Winter, G.
Performance of Compression Plates as Parts of Structural Members.
In George Winter (editor), Four Papers on the Performance of Thin Walled Steel Structures, pages 51-57. Cornell University, Ithaca, New York, November, 1950.
(Reprint from Research, Engineering Structures Supplement(Colston Papers, Vol II), p.179, London, 1949).

[68] Wolfe, P.
Secant Method for Simultaneous Nonlinear Equations.
Communications of the Association for Computing Machinery 2(12):12-13, December, 1959.

APPENDIX

NOMENCLATURE

A	Aspect ratio = a/b
A_f, A_w	Areas of flange and web of the stiffener
a	Length of plate or of stiffened plate
B,	Slenderness ratio of plate = $0.526(a/t)\sqrt{\epsilon_y}$ or $0.526(b/t)\sqrt{\epsilon_y}$
$\underline{B}$	Slenderness ratio of plate = B/0.526
b	Width of plate (length of the loaded edge of the plate)
b_f, b_t	width of flange of the transverse and longitudinal stiffeners
C_p	Matrix of constants for plates
C_s	Matrix of constants for stiffened plates
D_j	Deflection at the j-th junction (between transverse and longitudinal beams)
Dx	Total axial shortening of longitudinal beam
d_o	Stress constant for linear range of stress-strain behavior of plates
d_f, d_t	depth of web of the transverse and longitudinal stiffeners
E	Modulus of elasticity
E_r	Sum of squared errors

e	Relative strain = ϵ / ϵ_y
e_o	Limit of relative strain below which the stress-strain relationship is linear
F_x	Coordinate function of variable x
f_j	Element of coordinate function (individual function)
f_{ij}	Individual function for the j-th coefficient (term) at the i-th point
G	Ratio of the area of the flange to the area of the total stiffener
H	Matrix of exact values of the function
$\bar{H}$	Matrix of approximate values of the function
h_{ij}	Individual coordinate function for the j-th term of the i-th variable
L	Slenderness ratio of stiffened plate
M_i	Moment at the i-th cross section of the longitudinal beam
m	Number of terms in combined coordinate function
m_i	Number of terms in the coordinate function for the i-th variable
m'	Number of terms in the reduced coordinate function
n	Width ratio of residual stress, that is, nt is the width of the tensile residual stress at the edge of the plate
P	Total axial force
P_y	Axial force which causes full yielding of the cross section

Q	$= U^T H$
R	Ratio of the area of the stiffener to the area of the plate
R_j	Redundant force at the j-th junction between transverse and longitudinal beams
r	Radius of gyration of the stiffened plate (gross section of plate and stiffener) about its centroidal axis
S	Stress
S_r	Residual stress
S_{rc}	Compressive residual stress
S_{rt}	Tensile residual stress
S_r	Nondimensionalized residual stress variable
S_y	Yield stress of plate
S_{yf}, S_{yw}	Yield stress of flange and web of the stiffener
s	Relative stress (for plate and stiffened plate models)
s	Curve coordinate at the centroid of a longitudinal beam (Chapter 5)
t	Plate thickness
t_f, t_w	Thickness of flange and web of the stiffener
U	Matrix of values of component functions at given points
V	$= U^T U$ (a symmetrical matrix)
V_i	Shear at the i-th cross section of the longitudinal beam

W_o Maximum initial deformation of plate

W_{os} Maximum initial deformation of stiffened plate

w_o Nondimensionalized initial imperfection of plate = W_o/t

w_{os} Nondimensionalized initial imperfection of stiffened plate = W_{os}/a

ϵ Average strain

ϵ_i Centroidal strain at the i-th cross section of the longitudinal beam

ϵ_O Centroidal strain at the mid-length cross section of the longitudinal beam

ϵ_y Yield strain of plate or weighted average yield strain of stiffened plate

θ_i Slope at i-th cross section of the longitudinal beam

ϕ_i Curvature at i-th cross section of the longitudinal beam

ϕ_O Curvature at mid-length cross section of the longitudinal beam

VITA

The author is the youngest child of Mr. and Mrs. Sambas Atmadinata and was born on September 7, 1954 in Cimahi, West-Java Indonesia. He received most of his elementary school (S.D.) education in Jakarta (Indonesia) and the remainder at a lyceum in Bucharest (Romania). He then received his junior high school (S.M.P.) and senior high school (S.M.A.) education at Bogor, West-Java. In January 1973 he entered the Bandung Institute of Technology (I.T.B.) at Bandung West-Java where he received his Civil Engineer degree (Ir.) in June 1978. After having worked for six months as a construction supervisor in the Department of Mining and Energy of the Republic of Indonesia at Jakarta, he came to the United States in September 1979 for graduate study. He attended the Virginia Polytechnic Institute and State University at Blacksburg, Virginia, where he was awarded a Master of Science degree in Civil Engineering in December 1980. His studies at Lehigh University began in January 1981.